



NATIONAL AERONAUTICS AND SPACE ADMINISTRATION

MSC-PA-R-69-2
SUPPLEMENT 3

APOLLO 9 MISSION REPORT
SUPPLEMENT 3

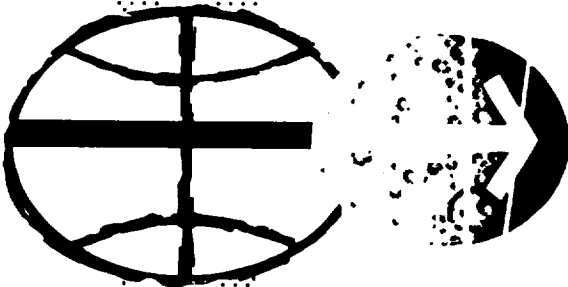
LM ABORT GUIDANCE SYSTEM POSTFLIGHT
ANALYSIS REPORT

(NASA-TM-X-72273) APOLLO 9 MISSION
REPORT. SUPPLEMENT 3: LM ABORT
GUIDANCE SYSTEM POSTFLIGHT ANALYSIS REPORT
(NASA) 108 p

N75-70487

Unclas
17410

00/98



MANNED SPACECRAFT CENTER
HOUSTON, TEXAS
NOVEMBER 1969

-

-

-

-

|

APOLLO 9 MISSION REPORT

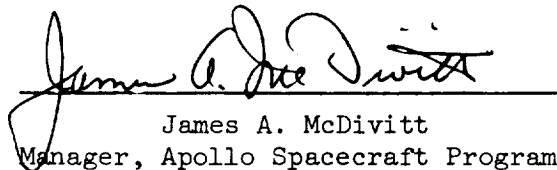
Supplement 3

LM ABORT GUIDANCE SYSTEM POSTFLIGHT
ANALYSIS REPORT

PREPARED BY

TRW Systems Group

APPROVED BY



James A. McDivitt
Manager, Apollo Spacecraft Program

NATIONAL AERONAUTICS AND SPACE ADMINISTRATION
MANNED SPACECRAFT CENTER
HOUSTON, TEXAS
November 1969

LM ABORT GUIDANCE SYSTEM
POSTFLIGHT ANALYSIS REPORT

Apollo 9 Flight
(LM-3)

1969 June

Prepared for

National Aeronautics and Space Administration
Manned Spacecraft Center, Houston, Texas
Under Contract No. NAS 9-8166

Approved by: *A. S. Gunnerson*
A. S. Gunnerson
Manager, Guidance System
Engineering Department

Approved by: *D. L. Meginnity*
D. L. Meginnity
LM/AGS Project Manager

TRW
SYSTEMS GROUP

|

CONTENTS

	Page
1. SCOPE, PURPOSE, AND SUMMARY	1-1
1.1 Scope and Purpose	1-1
1.2 Summary	1-1
1.2.1 Performance Measurements	1-2
1.2.1.1 Free Flight Mission Period Measurements	1-2
1.2.1.2 Thrusting Flight (Burn) Period Measurements	1-3
2. ANALYSIS METHODS	2-1
2.1 Data Sources	2-1
2.2 Analysis Performed	2-1
2.3 Analysis Computations	2-2
2.4 Analysis Accuracy	2-9
2.4.1 Quantization	2-9
2.4.2 PGNCS Errors	2-9
2.4.3 PGNCS/AGS Sample Time Differences and Oscillatory Angular Motion	2-10
2.4.4 AEA Computational Errors	2-11
3. SYSTEM PERFORMANCE	3-1
3.1 General	3-1
3.2 Velocity to be Gained Residual Comparisons	3-1
3.3 Guidance Solution Comparisons	3-3
3.4 PGNCS/AGS Alignment Accuracy	3-4
3.5 In-Flight Calibration (IFC) and Sensor In-Flight Bias Performance	3-5
3.5.1 Gyro Calibrations	3-5
3.5.2 Accelerometer Calibration	3-6
3.6 AGS Steering	3-7
4. SENSOR PERFORMANCE ANALYSIS	4-1
4.1 Docked Burn Analysis	4-2
4.1.1 Docked Burn Data	4-2
4.1.2 Docked Burn Accelerometer Analysis	4-2
4.1.3 Docked Burn Gyro Analysis	4-4
4.1.4 Direction Cosine Misalignment	4-4
4.2 LM AGS Burn to Depletion Analysis	4-5

CONTENTS (Continued)

	Page
4.3 Free Flight Interval Data	4-6
4.4 Other Burns	4-8
4.4.1 Insertion Burn	4-8
4.4.2 CSI Burn	4-8
4.5 Comparison of Sensor Analysis Results to AGS Error Models	4-9
4.5.1 Qualification of Derived Errors	4-9
4.5.2 Error Model Comparison	4-9
4.5.3 Initial Misalignment Error Comparisons . .	4-12
4.5.4 Sensor Bias Stability Comparisons	4-12
4.5.4.1 Accelerometer Bias Repeatability	4-13
4.5.4.2 Accelerometer Bias Time Stability	4-13
4.5.4.3 Gyro Bias Repeatability	4-14
4.5.4.4 Gyro Bias Time Stability	4-14
4.5.5 Unmodeled Errors	4-14
4.5.6 PGNCS Error Contributions	4-15
4.6 Sensor Error Analysis Conclusions	4-15
5. FUNCTIONAL PERFORMANCE	5-1
5.1 Flight Environment	5-1
5.1.1 Flight Vibration Levels	5-1
5.1.2 Input Voltages	5-1
5.1.3 ASA Temperature	5-1
5.2 AGS Functional Anomalies	5-2
5.2.1 Caution and Warning Electronic Assembly (CWEA) Signal	5-2
6. REFERENCES	6-1
APPENDICES	
I PREFLIGHT HISTORY AND PERFORMANCE	I-1
II TIMING ADJUSTMENTS	II-1
III QUANTIZATION INDUCED COMPUTATIONAL ERRORS IN THE TRANSFORMATION OF OUTPUTS OF THE BODY MOUNTED ACCELEROMETERS INTO INERTIAL COORDINATES	III-1

1. SCOPE, PURPOSE, AND SUMMARY

1.1 SCOPE AND PURPOSE

The results of the postflight analysis of the Abort Guidance Section (AGS) for the LM 3 are presented in this report. A summary of the analysis methods used, and the data sources employed, is given in Section 2. The analysis was done in accordance with the general method of the LM/AGS Postflight Data Reduction and Analysis Plan, Reference 1. The main source of quantitative data against which the AGS performance is evaluated is the telemetered Primary Guidance Navigation and Control System (PGNCS) output. PGNCS is a high accuracy, gimbaled inertial measurement unit and thus provides good measurement data against which to evaluate the AGS strapped down inertial measurement unit.

The objectives of the postflight analysis are to evaluate overall AGS performance to the extent possible with the available data. A particular objective is the evaluation of the inflight performance of the inertial sensors in order to confirm, or allow correction of, the AGS Capability Estimate, Reference 2.

The AGS overall system performance is described in Section 3. The sensor performance is described in Section 4.

The general functional performance of AGS, including any observed anomalies, is discussed in Section 5.

1.2 SUMMARY

The AGS functions of inflight state vector (position and velocity) initialization, alignment, accelerometer and gyro calibration, control of the LM during the execution of a "burn" (thrusting maneuver), control of the LM attitude in the attitude hold mode, radar data processing and guidance solution computation were all successfully accomplished. The functional performance appeared to be excellent with one exception, a DEDA keyboard pushbutton sometimes required repeated depression to properly function; this was an annoyance to the crew.

AGS operating procedures and guidance and control system interfaces were all validated during this flight. Minor crew, or ground, operating procedure deficiencies were identified.

There was an instrumentation failure in the LM Caution and Warning circuitry that caused a false indication of AGS failure early in the flight. An analysis of available system performance data established that no AGS failure had, in fact, occurred.

The quantitative evaluation of the AGS inertial measurement performance is based upon measurements made during the burns and during selected free fall portions of the mission. Table 2-2 of Section 2, indicates the mission time periods that were analyzed for inertial measurement performance.

1.2.1 Performance Measurements

1.2.1.1 Free Flight Mission Period Measurements

During the free flight mission periods, three In Flight Calibrations (IFC's) were performed. An IFC determines gyro biases (relative to PGNCS) and accelerometer biases (relative to the "zero g" of freeflight). The results of these IFC's are described in Section 3.

The gyro biases determined by these calibrations were all well within the expected range. The spread between the three IFC's was less than 0.25 deg/hr on any gyro. The accelerometer biases as determined by the IFC's were only available within a quantization level of 380 μ g (because of earth scaling of the lunar flight program). These did not shift at all during the flight nor did they indicate any shift from their preflight compensation values.

In addition to the IFC's, free flight data analysis of the accelerometer outputs over a 62 minute period prior to the first IFC and over several shorter free flight intervals was also made. The accelerometer biases over all these intervals were very stable. The apparent bias shift from the last preflight value was approximately three times the 1σ capability estimate on one instrument. The capability estimate for this bias shift is being re-examined.

Also the inertial attitude reference, or gyro drift, performance was analyzed over a 10 minute free flight interval between the CDH and TPI burns. This analysis is subject to error due to the fact that PGNCS and AGS attitude measurements are not available at common time, but may be as much as 1/2 second apart. The PGNCS data is interpolated to the AGS sample times. This can result in attitude errors as large as 63 arc seconds.

The relative attitude drifts between AGS and PGNCS during this period did not, however, exceed 0.3 deg/hr.

These results are described in Section 4.

1.2.1.2 Thrusting Flight (Burn) Period Measurements

There are two kinds of performance that are of basic interest over the burn periods (as well as over the free flight periods). These are: 1) the inertial reference, or gyro, drifts, and 2) the velocity measurement capability, or accelerometer performance.

The technique that has been used to evaluate gyro drift performance over the burn periods is to compare the AGS calculated direction cosines with the PGNCS gimbal angle CDU readouts. These quantities are the measures of the orientation of the LM vehicle axis system relative to the AGS and PGNCS inertial references, respectively, and thus any differences represent differences or relative drifts between AGS and PGNCS. Because the times at which PGNCS and AGS data is sampled are generally different (up to 1/2 second) there will be errors in this comparison. The errors will be larger during periods of large angular motion of the LM.

There were two burns, the docked burn and the depletion burn, that were of sufficient duration to provide some measure of the relative angular drift between AGS and PGNCS. These were each of approximately 6 minutes duration. The angular limit cycle motion during the docked burn was quite small and of low frequency. The motion was quite severe during the depletion burn. Therefore, throughout the docked burn angular comparisons between AGS and PGNCS were made, the differences resolved along the AGS axes and relative AGS/PGNCS drifts estimated. For the

depletion burn a total, end-to-end, drift check was made by comparing the AGS/PGNCS relative alignment after the burn with that before the burn.

The results of these comparisons indicate that AGS was performing within specification. They do show an apparent drift of AGS relative to PGNCS, in the X channel, of approximately three times the expected 1σ AGS drift. It is assumed, however, that much of this is error due to the nonsynchronization of the data timing.

The techniques for evaluating the velocity measurement, or accelerometer performance, over the burn period are the comparison of the velocity to be gained residuals and a comparison of integrated body axis accelerations.

To obtain an overall comparison of the accuracy of AGS and PGNCS velocity measurement capabilities, it is desirable to compare the two system's outputs in the inertial coordinate reference. For this mission, however, the AGS calculation of inertial quantities is of limited accuracy because of the scaling required in the AEA to accomplish the Earth mission. The AEA software is, of course, designed for a Lunar mission and the effect of the Earth rescaling is to increase the computational error enough to essentially hide the basic sensors errors.

The velocity to be gained, V_g , is calculated in an inertial reference frame, and is thus subject to these scaling errors. Furthermore, PGNCS and AGS are targeted with slightly different initial V_g 's to account for the fact that they perform different coordinate transformations on the input V_g to put it into the reference inertial coordinate system. Because of these effects the V_g residual comparison is not adequate to determine accelerometer measurement accuracy.

The comparison does, however, show agreement adequate for the AGS mission requirements. The V_g residual comparisons are shown in Section 3.

A better estimate of AGS accelerometer performance was obtained by resolving the PGNCS measured velocity changes (accelerations) onto body or AGS axes and summing (integrating) them for comparison with the integrated outputs of the AGS accelerometers. This process will suffer errors due to angular motions because the PGNCS gimbal angle measurements, used for the resolution, are only available once per second. Furthermore, there are errors due to gimbal misalignments and gimbal angle readout granularity. Nonetheless, this type of comparison during the docked burn (which was long and had the minimum amount of angular motion) indicated well under 100 μg accelerometer bias shift relative to the free flight values. This is well within required performance levels. The accelerometer performance estimates during the burns are given in Section 4.

|

2. ANALYSIS METHODS

2.1 DATA SOURCES

There are two possible sources of data for comparison with AGS data; namely,

- a) PGNCS acceleration and angle data.
- b) Radar tracking data.

The data that has been used to measure AGS performance during the flight is the PGNCS data. The reasons for this are:

- a) PGNCS, like AGS, is an inertial measurement unit and thus senses the same quantities, that is, accelerations, or velocity changes, and angular rotations.
- b) PGNCS accuracy is high relative to the required AGS performance levels.
- c) Radar data does not measure LM attitude.
- d) Radar velocity data, while very accurate when appropriately smoothed, does not provide as high a measurement accuracy of velocity transients as PGNCS.
- e) Radar data, unlike PGNCS, would have to be corrected to eliminate gravity and geoidal effects.

The PGNCS data that are used in the postflight analysis consist of six quantities: three measured velocities and the three gimbal angles. The velocities each represent the accumulation of inertial velocity during a two second interval along an inertial platform axis. The gimbal, or Euler, angles are a measure of the orientation of the LM body axes relative to the PGNCS platform.

2.2 ANALYSIS PERFORMED

The three basic errors discussed in this report are: accelerometer bias, gyro bias (or drift), and direction cosine misalignment. Accelerometer errors are modeled as biases. During non-thrusting intervals this bias quantity does, in fact, represent the accelerometer static bias. During thrusting intervals this error (apparent bias) can be attributed to static bias, dynamic bias, accelerometer scale

factor, or accelerometer misalignment. These effects are generally inseparable.

Gyro errors are also modeled as fixed drifts. These apparent fixed drifts include dynamic errors, g sensitive errors, scale factor and misalignment errors. The effects of Y and Z gyro drifts will be observed in the velocity data across a burn as well as in the angular data. X gyro drift is unobservable in the velocity domain because the velocity change during the burn is along the X axis. Direction cosine misalignment is modeled as a constant angular error initialized at the beginning of each burn. Therefore, the direction cosine misalignment that is determined includes the initial AGS direction cosine alignment error and the system drift between the time of alignment and the start of the burn.

Table 2-1 shows the flight periods which were analyzed and which quantities were estimated in each period. Tables 2-2 and 2-3 summarize related flight events, analysis intervals, and vehicle dynamics.

2.3 ANALYSIS COMPUTATIONS

Three computer programs are used to process the AGS data. (See Reference 1). The AGS Edit Program (Figure 2-1, Block 1) is used to edit the telemetry data, merge and interpolate PGNCS gimbal angles with AGS data and compute quantities including body thrust acceleration (A_A), direction cosines from the gimbal angles (a_G), body turning rates from both AGS and gimbal angle data (ω_A, ω_G), and the integral of body rate differences $\int(\omega_A - \omega_G)$. This integral indicates the drift in each AGS gyro if no PGNCS drift error is present. Thus, gyro bias is computed from this data. Also, initial misalignment is computed by subtracting CDU angles from equivalent angles computed from the AGS direction cosine matrix at the initial time.

The AGS Error Analysis Program (EAP) (Figure 2-1), Block 3) computes the partial derivatives of thrust velocity and accumulated angular drift with respect to the modeled AGS errors. These partials multiplied by the calculated error coefficients of the modeled AGS errors (K_i)

Table 2-1. Flight Periods

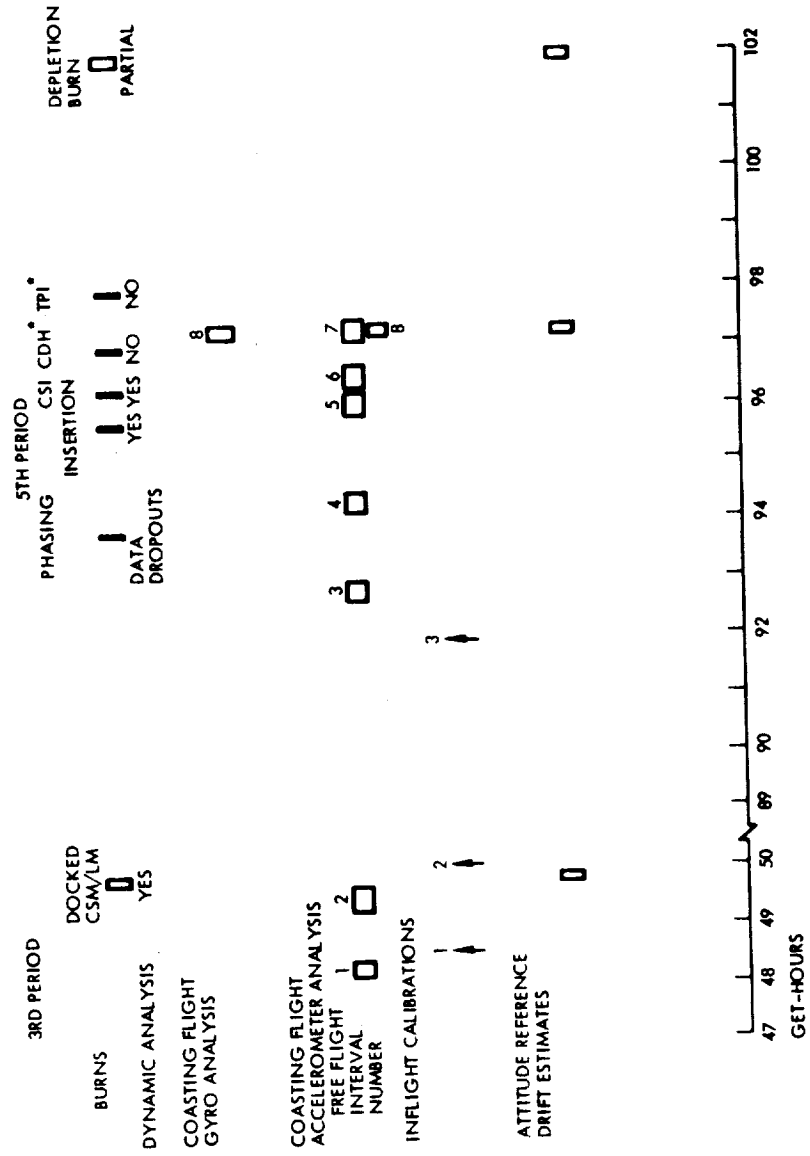
Flight Period	Time	Errors Estimated*		
		B _A	B _G	IM
IFC 1	48:30	-	-	-
Docked Burn	49:41:35	X, Y, Z	X, Y, Z	X, Y, Z
IFC 2	49:59:04	-	-	-
IFC 3	91:49:04	-	-	-
Insertion	95:39:08	-	-	-
CSI	96:16:04	-	-	-
Depletion	101:53:15	-	X, Y, Z**	X, Y, Z
Coast (1)	47:20:12	X, Y, Z***	-	-
(2)	49:17:1	X, Y, Z	-	-
(3)	92:35:49	X, Y, Z	-	-
(4)	94:06:51	X, Y, Z	-	-
(5)	95:44:1	X, Y, Z	-	-
(6)	96:17:19	X, Y, Z	-	-
(7)	97:03:12	X, Y, Z	-	-
(8)	97:08:0	X, Y, Z	X, Y, Z	X, Y, Z

* B_A, B_G, IM: accelerometer bias, gyro bias, initial misalignment

** Gimbal angle differences across the burn (Table 4-2).

*** Actual instrument biases

Table 2-2. Summary Time Line of Burns and Analysis Periods



* NO DATA AVAILABLE FOR CDH AND TPI BURNS

Table 2-3. Summary Time Line of Burns and Analysis Periods

BURN	ENGINE USED	GUIDANCE USED	DURATION(SEC)	SENSED ΔV_x (FT/SEC)	MAXIMUM THRUST ACCELERATION (FT/SEC ²)	LIMIT CYCLING			
						EXPECTED DYNAMICS		MEASURED DYNAMICS ⁽³⁾	
						PERIOD (SEC)	RATE P-P (DEG/SEC)	PERIOD (SEC)	RATE P-P (DEG/SEC)
DOCKED	DPS	PGNCS	369.7	1740	6	2-3 ⁽¹⁾	<0.009 ⁽¹⁾	YAW 2.9 ⁽⁴⁾ PITCH 2.4 ROLL 2.6	0.5 (CSM Rate -0.5) 0.5 (CSM Rate -0.3) 0.6 (CSM Rate -0.2)
PHASING	DPS	AGS	18.6	90.5	5.8	0.12-0.4 ⁽²⁾	.05 ⁽²⁾		
INSERTION	DPS	PGNCS	24.9	44.0	2	0.4 ^(1&2)	0.009 ^(1&2)	YAW 4.5 PITCH 5 ROLL 5	0.5 ⁽⁵⁾ 1.5 2.5
CSI	RCS	PGNCS	30.3	40.0	1.25	0.3-1 ⁽¹⁾	8 ⁽¹⁾		
CDH	APS	PGNCS	-----	-----	-----	0.3-1 ⁽²⁾	8 ⁽²⁾		
TPI	RCS	PGNCS	-----	-----	-----	0.3-1 ⁽¹⁾	8 ⁽¹⁾		
DEPLETION	APS	PGNCS	350	5375.0	12.0	0.3-1 ⁽¹⁾	8 ⁽¹⁾	YAW 1.8 PITCH 2.8 ROLL 2.8	2 10 10

(1) Data Source, GAEC/TRW Telecon

(2) Data Source, P&I Spec, Reference 6

(3) Data Source, NASA Report MSC-PA-R-69-2, "Apollo 9 Mission Report" Reference 4

(4) These oscillations appear during only about 20% of the burn, with greatest amplitudes near the end of auto throttling. They were superimposed upon continuous frequency oscillations with periods on the order of 50 sec and rates (P-P) of 0.2 deg/sec.

(5) These motions due to slosh were continuous throughout the insertion burn, and were evidently not considered in the expected dynamics quoted.

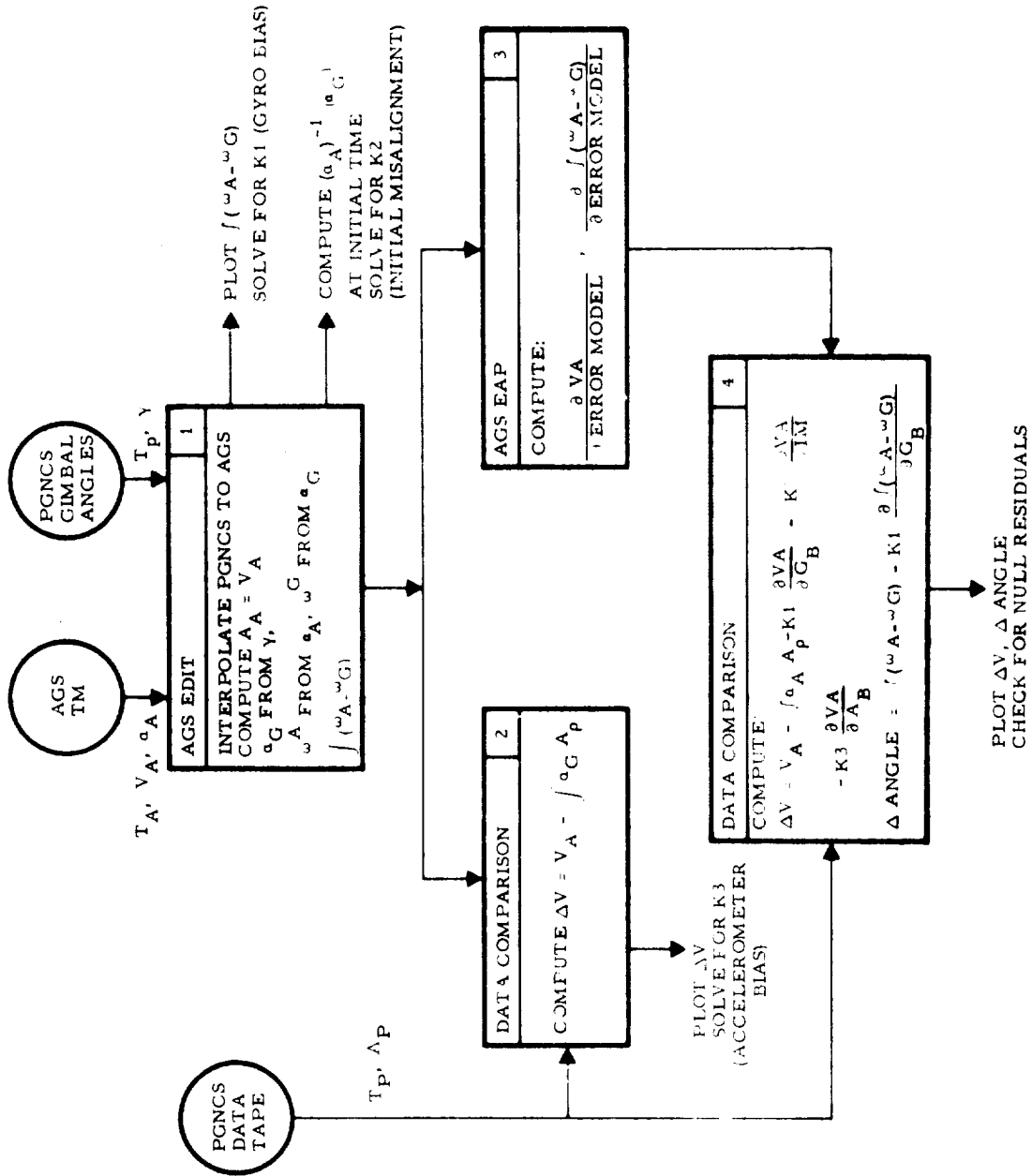


Figure 2-1. Postflight Analysis Block Diagram

Table 2-4. Key to Analysis Block Diagram (Figure 2-1)

T_A = AGS Time

T_P = PGNCS Time

V_A = AGS Body Thrust Accumulation

a_A = AGS Direction Cosines

γ = Gimbal Angles

A_A = AGS Body Thrust Acceleration

a_G = Direction Cosines from Gimbal Angles

ω_A = Body Rates from AGS

ω_G = Body Rates from Gimbal Angles

$\int(\omega_A - \omega_G)$ = Accumulated AGS Body Angular Difference

K_1 = Gyro Bias Coefficients

A_P = PGNCS Platform Thrust Acceleration

$V_A - \int a_G A_P$ = Velocity difference due to accelerometer errors

K_3 = Accelerometer Bias Coefficient

$K_1 \frac{\partial V_A}{\partial G_B} = K_1 \times \frac{\partial V_A}{\partial \text{Gyro Bias}} = \text{Velocity Difference due to } K_1 \text{ units of Gyro Bias.}$

$K_3 \frac{\partial V_A}{\partial A_B} = K_3 \times \frac{\partial V_A}{\partial \text{Accelerometer Bias}} = \text{Velocity difference due to } K_3 \text{ units of Accelerometer Bias}$

K_2 = Direction Cosines Misalignment Coefficient.

$K_2 \frac{\partial V_A}{\partial \text{IM}} = K_2 \times \frac{\partial V_A}{\partial \text{Misalignment}} = \text{Velocity Difference Due to Direction Cosine Misalignment.}$

$V_A - \int a_A A_P - K_1 \frac{\partial V_A}{\partial G_B} - K_2 \frac{\partial V_A}{\partial \text{IM}} - K_3 \frac{\partial V_A}{\partial A_B} =$

= Velocity Difference Compensated for all errors.

$K_1 \frac{\partial \int(\omega_A - \omega_G)}{\partial G_B} = \text{Body Coordinate Angular Differences Due to Gyro Bias}$

$\int(\omega_A - \omega_G) - K_1 \frac{\partial \int(\omega_A - \omega_G)}{\partial G_B} = \text{Compensated body Coordinate Angular Difference.}$

represent the velocity and angular drift errors accounted for by these modeled errors. Hence, in Block 4 of Figure 2-1 the components of gyro bias ($K1 \partial V_A / \partial G_B$), initial misalignment ($K2 \partial V_A / \partial IM$) and accelerometer bias ($K3 \partial V_A / \partial A_B$) are subtracted from the AGS minus PGNCS velocity residuals in order to check how much residual error is unaccounted for by the modeled errors.

The AGS Data Comparison Program computes AGS/PGNCS thrust velocity and angular differences in body coordinates. When PGNCS accelerometer data is transformed through gimbal measured transformation (α_G) no AGS or PGNCS gyro error is involved because the gimbals measure the orientation of the body axes relative to the PGNCS platform independent of any gyro drift. Thus, the velocity residual is only due to accelerometer differences (Block 2). Accelerometer biases are therefore computed from this data. When PGNCS accelerometer data is transformed through AGS direction cosines, AGS to PGNCS misalignment errors are present in the velocity residuals. By removing the calculated gyro drift, initial misalignment and accelerometer errors (Block 4) the velocity residuals should be nulled. Likewise, the angle residuals, $\int(\omega_A - \omega_G)$, are compensated for the calculated gyro drift and initial misalignment. They too should be nulled. This process should complete the fitting. Recycling through the process can be done if misfit residuals are seen, but this was not required in the present analyses.

The above analysis depends upon being able to integrate acceleration and body rates across the analysis interval. However, this was not possible during the depletion burn (see Section 4), because of large angular acceleration and rates. However, it is possible to solve for the initial misalignment and alignment after the burn. The changes in alignment across the burn is due to the accumulated AGS/PGNCS gyro drift. The magnitude of this change should bound the amount of AGS gyro drift, although the drift cannot be accurately resolved into AGS gyro coordinates.

2.4 ANALYSIS ACCURACY

The determination or estimation of the modeled sensor errors (accelerometer biases (B_A), gyro drifts (B_G) and inertial reference misalignments (IM) is subject to a number of errors. These include errors caused by the following effects.

- Data readout quantization
- PGNCS errors
- AEA Computational Errors
- PGNCS/AGS sample time differences
- Oscillatory angular LM motion

These are discussed below.

2.4.1 Quantization

There are two quantizations that have a significant effect on the analysis. The AGS body axis velocity outputs (V_{dx} , V_{dy} , V_{dz}) are quantized at 0.25 ft/sec. These are the basic AGS quantities used in estimating accelerometer biases. The effect of this is to introduce an uncertainty into the biases that is equal to the quantization divided by the time interval over which the biases are estimated. This amounts to $\pm 10 \mu g$ over the docked burn.

The PGNCS gimbal angle CDU readouts are quantized at $40 \widehat{\text{sec}}$. These are the source of the PGNCS angular measurements and are thus responsible for uncertainties of $\pm 20 \widehat{\text{sec}}$ in the estimates of IM and in errors of $\pm \frac{20}{t} \widehat{\text{sec}}$ in the estimate of gyro bias, B_G , where t is the analysis time interval in seconds.

In the docked DPS burn and APS burn to depletion the quantization errors were small compared to other errors. In all other (short) burns however, the data quantization error alone prohibited resolution of the sensor errors.

2.4.2 PGNCS Errors

In general the PGNCS errors are very small relative to the AGS accuracy. The particular PGNCS on this flight did have an out-of-tolerance X-gyro mass unbalance drift of slightly over 0.75 deg/hr per g

just prior to launch, (reference 4). This would affect the B_G estimate over the docked burn by about 0.14 deg/hr and, of course, if this condition had increased during the flight the effect would be greater.

2.4.3 PGNCS/AGS Sample Time Differences and Oscillatory Angular Motion

Both PGNCS and AGS data are telemetered at a rate of one sample per second. This sampling frequency limitation results in uncertainties, particularly during periods of transient or high frequency motion. The most significant effect is not only that the sample frequency is low, but that the AGS data and PGNCS data are valid at different time points within the one second sample cycle.

Thus if the outputs are changing, it is not possible to get PGNCS and AGS data that represent the same LM state. In the analysis, linear interpolation was used to adjust AGS and PGNCS data to a common time. This method of interpolation introduces errors if the LM angular rates are not constant over the interpolation interval.

Oscillatory motion also introduces commutativity errors in resolving the inertial drift angle data into body (sensor) coordinates and inertial velocities into body coordinates.

In the primary analysis interval (the docked DPS burn), for this report, the observed vehicle angular motions were relatively mild; a limit cycle was observed (see Table 2-3) with approximately 50 second period, 0.2 deg/sec rate, plus occasional sloshing motion with a period of approximately 2.5 seconds and p/p rates up to .5 deg/sec.

A limit on the measurement errors introduced by sample time differences and oscillatory motion in the docked DPS burn is estimated as 0.2 deg/hr gyro drift uncertainty and 25 μ g accelerometer bias uncertainty.

The APS depletion burns had much more severe limit cycling periods of 2-3 seconds with rates to 10 deg/sec pp.

The sampling problem is severe and processed data was extremely noisy. It is estimated that the processing errors exceed 1.0 deg/hr and the results are not useful.

In general it appears that long LM descent engine burns (200 seconds) will give useful sensor analysis results, using the methods herein, but that ascent engine burns may not, because of characteristically high rate, high frequency limit cycles.

Other effects of oscillatory motion are tangential and centripetal accelerations which corrupt the AGS accelerometer bias estimates, and, in coasting flight, gyro rectification errors which degrade attempts to determine the fixed drift.

The combined oscillatory, vibratory motion during the free flight analysis interval (staged) is estimated as contributing $0.1^\circ/\text{hr}$ uncertainty to the gyro fixed drift determination (from reference 2).

The combined oscillatory/vibratory motion error contribution to free flight determination of accelerometer bias is approximately $(10 \oplus \frac{100}{T}) \mu\text{g}$, where T is the analysis measurement interval in minutes and \oplus signifies a root sum square. This error is based on the In Flight Calibration measurement error of reference 2.

2.4.4 AEA Computational Errors

In addition to quantization the primary AGS data from which these analyses are made contains some AEA computational error unrelated to sensor error.

The AEA computational error in the attitude reference (direction cosine) data, due to truncation, roundoff and algorithm errors can be as large as $14^\circ/\text{hr}$ according to reference 2.

The only other significant AEA errors are those which appear in the inertial velocity and velocity to be gained magnitudes. In the present analysis these errors were such as to prohibit the use of this data for sensor error determination. This velocity error, in feet per second, is bounded by a quantization error of $.1 t$ (where t is the burn duration in seconds), but is generally much smaller. A more detailed discussion of this error is contained in Appendix IV.

From consideration of all the error sources discussed, as well as consideration of the repeatability of results and the noise on processed data, the uncertainties of all results of this analysis were estimated and are presented in Table 2-5.

Table 2-5. Measurement Error Estimates

Period	Analysis Interval sec	Fixed Bias	Accelerometer μ g Total Error	Fixed Drift	Gyro $^{\circ}$ /hr Total Error	PGNCS/AGS Attitude Differences sec
Free Flight						
Periods 1 thru 7	*	10				
Period 8	600	21		.12		63
Docked DPS	370		27		.27	63
Phasing	18					
Insertion	25		150		0.6 $^{\circ}$ /hr	
CSI	30					
Depletion	350		100		1.0	63
Gyro IFC				.3		
Mean of Two Gyro IFC's				.21		

* Minimum interval = 1132 seconds

The only PGNCS error sources considered in these measurement error estimates are:

- 1) The gimbal angle data quantization
- 2) The reported X gyro mass unbalance shift (uncertainty).

|

3. SYSTEM PERFORMANCE

3.1 GENERAL

AGS performance was excellent in all respects. Velocity-to-be-gained computed by AGS and PGNCS agreed very closely on all burns, and the inflight calibration results were excellent. Gyro and accelerometer bias determinations were in good agreement with preflight values.

Although no AGS software problems were found as a result of the flight analysis, there were several AGS related anomalies during the flight. The majority of these are attributed to procedural problems and in one case to a LM system interface constraint not recognized prior to flight. These anomalies are discussed in the MSC Mission Report for Apollo 9.

The state vector initialization functions, (transfer of state vectors from PGNCS to AGS) for both LM and CSM states were repeatedly accomplished without problem. The AGS calculated state vectors (AGS navigation) behaved as anticipated during flight. They are not directly comparable to the PGNCS calculated state vectors because of AGS computational simplifications. These simplifications are designed to give relative LM/CSM navigational accuracy adequate for safe abort guidance, although they do not result in accurate calculation of absolute position and velocity.

3.2 VELOCITY TO BE GAINED RESIDUAL COMPARISONS

The term "velocity residuals" may be used to denote many different quantities. The quantities of most interest from an AGS analysis standpoint are targeted vs actual velocities achieved at engine shutdown (cutoff velocity residuals); and the difference between PGNCS and AGS velocity-to-be-gained (V_g) at the end of a burn. The first of these is only of interest during an AGS-controlled burn; the second is of interest after any burn. With perfect control, the velocity to be gained at the end of a burn (V_g residual) would be zero in all components, at least for the guidance system controlling the burn. Furthermore, the differences between the AGS and PGNCS V_g 's at the end of a burn represent the differences between the velocities that would have been achieved with AGS in control and those

obtained with PGNCS in control. Thus, such a comparison will show the velocity error that would result (relative to PGNS) if AGS, rather than PGNCS, had performed the burn.

The V_g residuals alone do not allow a determination of specific sensor performance for a number of reasons. These include the following.

- 1) PGNCS and AGS V_g's are not available in the same coordinate system – PGNCS's inertial, AGE in body axes
- 2) PGNCS and AGS V_g readouts are not valid at the same time
- 3) DSKY and DEDA have different quantizations
- 4) AEA computed velocity errors due to Earth scaling (see Appendix IV)

What these differences in PGNCS and AGS V_g's effectively mean, relative to evaluating AGS performance, is that V_g comparisons do not provide enough information to calculate or estimate specific AGS sensor error parameters. The residual V_g comparisons do, however, very definitely show that the overall AGS performance during the burns was well within the accuracy required for it to have successfully guided the LM through the burns.

The V_g residuals for those burns with telemetry coverage are shown in Table 3-1.

Table 3-1. Velocity-to-be-Gained Residual Magnitudes

Burn Period	V _G Magnitude - FPS	
	AGS	PGNCS
Docked	5.5	4.24
Phasing	1.0	1.38
Insertion	1.0	0.70
CS1	1.5	1.18

3.3 GUIDANCE SOLUTION COMPARISONS

Guidance solutions, i. e., velocity to be gained, were computed prior to the CSI, CDH and TPI burns. The solutions are summarized in Table 3-2.

Table 3-2. Comparison of Guidance Solutions

Parameter	AGS	Ground Solution
<u>CSI</u>		
V_G (fps)	86	81*
<u>CDH</u>		
V_G (fps)	42	41.1
<u>TPI</u>		
V_G (fps)	21 to 26**	22.2
<u>TPI₀</u>		
V_G (fps)	20	20.1

*Solution computed using nominal (Operational Trajectory) states and Second Apsis ($S_{16} = 1$) targeting. Crew debriefing indicated that PGNCS solution was in agreement with AGS for second apsis targeting. Time did not permit retargeting AGS for first apsis.

**Solution varies due to measurement errors during radar data processing. Bit-by-bit simulation shows that reasonable measurement errors cause TPI V_g solution variations from 21 to 27 fps. The final TPI solution was not available since the LM went out of telemetry station range during radar processing.

For CDH, AGS calculated a V_G of 42 fps. The ground solution was 41.1 fps. The corresponding numbers for TPI_0 were 20 fps for the AGS and 20.1 fps for the ground solution. The TPI solution varied from 21 to 26 fps while radar updating was being performed, excluding those solutions obtained during the transient response of the radar filter. The final TPI solution was not available since telemetry coverage was lost prior to that time. The ground solution for this burn was 22.2 fps.

The range of values obtained during the radar updating of the TPI V_V (21 to 26 fps) is considered excellent. A bit-by-bit simulation of this calculation using the operational trajectory and having as the only radar measurement error a round-off of the range measurement to the nearest 0.5 nmi showed a variation of from 21 to 27 fps. The precision with which the range tape meter can be read is expected to be 0.5 nmi at these ranges.

3.4 PGNCS/AGS ALIGNMENT ACCURACY

The alignment of the AGS inertial attitude reference is accomplished by computing direction cosines from the CDU angles input to AGS from PGNCS. The CDU values are measurements of the three PGNCS IMU gimbal angles. This PGNCS to AGS alignment was successfully accomplished many times during the third and fifth periods. Eleven known AGS alignments were performed.

Table 3-3 summarizes the results of three alignments where data were available immediately after the alignment. The alignment transfer

Table 3-3. Alignment Update Accuracy

Alignment Update	CDU - AEA Angular Differences		
	X (degrees)	Y (degrees)	Z (degrees)
91:49:35	0.0	0.02	-0.003
93:40	0.005	0.002	0.02
94:50	0.04	0.02	0.01

accuracy is seen to be within the specification accuracy of 0.067 degree (4 arc minutes).

An alignment attempt apparently out of sequence occurred early in the fifth period and PGNCS/AGS alignment was not accomplished.

3.5 IN-FLIGHT CALIBRATION (IFC) AND SENSOR INFLIGHT BIAS PERFORMANCE

A total of three in-flight calibrations (IFC's) were performed, two during the third period of activities and one during the fifth period. IFC's of both gyros and accelerometers indicated shifts that were well within the 3σ estimates of expected shifts.

3.5.1 Gyro Calibrations

The gyro bias measurements, as obtained from the IFC's are given in Table 3-4. Included are the final pre-installation calibration (PIC) values (which were the flight compensation values) and the final earth prelaunch calibration (EPC) values.

Table 3-5 shows shifts between the final PIC and the first IFC, the final EPC and the first IFC, and between successive IFC's. Also included in the table are 3σ estimates of expected shifts between EPC/IFC and IFC/IFC as given in reference 7. These expected bounds were derived from ensemble behavior, measurement error and environmental errors by the methods given in reference 1.

Table 3-4. Gyro Bias Measurements, IFC Results

Channel	Final PIC (1/10/69)	Final EPC (2/16)	Equivalent Bias Compensated		
			IFC #1 (3/5-48:00 get)	IFC #2 (3/5-50:00 get)	IFC #3 (3/7-91:30 get)
X (deg/hr)	-0.27	-0.33	-0.21	-0.07	-0.19
Y (deg/hr)	-0.47	-0.56	-0.36	-0.28	-0.13
Z (deg/hr)	-0.06	+0.16	+0.20	0.00	+0.01

Table 3-5. Gyro Bias Shifts

Channel	Gyro Bias Shifts (Deg/Hr)			
	(IFC #1) - (Final PIC)	(IFC #1) - (Final EPC)	(IFC #2) - (IFC #1)	(IFC #3) - (IFC #2)
X	+0.06	+0.12	+0.14	-0.12
Y	+0.11	+0.20	+0.08	+0.15
Z	+0.26	+0.04	-0.20	+0.01
RMS	0.17	0.14	0.13	
3 σ estimates of allowable shifts	--	± 0.88	± 0.60	

Of the 0.6^o/hr allowable shift, 0.42^o/hr was estimated for IFC measurement errors (3 σ). The total repeatability is considerably better than this, which is interpreted as confirmation of the existing IFC measurement error estimates, with the possibility that performance is somewhat better than estimated.

It is considered a milestone in AGS testing that the adequacy of the gyro In-Flight Calibration scheme has been demonstrated. Furthermore, the IFC results were the prime means of verifying AGS integrity when a question was raised by an (erroneous) indication of failure by the Caution and Warning Indicator.

3.5.2 Accelerometer Calibration

The accelerometer bias measurements obtained from the IFC's are given in Table 3-6. The final PIC accelerometer bias values and Flight Program Three tape compensated biases are also included in the table. The compensation values differ from the PIC values only because of the 95 μ g accelerometer bias compensation quantization in FP 3.

Table 3-6. Accelerometer Bias Measurements, IFC Results

Channel	Last PIC	Bias Compensated by FP3 Tape	DEDA Indicated Bias Compensation		
			IFC #1	IFC #2	IFC #3
X (μg)	124	95	0	0	0
Y (μg)	45	0	0	0	0
Z (μg)	185	190	380	380	380

IFC results were not read out within range of telemetry coverage, and were therefore recorded only to the quantization level of the DEDA readout, 380 μg , rather than the AEA quantization level of 95 μg . The DEDA readouts (presented in Table 3-6) are too coarse to confirm the inflight bias values or the expected calibration accuracy, i. e., 185 μg 3σ , shift between successive IFC's (from reference 7). However, the IFC accuracy was demonstrated by free flight data analysis. Accelerometer biases after IFC were determined from free flight velocity data and are presented in Table 4-7 of the sensor analysis section. This shows the calibration compensation accuracy to be within the 95 μg quantization level.

3.6 AGS STEERING

During the DPS phasing burn, the AGS guidance commands were satisfactory. The engine cutoff signal was generated at the proper time and the vehicle was steered in the proper direction as indicated by the velocity increments along each axis. Steering commands were normal, and the thrust vector orientation was maintained within acceptable limits.

Control transients occurred at thrust initiation and at each change of thrust level (throttling changes), apparently because of the c. g. offset, thrust vector misalignment, and engine mount compliance. However, these transients were of short duration and the resulting attitude errors and attitude rates did not exceed 0.8 degree and 2.0 deg/sec (P-P) respectively. For the remaining portions of the burn period, the vehicle attitude was reflecting a low frequency (2-4 sec period) limit cycle with maximum P-P rates less than 1.0 deg/sec. Attitude excursions occasionally exceeded the deadband as expected with control by both RCS jet firing and engine gimbaling.

4. SENSOR PERFORMANCE ANALYSIS

This section describes the analyses performed in order to evaluate the AGS sensor performance during the flight. The general procedures used are as described in Section 2.0.

The AGS sensor performance was studied carefully over the Docked burn and again over an interval of free flight between the CDH and TPI burns. A study was also made of the Depletion burn but the sampling and limit cycling problems discussed in Section 2 precluded a quantitative sensor analysis. Velocity comparisons with the PGNCS system were taken over the Insertion and CSI burns, the only other burn periods with adequate telemetry coverage.

Table 4-1 summarizes the accumulated thrust velocity error (relative to PGNCS) at the end point of the burns. With the exception of the Docked burn Y and Z velocities these comparisons are all within the 0.25 ft/sec AGS velocity quantization. Furthermore, since the Docked burn was a rather large velocity gain along the X axis, the Y and Z velocity comparisons are subject to uncertainties due to the imperfect inertial to body axis resolution resulting from the once per second gimbal angle sampling.

Table 4-1. Final AGS Thrust Velocity Residual (ft/sec)

	$\Delta\dot{X}$	$\Delta\dot{Y}$	$\Delta\dot{Z}$
Docked Burn	0.15	-2.39	-1.97
Insertion Burn	0	-0.15	-0.05
CSI Burn	0	-0.1	0

End point velocity errors have an uncertainty of 0.25 ft/sec quantization uncertainty.

Attitude differences were analyzed and comparisons made in body gyro coordinates for the docked burn and for one free flight interval. These comparisons yield drift rates which can be interpreted as individual gyro drifts. Inertial attitude differences were also taken at the beginning and end of each interval. The changes observed in inertial attitude (see Table 4-2) are comparable to the changes in body attitude in both cases.

The changes in inertial attitude during the depletion burn were also checked and were comparable with those observed over the docked burn.

Table 4-2. AGS/PGNCS Attitude Differences

Interval	(Arc Seconds)											
	Body Gyro Drift Over Interval			Inertial Attitude Difference (Start)			Inertial Attitude Difference (End)			Change in Inertial Attitude		
	Body X	Body Y	Body Z	PGNCS X	PGNCS Y	PGNCS Z	PGNCS X	PGNCS Y	PGNCS Z	PGNCS X	PGNCS Y	PGNCS Z
Docked Burn (400 sec)	-340	-72	-108	-140	174	-33	-410	279	-146	-270	105	-113
Free Flight Interval (600 sec)	18	-44	60	-360	-20	-80	-380	-200	-180	-20	-180	-100
Depletion Burn (400 sec)	*	*	*	-550	440	550	-860	540	750	-310	100	200
Uncertainty	Docked ± 108 sec Free Flight ± 72 sec			± 63 sec			± 63 sec			± 88 sec		

*Data could not be calculated.

4.1 DOCKED BURN ANALYSIS

4.1.1 Docked Burn Data

The docked burn consists of about 5.5 ft/sec^2 acceleration for about 300 seconds, (Figure 4-1). Most of the acceleration occurs along the X-body axis although small thrust velocity profiles along the other axes are shown in Figure 4-2. A distinctive 1 degree angular limit cycling with fifty second period and a higher frequency shock motion is seen about the X (outer gimbal) axis in Figures 4-3 and 4-6. The line plots in Figures 4-6 through 4-8 display the body rates as computed from the AGS direction cosine data while the point plots display those rates as computed from the PGNCS gimbal angles. The AGS time base on the plots is ground elapsed time in seconds less 40 hours, 0 min., 0.288 sec.

4.1.2 Docked Burn Accelerometer Analysis

AGS accelerometer static biases for comparison with biases calculated over the docked burn, were computed as the average rate of change of AGS thrust velocity over a 24 minute interval just prior to the docked burn. These biases are shown in column 2 of Table 4-3.

The components of AGS error which could significantly affect the apparent accelerometer biases during the docked burn include dynamic biases, X-accelerometer scale factor, Y- and Z- accelerometer misalignments towards X. Because of the nearly constant acceleration profile,

these errors are not separable. To observe these errors, the AGS velocity data must be compared with some independent source such as PGNCS. PGNCS thrust velocity data transformed to body coordinates is used for comparison with AGS accelerometer data. These data contain all of the PGNCS accelerometer errors as well as AGS errors. The transformation from PGNCS to AGS was made using the PGNCS gimbal angles. Since the gimbals are fixed to the platform and the body, no gyro drift error is introduced into the comparison, but gimbal angles have misalignment and quantization errors which do affect the comparison.

To obtain estimates of bias errors, the transformed PGNCS data were subtracted from the AGS data. These comparisons are shown as the point plots (points not connected) in Figures 4-9 through 4-11. For the Y and Z comparisons, it was straightforward to fit a straight line to the velocity residuals and compute its slope as the bias. The effect of the Y-accelerometer bias (B_Y^A) at the end of the burn is shown in Figure 4-10, and the effect of the representative Z-accelerometer bias (B_Z^A) at the end of the burn is shown in Figure 4-11. These docked-burn-biases are given in the second column of Table 4-3. The apparent level shift of 0.25 ft/sec in the X velocity residuals (Figure 4-9) is due to a PGNCS data dropout and automatic fill-in by the PGNCS Data Processor program. The fill-in was computed over a 4 second interval of changing acceleration using linear interpolation. No identifiable X-accelerometer error was observed other than the jump due to processing.

Table 4-3. Docked Burn

Estimated Representative Accelerometer Biases (μG) and Uncertainties		
Axis	Bias During Free Flight	Bias During Docked Burn
X-Accelerometer	+27 \pm 10	0 \pm 27
Y-Accelerometer	-43 \pm 10	-131 \pm 27
Z-Accelerometer	-54 \pm 10	-16 \pm 27

The fourth column of Table 4-3 gives the docked burn representative bias minus the free flight measured bias. These accelerometer bias values represent the combined effects of AGS accelerometer dynamic bias, AGS accelerometer scale factor error, AGS accelerometer misalignment, PGNCS gimbal angle transformation error, and the total PGNCS accelerometer error.

4.1.3 Docked Burn Gyro Analysis

During the docked burn, AGS gyro shifts relative to the PGNCS gyros were computed by fitting straight lines to the integrated body rate differences (Figures 4-12 through 4-14). Apparent jumps in the data are due to numerical integration of numerically differentiated and interpolated data. Numerical integration turns the resulting wild points into level shifts of the residuals. This is purely a postflight data processing problem. Since the integration starts at zero, initial misalignments cannot be computed this way. However, they can be computed by differencing initial gimbal angles with equivalent angles computed from the AGS direction cosines. The gyro biases were computed over intervals in which no jumps occurred. The results are listed in column 2 of Table 4-4.

As in the case of the accelerometers, observed gyro drift during the burn is the resultant of several inseparable error sources. Principal error sources include AGS static and dynamic gyro biases, AGS X-gyro spin axis mass unbalance, and combined PGNCS gyro bias and g-dependent drifts.

4.1.4 Direction Cosine Misalignment

The line plots in Figures 4-9 through 4-11 show the AGS/PGNCS velocity residuals with the PGNCS thrust velocities transformed to body coordinates using the AGS direction cosines. These residuals are the resultant of AGS and PGNCS accelerometer errors (described in the above paragraph), the gyro errors, and direction cosine misalignments at the beginning of the burn.

The direction cosine misalignments of the AGS to the PGNCS include AGS/PGNCS alignment computational errors, quantization of the gimbal

Table 4-4. Docked Burn Estimated Gyro and Misalignment Errors

Error Source	Error Coefficient	Corresponding Velocity Error	Corresponding Angle Error
X-Gyro Bias *	$-.85^{\circ}/\text{hr} \pm .27^{\circ}/\text{hr}$	---	-330 sec
Y-Gyro Bias *	$.18^{\circ}/\text{hr} \pm .27^{\circ}/\text{hr}$	$-.3\text{ft}/\text{sec}(\dot{Z})$	70 sec
Z-Gyro Bias *	$-.27^{\circ}/\text{hr} \pm .27^{\circ}/\text{hr}$	$-.46\text{ft}/\text{sec}(\dot{Y})$	-105 sec
Initial Misalignment About X**	$-140 \text{ sec} \pm 63 \text{ sec}$	---	-140 sec
Initial Misalignment About Y**	$174 \text{ sec} \pm 63 \text{ sec}$	$-1.47\text{ft}/\text{sec}(\dot{Z})$	174 sec
Initial Misalignment About Z**	$-33 \text{ sec} \pm 63 \text{ sec}$	$-.28\text{ft}/\text{sec}(\dot{Y})$	-33 sec

*Include static and dynamic bias, mass unbalance and PGNCS gyro drift.

**Include alignment computational error, gimbal quantization and drift since initialization.

angles, and accumulated AGS/PGNCS relative drift from alignment to burn. The direction cosine misalignment angles were determined by comparing angular measurements made by the two systems interpolated to the same time. These misalignments are presented in Table 4-4. The misalignment causes an error in the thrust velocity measured during the burn. The velocity errors caused by the estimated misalignments for the docked burns on this flight are shown in Figures 4-10 through 4-11.

The compensated thrust-velocity and integrated body-rate-difference residuals appear in Figures 4-15 through 4-20. Jumps were not removed during the compensation process.

4.2 LM AGS BURN TO DEPLETION ANALYSIS

The depletion burn presented the most severe dynamic conditions for AGS operations. However, large amplitude ($\pm 5 \text{ deg}/\text{sec}$) angular limit cycling occurred during the burn at rates comparable to the telemetry data sampling rate, invalidating most of the data reduction techniques. Gimbal angle limit cycling roughly once per three seconds was observed. Total,

end to end, inertial reference drift was determined across this burn. These components were shown in Table 4-2.

4.3 FREE FLIGHT INTERVAL DATA

A ten minute interval with continuous telemetry was chosen for free flight analysis, beginning about 97 hours 8 minutes GET. Thrust position data was plotted (Figure 4-21), and since no abrupt changes occurred to indicate thrusting, it was assumed that all measured velocity changes are errors due to the AGS. The time base in the plots is GET less 90 hours 0 minutes 54 seconds.

The gimbal angle plots, Figures 4-22 through 4-24, show relatively slow wideband limit cycling plus an orbital turning rate about the inner gimbal. The corresponding body rate data are given in Figures 4-25 through 4-27. The line plots represent body rates computed from the gimbal angles.

AGS-Gyro/PGNCS-gimbal-angle comparisons were made over this free flight interval. The body rates computed from the two systems (by differentiation) were differenced and the result integrated. As in the docked burn, these results suffered from some data processing jumps, particularly when the body rate is discontinuous at the turning points in the limit cycling. These data are presented in Figures 4-28 through 4-30. The results are given in Table 4-5.

Table 4-5. Free Flight AGS Gyro Biases
(Relative to PGNCS)

	Start Time (1)	Stop Time (1)	Delta Time	Representative Drift
X-Gyro	25700	26300	600	.03 ±0.12°/hr
Y-Gyro	25720	26300	580	-.14 ±0.12°/hr
Z-Gyro	25720 25980	25960 26190	240	.10 ±0.12°/hr

(1) AGS absolute time in seconds.

Accelerometer bias estimates were calculated over a number of free flight intervals. The first of these was just prior to the first in flight calibration and the last was the same interval analyzed for gyro drift. The results of these free flight accelerometer bias estimates are summarized in Table 4-6.

Table 4-6. Free Flight Accelerometer Biases

Interval Number	1*	2	3	4	5	6	7	8**
Start Time (HR:MIN:SEC)	47:20:12	49:17:1	92:35:49	94:6:51	95:44:1	96:17:19	97:3:12	97:8:0
Duration (min)	62	24	19	22	32	23	22	10
AGS Accelerometer Static Bias (μg)	Prior to IFC	→ Measurements After Initial IFC						
B_x^A	-149	26.8	13.7	11.5	8.1	11.2	11.4	-1
B_y^A	-41	-43.0	-41.1	-40.2	-44.6	-50.2	-45.5	-41
B_z^A	-41	-53.8	-82.2	-51.8	-65.0	-72.6	-56.9	-58
Measurement Error	± 10	± 10	± 10	± 10	± 10	± 10	± 10	± 21

Standard Deviation of Bias Repeatability after IFC. / Error Budget Repeatability Value is 20 μg

$$B_x^A = 6.6 \mu\text{g} \quad B_y^A = 3.6 \mu\text{g} \quad B_z^A = 11.9 \mu\text{g}$$

* Interval Number 1 is an interval before the first IFC. Between interval 1 and 2 an IFC was performed which changed the value of the X accelerometer bias compensation by 190 μg . If the IFC had been performed before interval 1 then the resulting uncompensated bias would be +41 μg .

** Interval Number 8 is contained in interval number 7. It is the interval of continuous telemetry used in the plots.

4.4 OTHER BURNS

Since the CDH and TPI burns were not covered by telemetry, no data are available for analysis. Telemetry signals were received during the phasing burn, but numerous dropouts in the PGNCS downlink data resulted in reconstructed PGNCS thrust velocity data of questionable value. As in all the short burns, the AGS and PGNCS errors do not propagate to a magnitude sufficient for detection.

The two burns which provided reliable telemetry data are discussed below.

4.4.1 Insertion Burn

The insertion burn lasted about 56 seconds during which the acceleration along the X body axis reached a maximum level of 2 ft/sec^2 . The sensed velocities at the end of the thrust period were

X	44.0	ft/sec
Y	0.75	ft/sec
Z	0.75	ft/sec

These values are quantized to 0.25 ft/sec. The AGS-PGNCS velocity differences are shown in Figures 4-31, 4-32, and 4-33. The magnitudes of the differences are within one AGS quantization interval.

4.4.2 CSI Burn

The velocities gained along AGS body axes were:

X	40	ft/sec
Y	0	ft/sec
Z	-1.25	ft/sec

The values were recorded from the AGS downlink telemetry data and are accurate to within a quanta, 0.25 ft/sec. The data span over which the acceleration was non-zero was approximately 52 seconds.

The velocities measured by the PGNCS (expressed in body coordinates) were equal to the AGS velocities, to within the accuracy stated.

This is shown by Figure 4-34, Figure 4-35, and Figure 4-36. It is evident that neither the length of the burn nor the magnitude of thrust acceleration (1.25 ft/sec/sec) are great enough to allow accurate detection of sensor errors. For example, an accelerometer bias of 150 μ g would be within the AGS downlink quantization.

4.5 COMPARISON OF SENSOR ANALYSIS RESULTS TO AGS ERROR MODELS

4.5.1 Qualification of Derived Errors

The low thrust short duration burns of LM 3 coupled with fairly high rate vehicle limit cycling and a low telemetry data rate, present a situation poorly suited to inertial instrument evaluation and parameter separation. Nevertheless the results do substantiate the existing performance error models to a considerable extent.

In comparing the derived errors to expected values it must be remembered that the values treated as AGS errors are relative errors, that is they include PGNCS errors, as well as measurement and processing errors. PGNCS errors were not removed because:

- 1) The PGNCS error estimates available (reference 5) are also relative errors, i. e., PGNCS compared to CSM guidance data
- 2) No PGNCS gyro drift data was available for the burn intervals analyzed.

4.5.2 Error Model Comparison

Tables 4-7, and 4-8 present the inflight error estimates in the form of the error model used in the AGS Capability Estimate.

Two comparison models are listed. The first is a preflight estimate for ASA 015. It is the ensemble capability estimate error model of reference 2, as modified by ASA 015 test data.* The second comparison model is the error budget (spec values) also from reference 2.

*Such a preflight estimate is contained in the ASA 015 error model as contained in reference 8. The model used here agrees except that the accelerometer stability terms have been updated to the latest (May 69) Capability Estimate for consistency.

Table 4-7. Accelerometer Errors (Powered Flight), μg

	Channel	ASA 015	ASA 015		Error Budget From
		Inflight Estimate	Preflight Estimate	Mean	Gaussian 3 σ
					Gaussian 3 σ
Accelerometer Bias and Nonlinearity (1)	X	+27 \pm 10	0	45	240
	Y	-43 \pm 10	0	121	240
	Z	-54 \pm 10	0	121	240
X-Scale Factor and Dynamic Errors (2)	X	-27 \pm 29	+13	53	105
Y and Z Dynamic Errors, ASA Accelerometer Internal Misalignment and ASA to IMU Mounting Points Misalignment (2)	Y	-88 \pm 29	+13	100	147
	Z	+38 \pm 29	-1	99	147
<hr/>					
Total (μg) (3)	X	0 \pm 27	+13	69	262
	Y	-131 \pm 27	+13	157	282
	Z	-16 \pm 27	-1	156	282

- Notes: (1) Inflight Estimate: From Free Flight Data
(2) Inflight Estimate: Difference between measured total error and measured fixed bias.
(3) Inflight Estimate: Derived from velocity comparisons.

Table 4-8. Gyro Errors (Powered Descent), deg/hr

	Channel	ASA 015	ASA 015		Error Budget From
		Inflight Estimate	Preflight Estimate		Capability Estimate
			Mean	Gaussian 3 σ	Gaussian 3 σ
Gyro Fixed Drift (1)	X	$-.14 \pm .21$	0	.52	.54
	Y	$-.32 \pm .25$	0	.53	.55
	Z	$+.10 \pm .21$	0	.53	.55
X-Gyro Dynamic Drift (2)	X		+ .02	.35	.63
			0	.11	.19
X-Gyro Spin Axis Mass Unbalance (2)	X				
Y and Z Gyro Dynamic Drift (2)	Y	$+.50 \pm .34$	-.21	.30	.62
	Z	$-.37 \pm .34$	+ .11	.30	.72
Total (deg/hr) (3)	X	$-.85 \pm .27$	+ .02	.64	.85
	Y	$+.18 \pm .27$	-.21	.61	.83
	Z	$-.27 \pm .27$	+ .11	.61	.91

Notes: (1) Inflight Estimate: Mean of IFC No. 1 and IFC No. 2

(2) Inflight Estimate: Difference between measured total error and measured fixed bias

(3) Inflight Estimate: Derived from attitude rate comparisons.

4. 5. 3 Initial Misalignment Error Comparisons

The AGS Direction Cosine Misalignments at the beginning of the Docked DPS burn (from Table 4-2) are compared to the capability estimate (Reference 2) in Table 4-9.

Table 4-9. AGS Direction Cosine Initial Misalignment Error

	Derived From Inflight Data	Capability Estimate
PGNS/AGS Computational Transfer Error		2.64 min = 155 $\widehat{\text{sec}}$
AGS Drift from Align to Burn*		.57t = 1260 $\widehat{\text{sec}}$
PGNS Drift from Align to Burn*		.1t = 216 $\widehat{\text{sec}}$
	<hr/>	
Total	X -140 $\pm 63 \widehat{\text{sec}}$	X 1287 $\widehat{\text{sec}}$
	Y 174 $\pm 63 \widehat{\text{sec}}$	Y 1287 $\widehat{\text{sec}}$
	Z -33 $\pm 63 \widehat{\text{sec}}$	Z 1287 $\widehat{\text{sec}}$

* 37 Minutes

4. 5. 4 Sensor Bias Stability Comparisons

In addition to the terms listed in Tables 4-7 through 4-9, this analysis yielded data on gyro and accelerometer long term stability and short term repeatability, which is compared here to capability estimates.

4.5.4.1 Accelerometer Bias Repeatability

From Table 4-6 the standard deviations of accelerometer biases over the flight interval were:

$$B_X^A = 6.6 \mu\text{g}$$

$$B_Y^A = 3.6 \mu\text{g}$$

$$B_Z^A = 11.9 \mu\text{g}$$

$$\text{RMS} = 8.1 \mu\text{g}$$

This compares well with the error budget value for accelerometer bias repeatability, which is 20 μg (3σ).

4.5.4.2 Accelerometer Time Stability

Accelerometer instrument biases were derived from the free flight data prior to the first IFC by determining the apparent bias from velocity data and adding the flight compensation value. The inflight bias values are compared to the preflight bias values measured in the BTME lab 54 days earlier in Table 4-10.

Table 4-10. Accelerometer Bias Stability

Channel	Last PIC	Inflight Prior to IFC No. 1	Bias Shift 54 Days
X μg	124 \pm 4	-54 \pm 10	-178 \pm 11
Y μg	45 \pm 4	-41 \pm 10	- 86 \pm 11
Z μg	185 \pm 4	116 \pm 10	- 69 \pm 11
3 σ Estimate of expected shifts from:		Capability Estimate ** Error Budget (Spec) **	168 594

* Time span of data: from 47:20:12 to 48:22:39 - a total time of 62 min 27 sec. Data uncertainty is estimated to be 10 μg .

** From Reference 2, AGS Capability Estimate.

The X accelerometer bias shift was greater than the latest revision of the capability estimate which decreased the estimate of the bias shift from 300 μg to 168 μg (3). The bias shift of 178 μg was however within the error budget value of 594 μg .

A long time period (62 minutes) was used to determine the bias value and various subsets within the time period gave nearly identical bias values. Venting or a residual thrust from either the CSM or LM could have contributed to the shift observed, however a check of PGNCs accelerometer results has indicated no residual thrusting.

Inasmuch as the capability estimate represents an a priori estimate of flight performance, this measurement is the first flight data actually used to compare with preflight estimates. Thus this bias shift should be considered in future revisions of the Capability Estimate.

From the mission viewpoint, it is concluded that this shift (even in the absence of subsequent accelerometer IFC's) would not prevent mission objectives from being achieved. Later free flight data from the X accelerometer indicated a stable instrument with excellent repeatability.

4.5.4.3 Gyro Bias Repeatability

It was shown in Table 3-4 that the gyro inflight bias repeatability was considerably better than precomputed limits based on IFC measurement error and bias non-repeatability.

4.5.4.4 Gyro Bias Time Stability

From Table 3-4 the maximum gyro shift from Earth Prelaunch Calibration (EPC) to IFC was 0.20^o/hr. The Capability Estimate is 0.54^o/hr.

4.5.5 Unmodeled Errors

Gyro scale factor and misalignment errors were verified by satisfactory navigation results, but they were not recoverable from this analysis because of inadequate data during a large turning maneuver.

Those accelerometer scale factors and misalignments which are not listed in Table 4-7, have no significant effect on the velocity errors.

4.5.6 PGNCS Error Contributions

The inflight error estimates contain PGNCS as well as AGS errors. In most cases this can be neglected as the combined error is very reasonable. However in the case of the Y accelerometer bias error during powered flight, the $-131 \mu\text{g}$ error in Table 4-9 appears rather large compared to the preflight estimates. The PGNCS Y accelerometer bias estimate from reference 7 of $44 \mu\text{g}$ can account for a significant part of the error, and the residual ($-87 \mu\text{g}$) is very reasonable.

The other parameter in the error models that is rather large compared to budgets is the X gyro drift in powered flight. No estimate of the PGNCS gyro drift during this burn is available for comparison.

4.6 SENSOR ERROR ANALYSIS CONCLUSIONS

The estimates of the sensor errors that were derived from the flight data are all essentially within the ranges expected based on the AGS capability estimate, and are all within the AGS error budget (spec.) The limitations of the available data and the resultant uncertainties in the estimated sensor errors, together with the fact that no gross errors were observed, prevent any detailed analysis of individual error effects. The general conclusion is that ASA 015 performed with high accuracy that was within the error budget and was consistent with its expected performance.

The largest single error, relative to the capability estimate, was the estimate of X gyro drift during the Docked DPS burn, the only burn over which gyro drift could be estimated. This was at a value just over the 3σ capability estimate for this drift and just within the error budget. This effect is most likely due to one, or some combination, of the following:

- 1) Errors inherent in the measurement and data processing
- 2) Larger than expected AGS dynamic gyro drifts, possibly indicating vehicular angular motions more severe than expected. Such motions, e. g., navigation base coning, are not directly measureable on this mission.

Additional data and further analysis would be needed to establish the specific contributing causes. The effect was not, however, large enough to cause any loss of confidence in the performance capability of AGS.

The flight performance has demonstrated that AGS is capable of successfully performing the role of back-up guidance for LM.

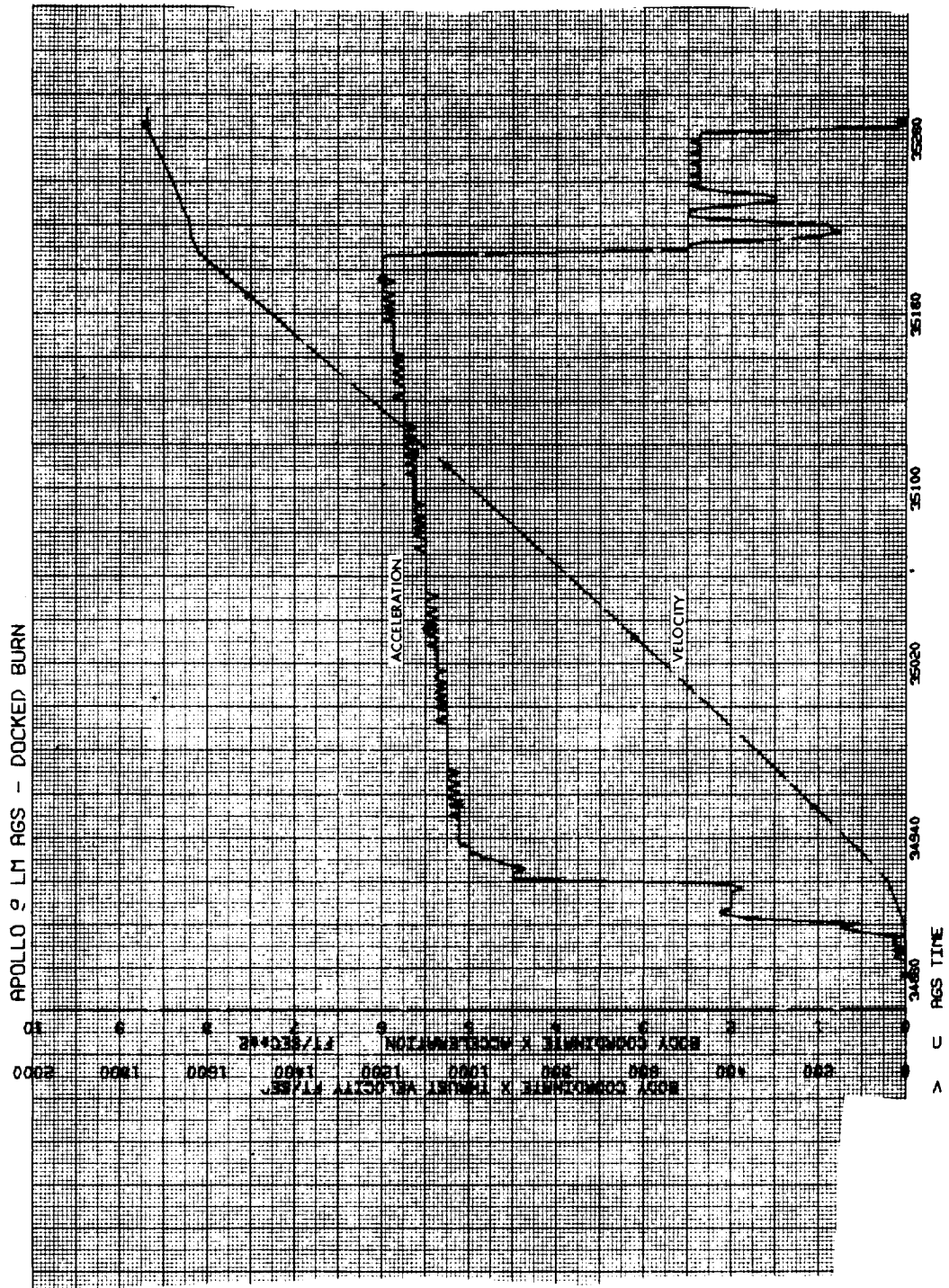


Figure 4-1. X Body Coordinate Thrust Measurements

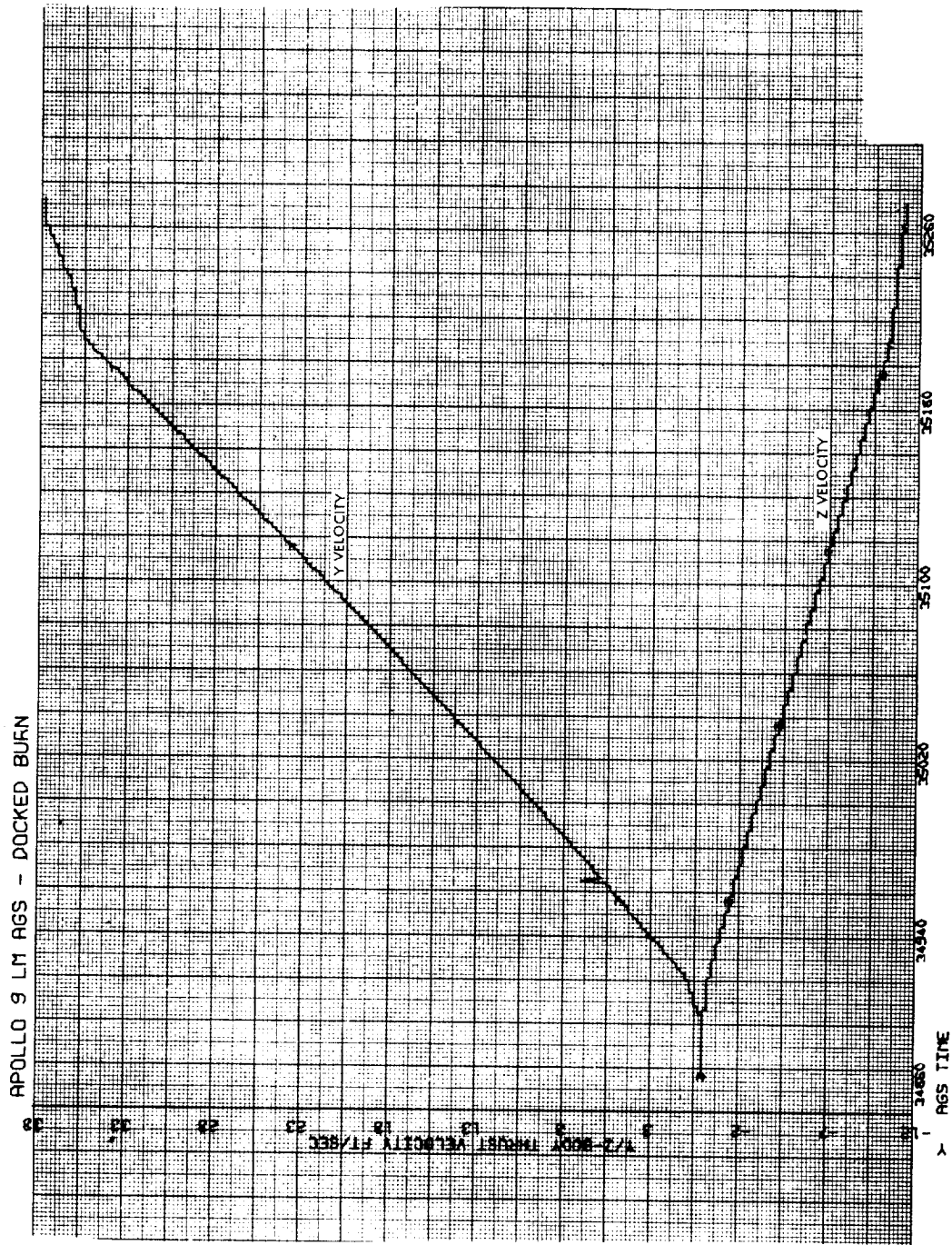


Figure 4-2. Y/Z Body Thrust Velocity

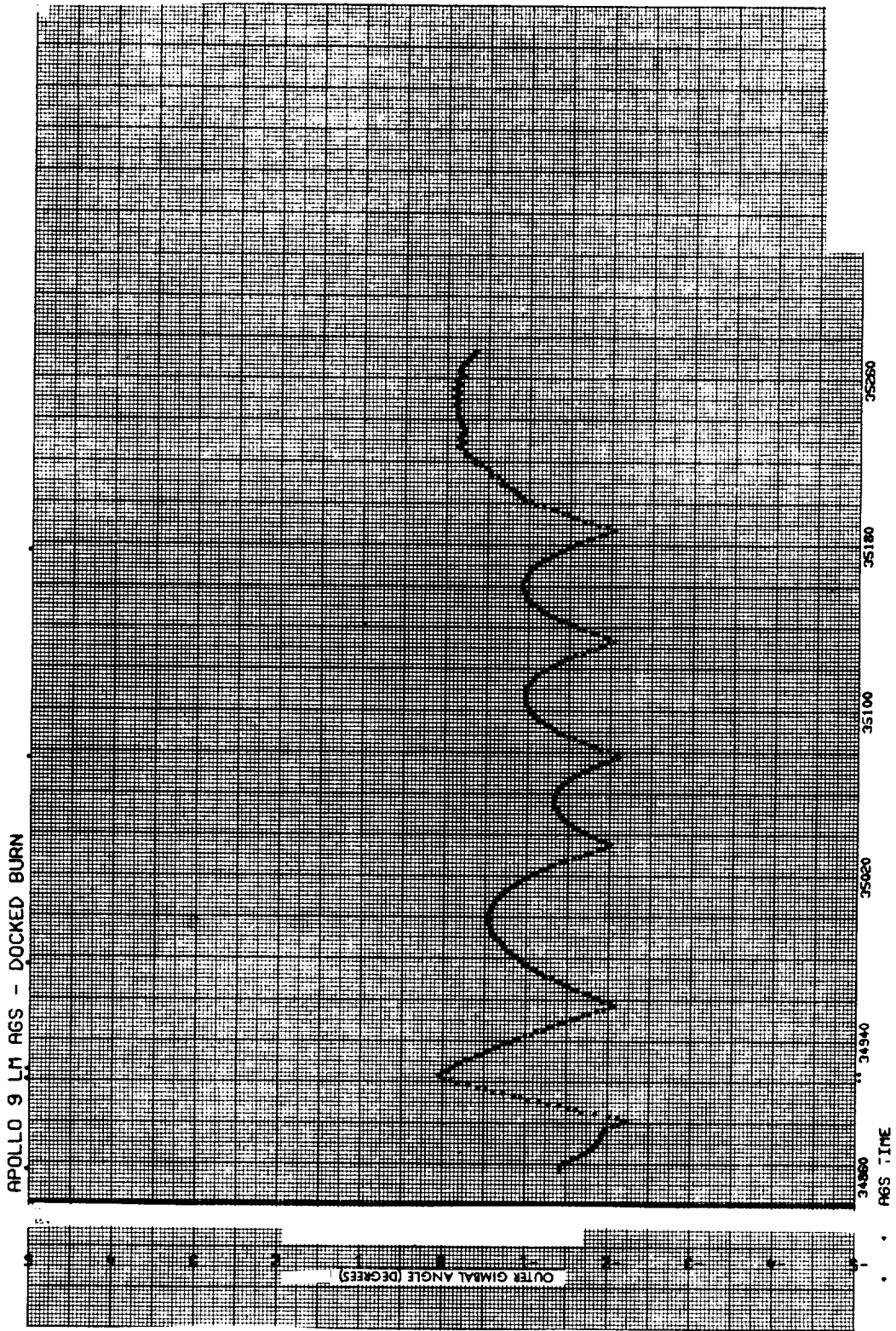


Figure 4-3. Outer Gimbal Angle

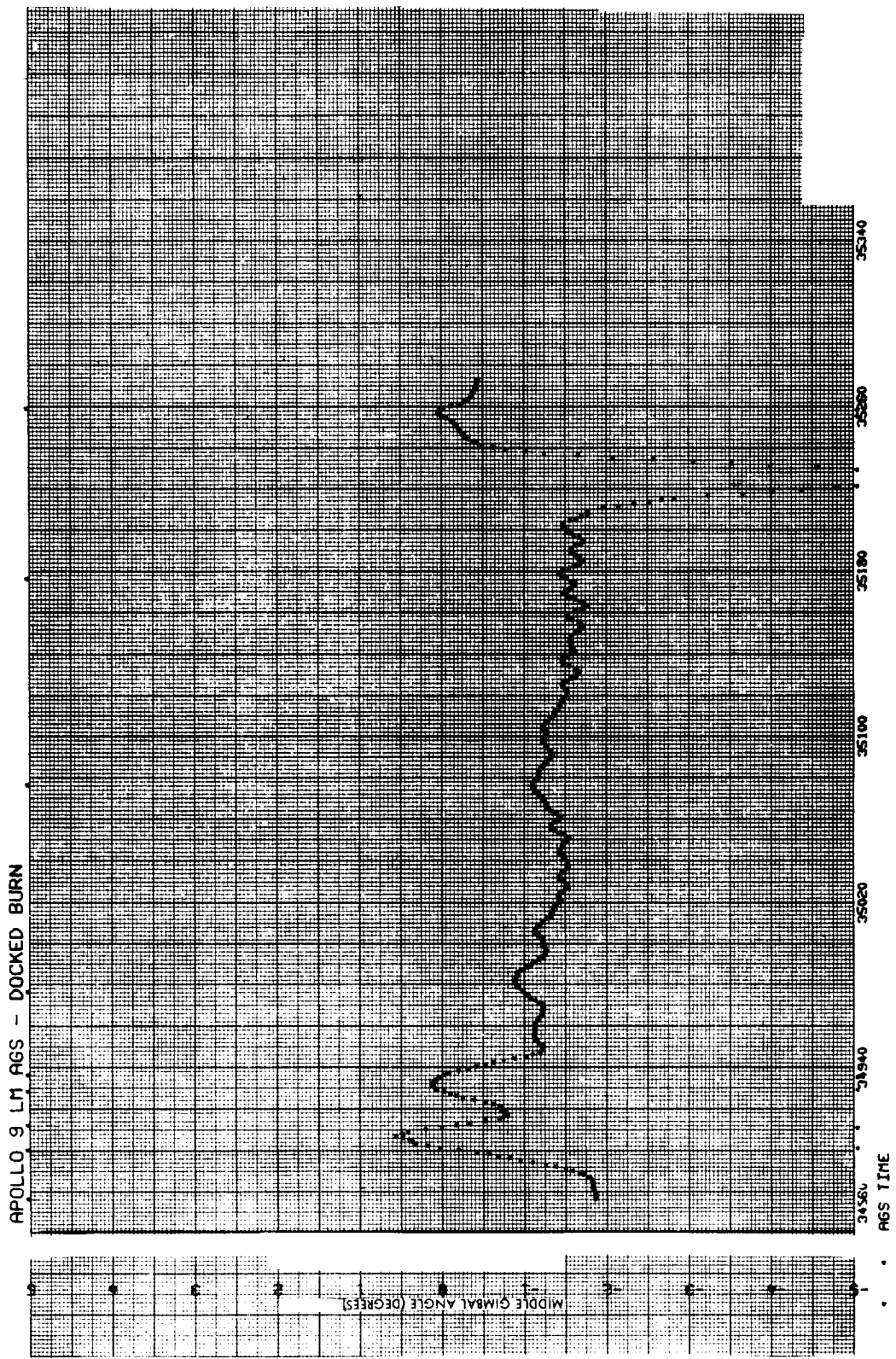


Figure 4-4. Middle Gimbal Angle

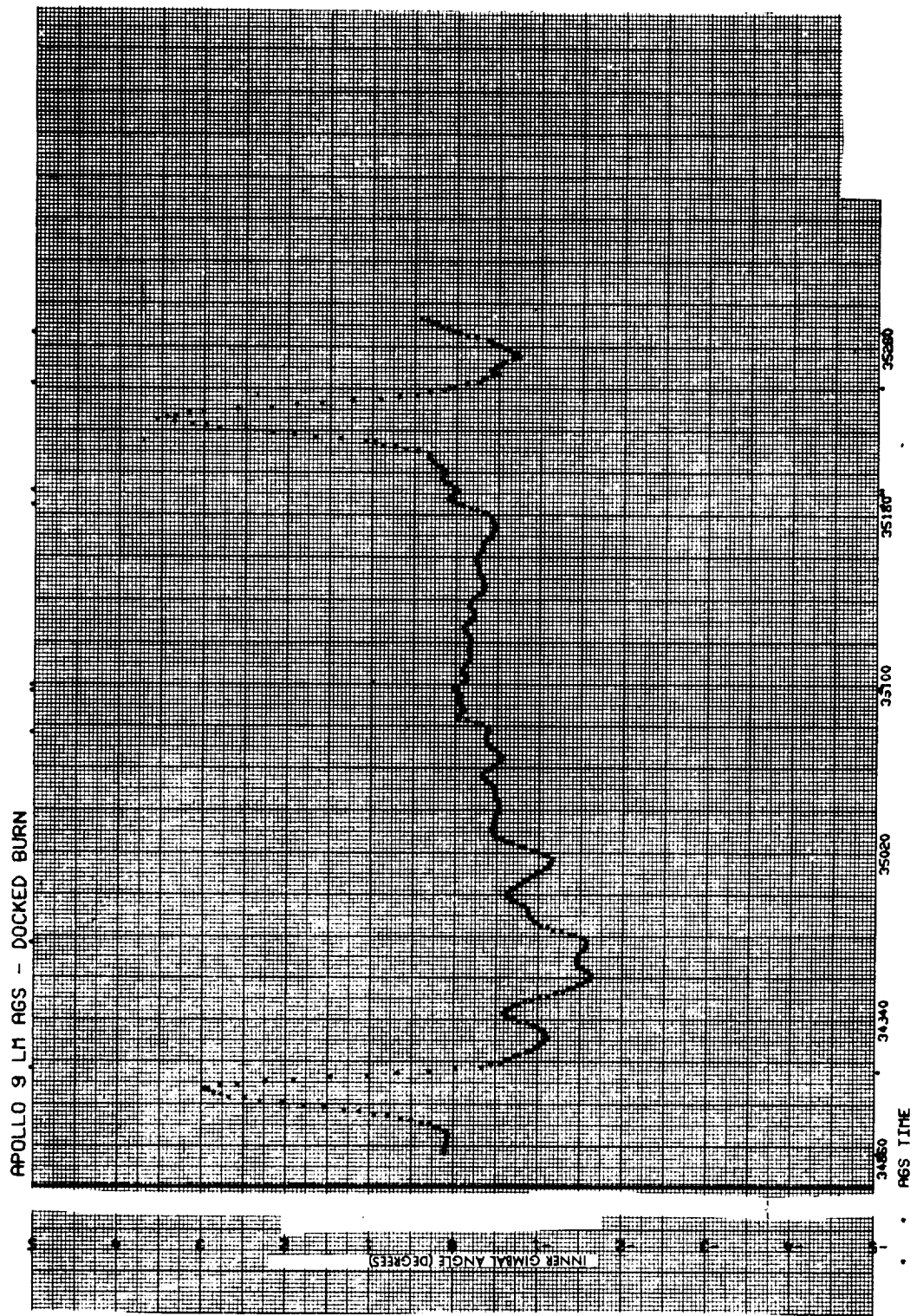


Figure 4-5. Inner Gimbal Angle

APOLLO 9 LM AGS - DOCKED BURN

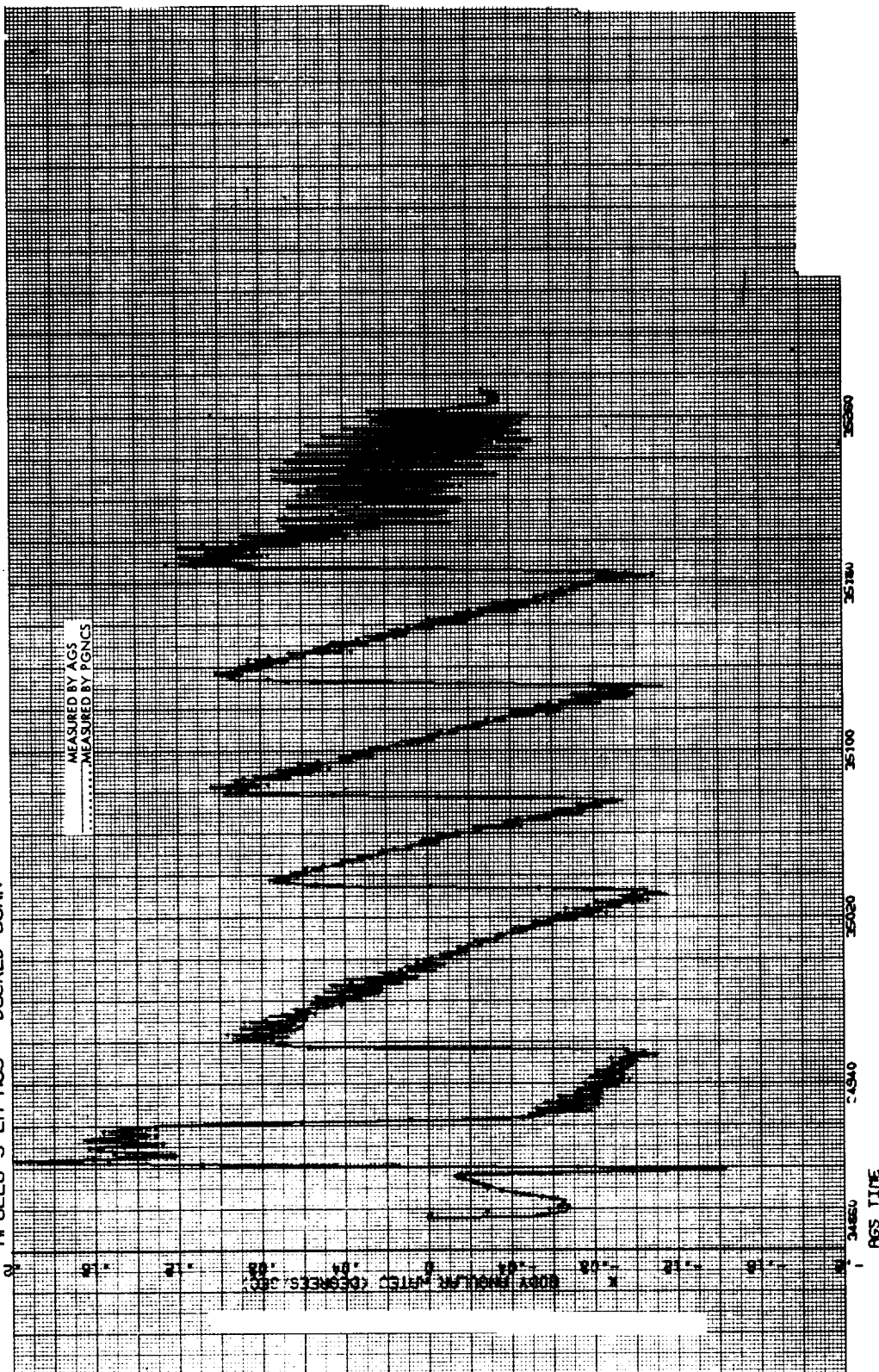


Figure 4-6. X-Body Angular Rate

APOLLO 9 LM AGS - DOCKED BURN

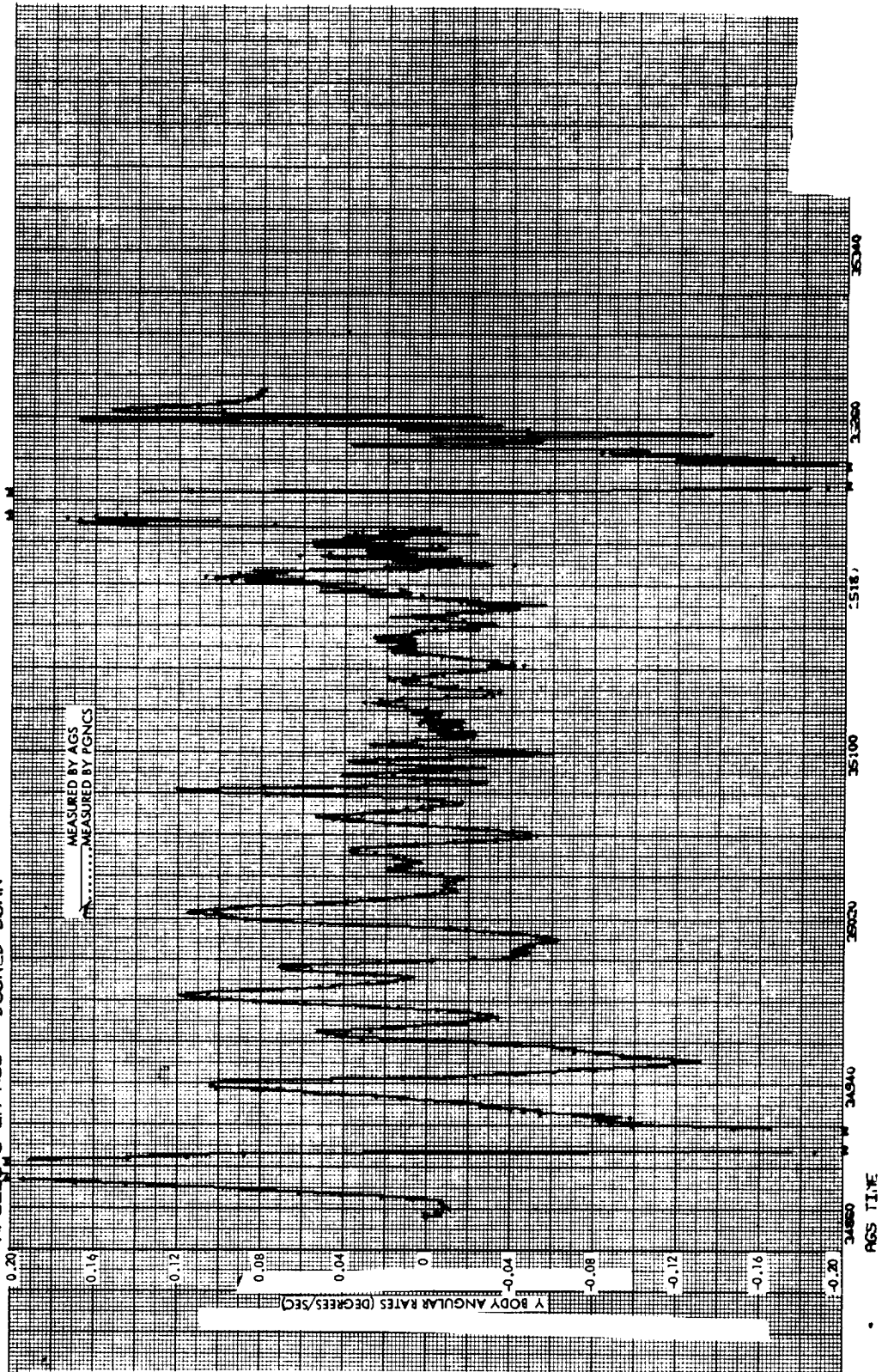


Figure 4-7. Y Body Angular Rate

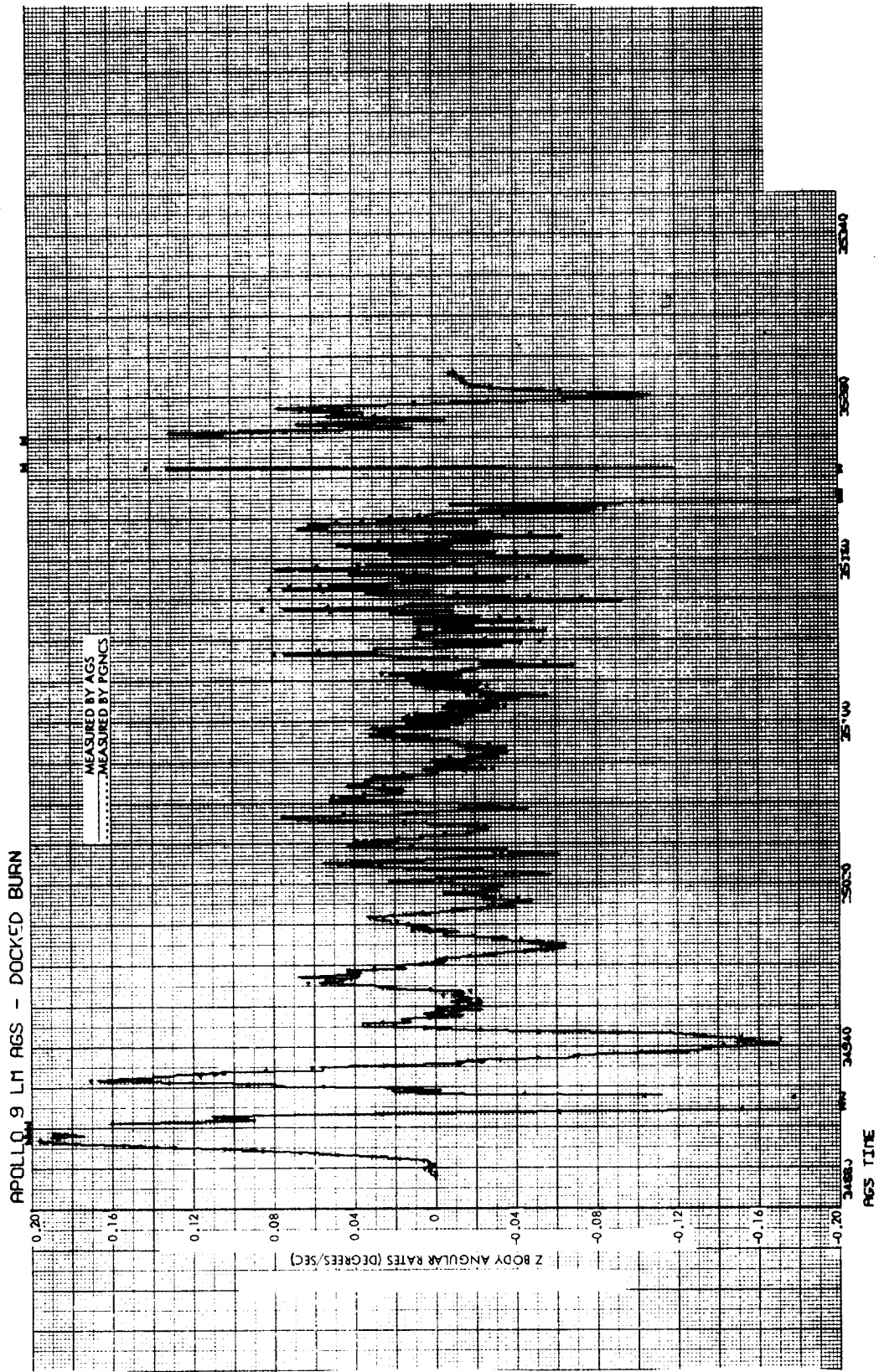


Figure 4-8. Z Body Angular Rate

APOLLO 9 LM RGS DOCKED BURN

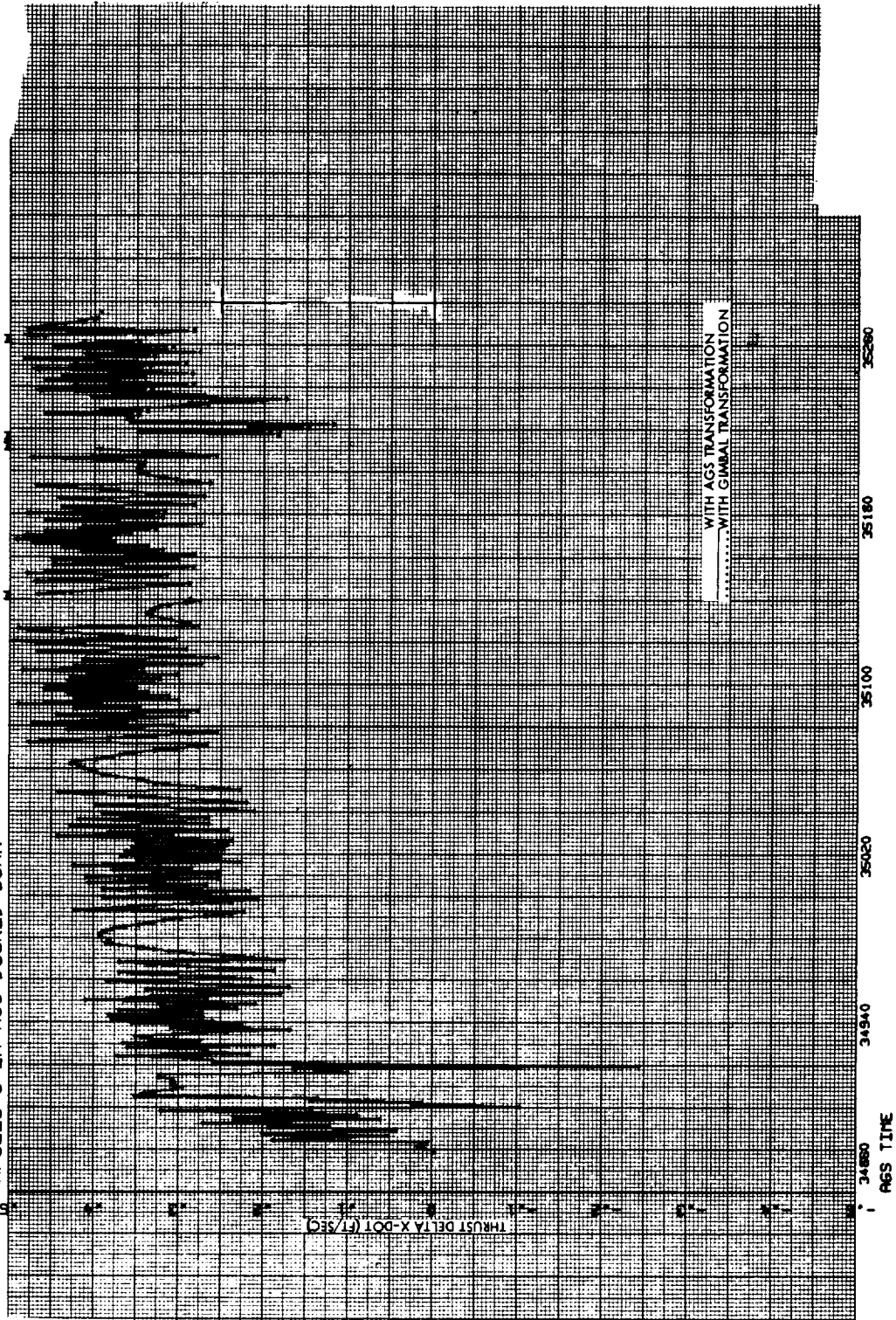


Figure 4-9. X Thrust Velocity Difference

APOLLO 9 LM AGS DOCKED BURN

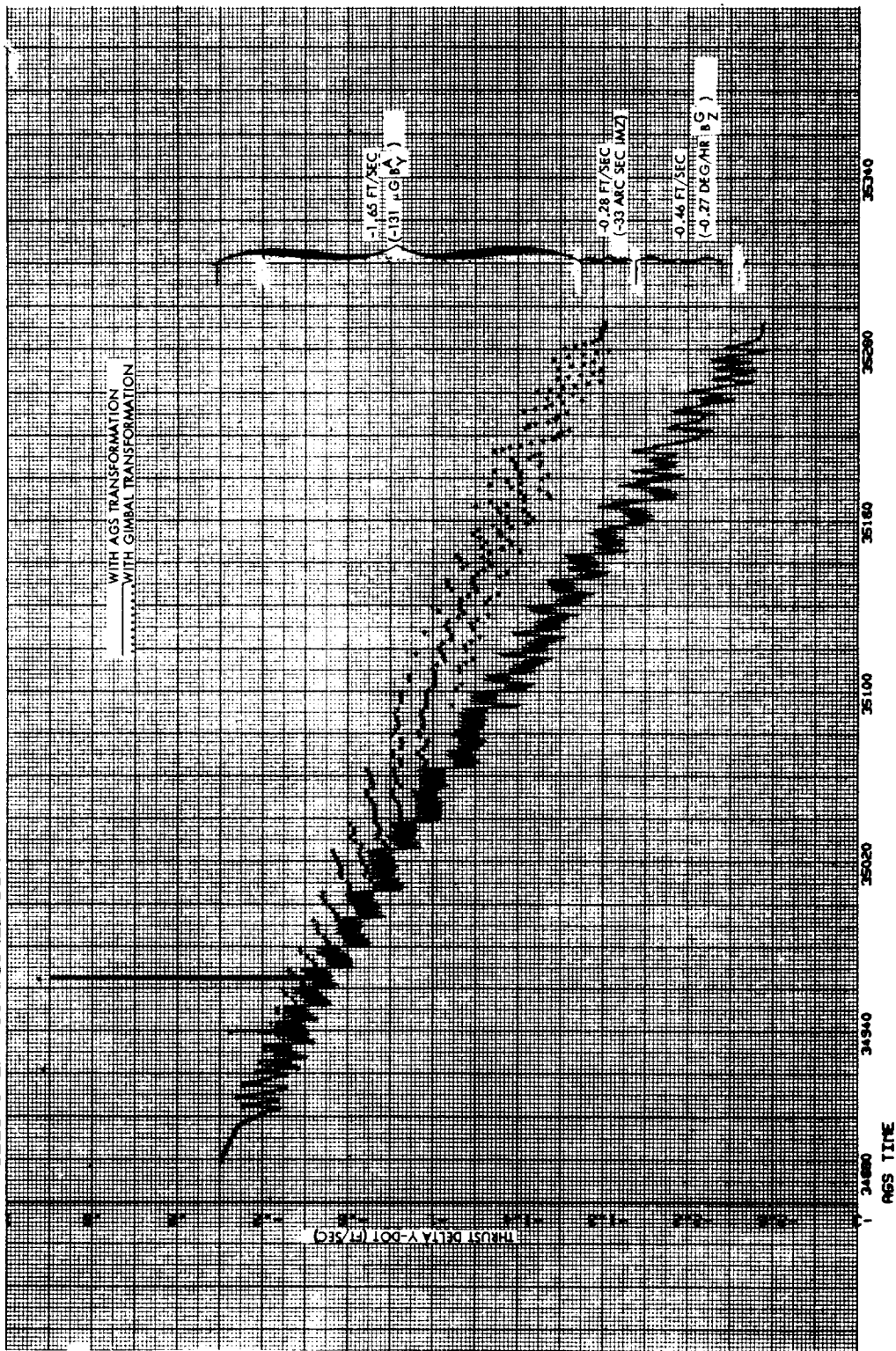


Figure 4-10. Y Thrust Velocity Difference

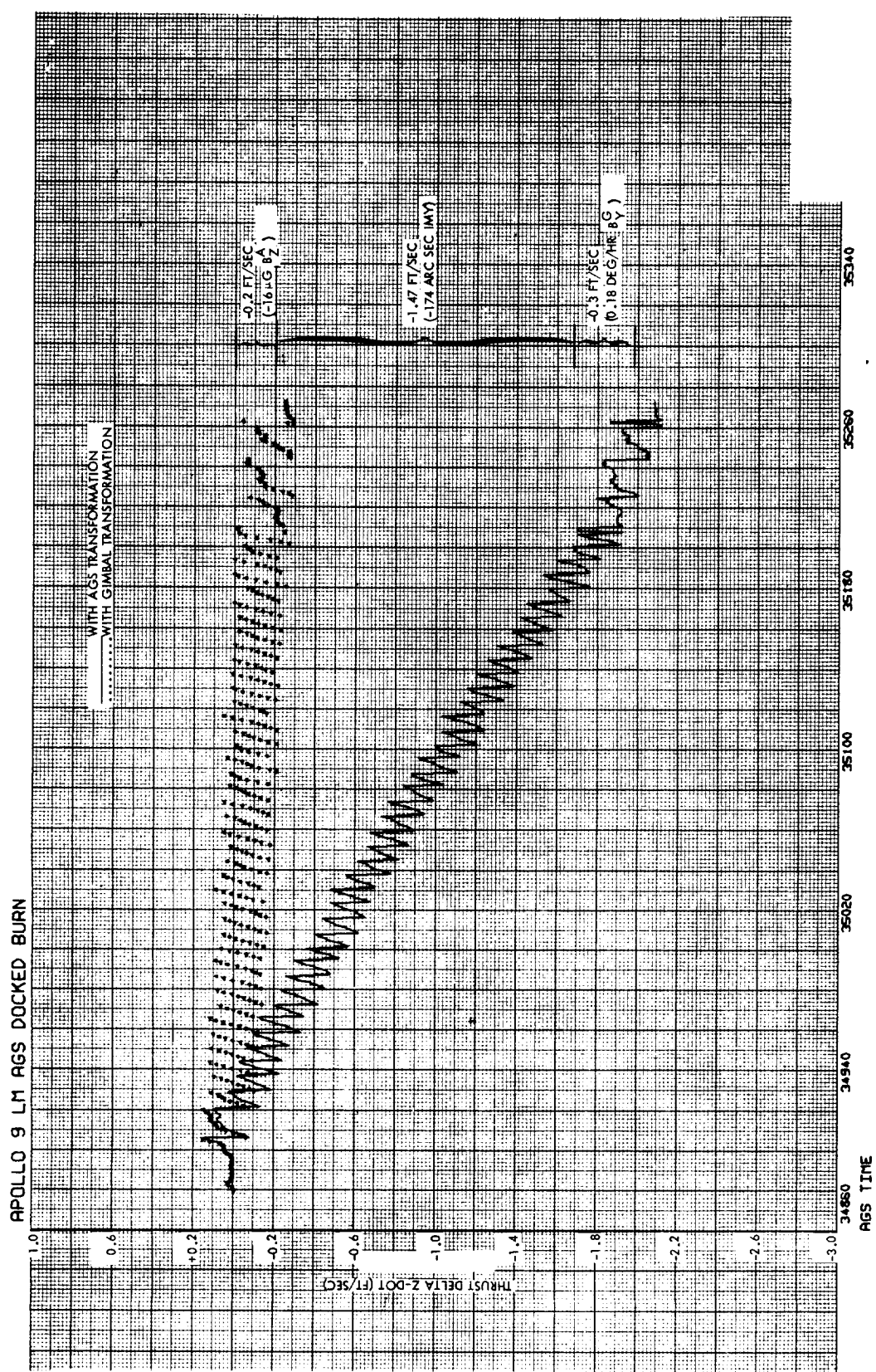


Figure 4-11. Z Thrust Velocity Difference

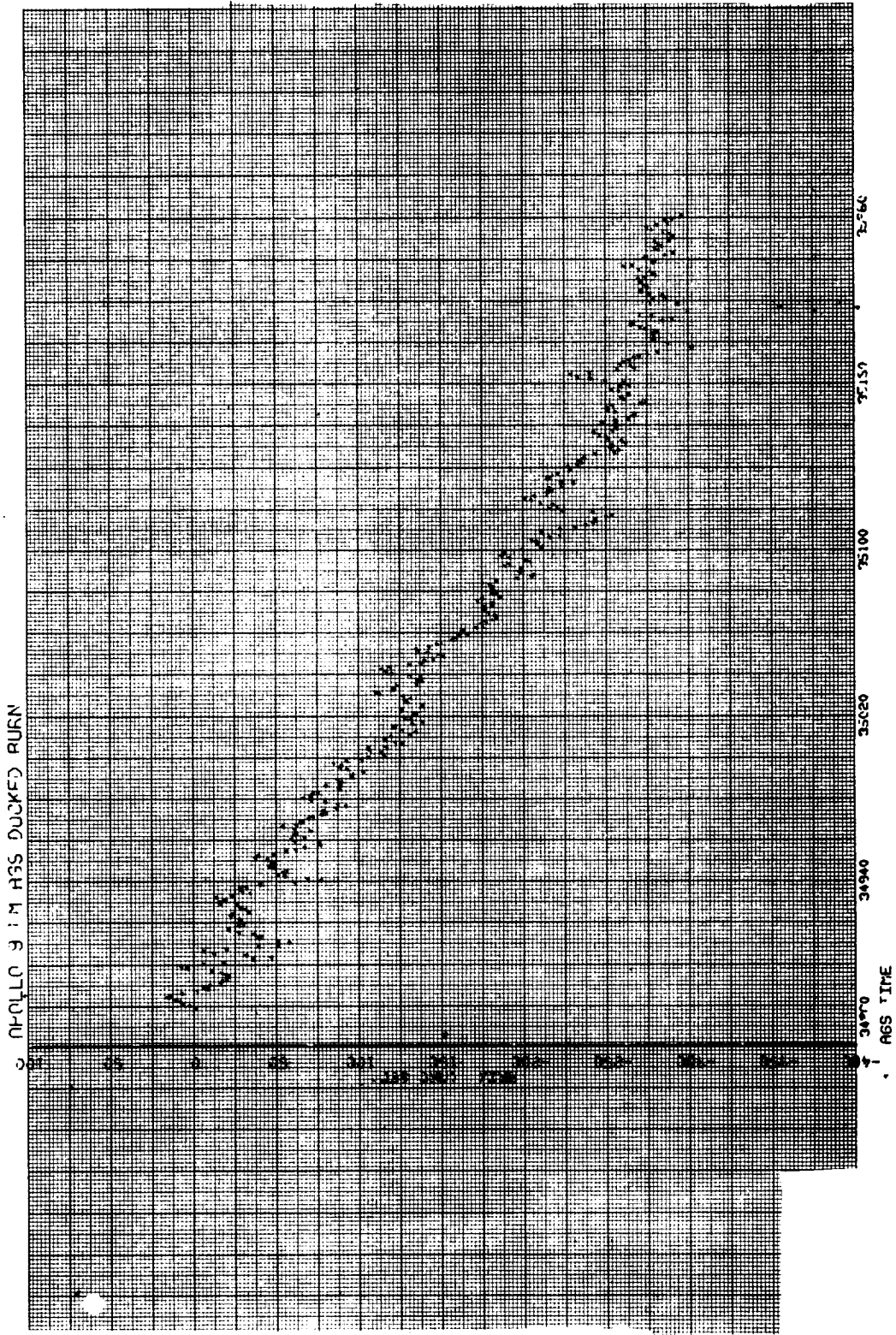


Figure 4-12. Integrated AGS/PGNCS Body Rate Differences (X)

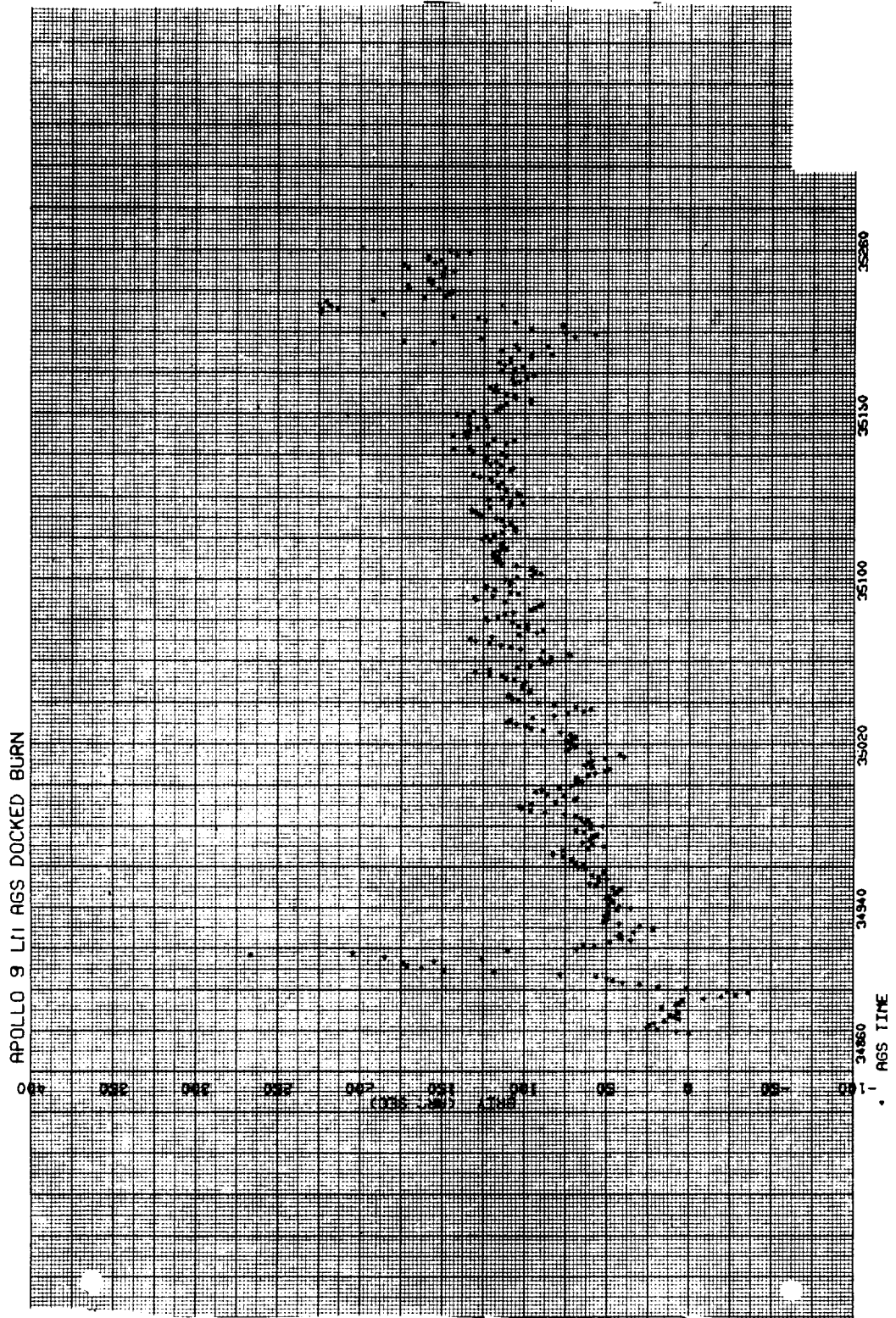


Figure 4-13. Integrated AGS/PGNCS Body Rate Differences (Y)

APOLLO 9 LM AGS DOCKED BURN

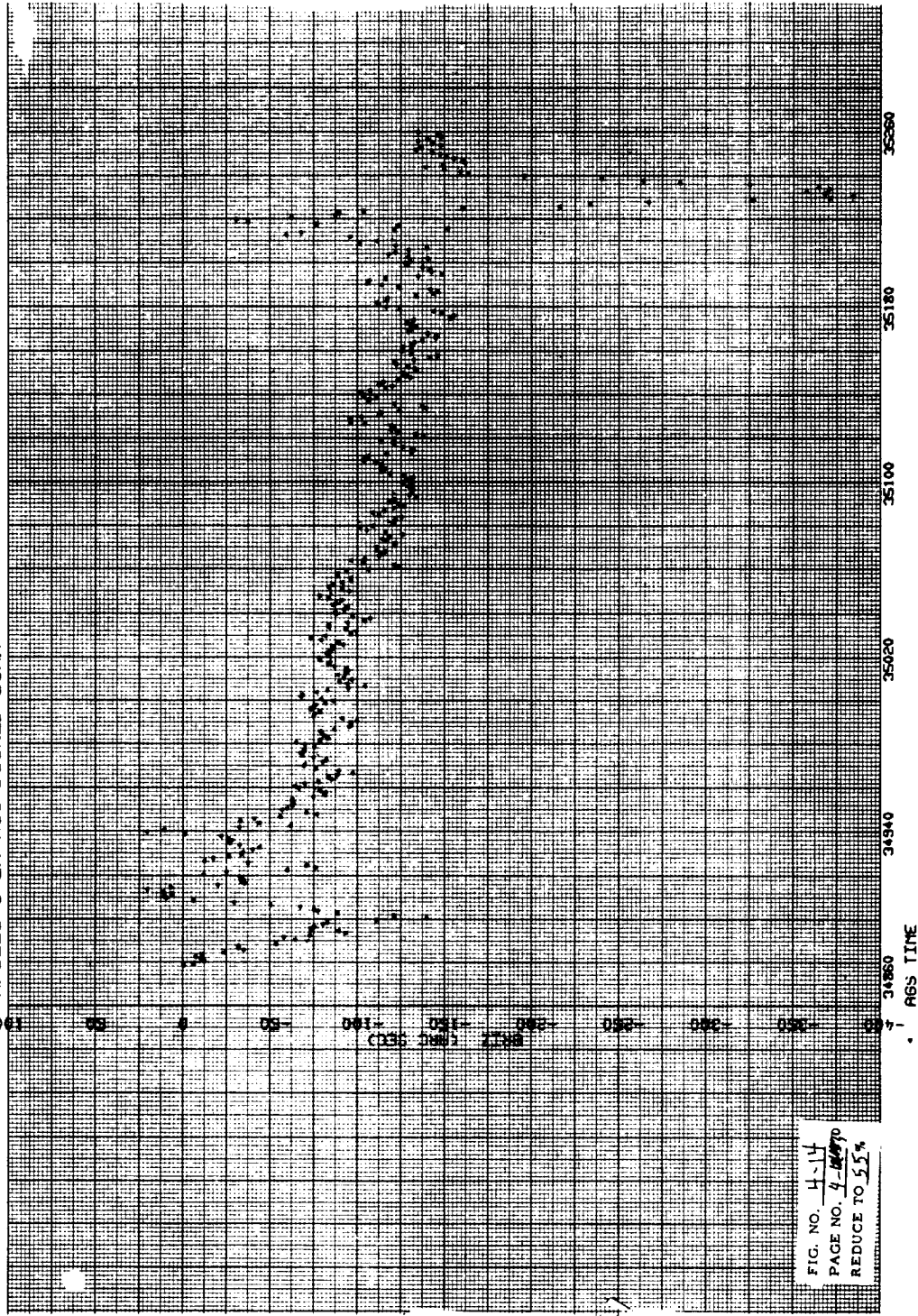


Figure 4-14. Integrated AGS/PGNCS Body Rate Differences (Z)

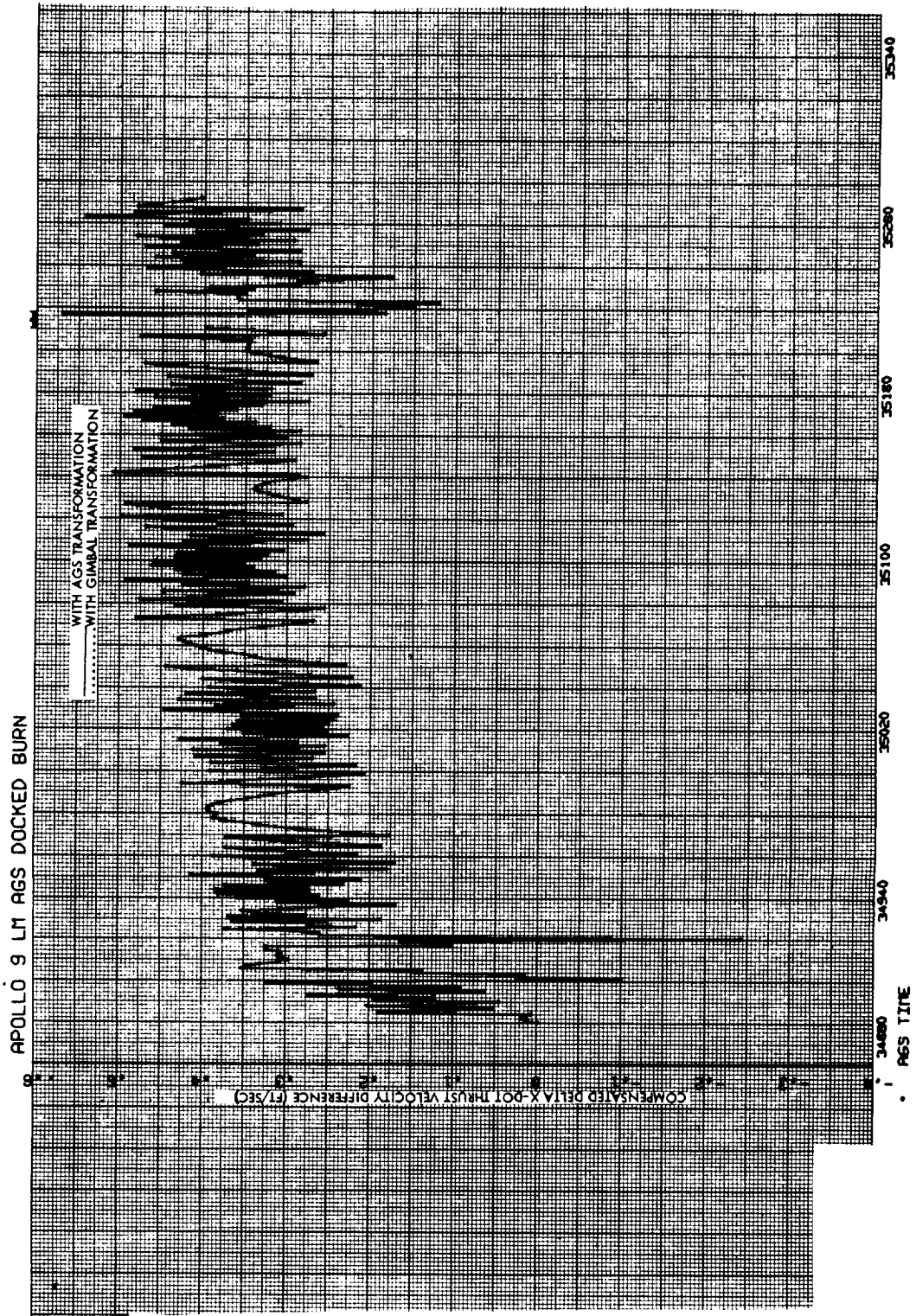


Figure 4-15. Compensated Thrust Velocity Difference (X)

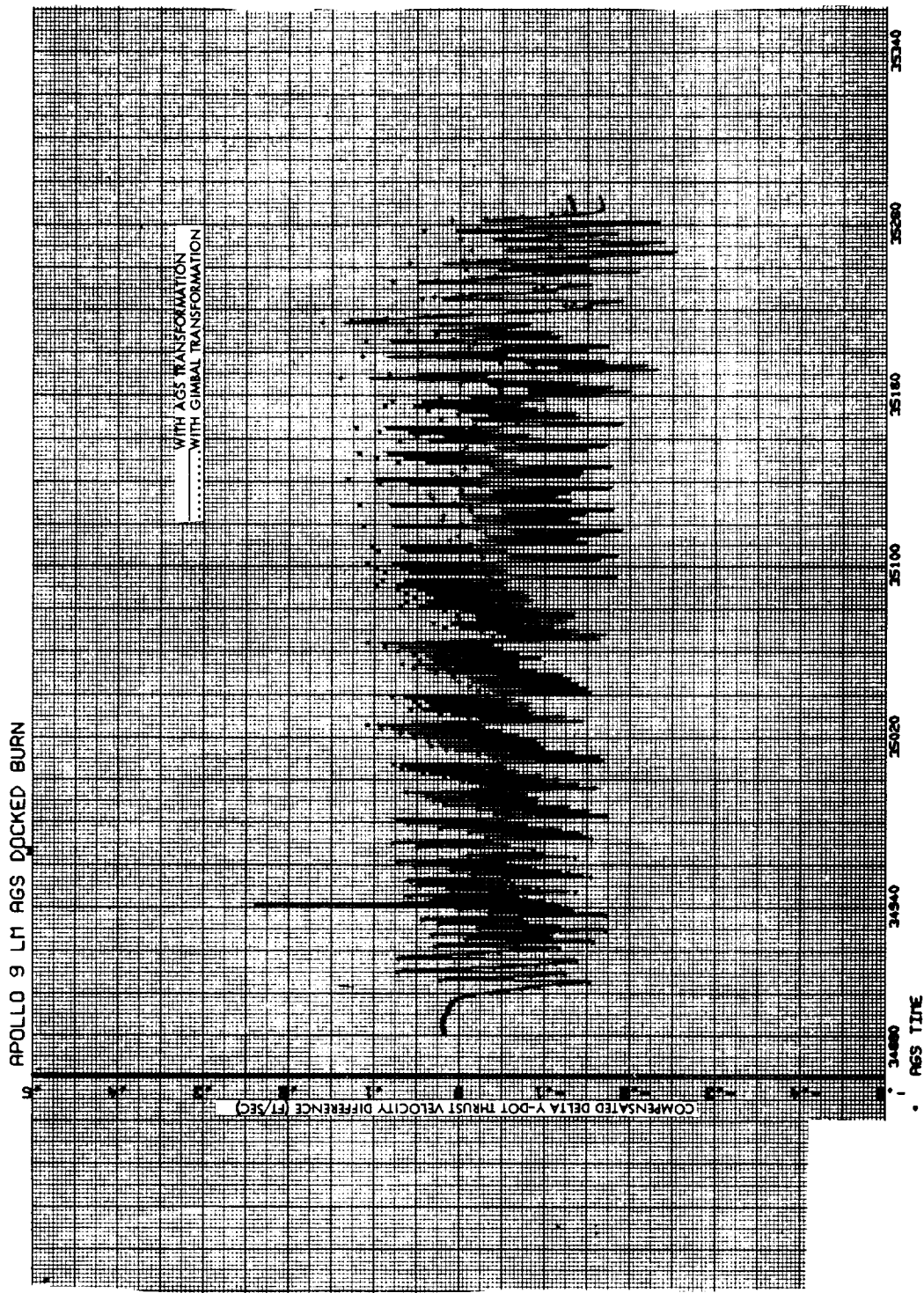


Figure 4-16. Compensated Thrust Velocity Differences (Y)

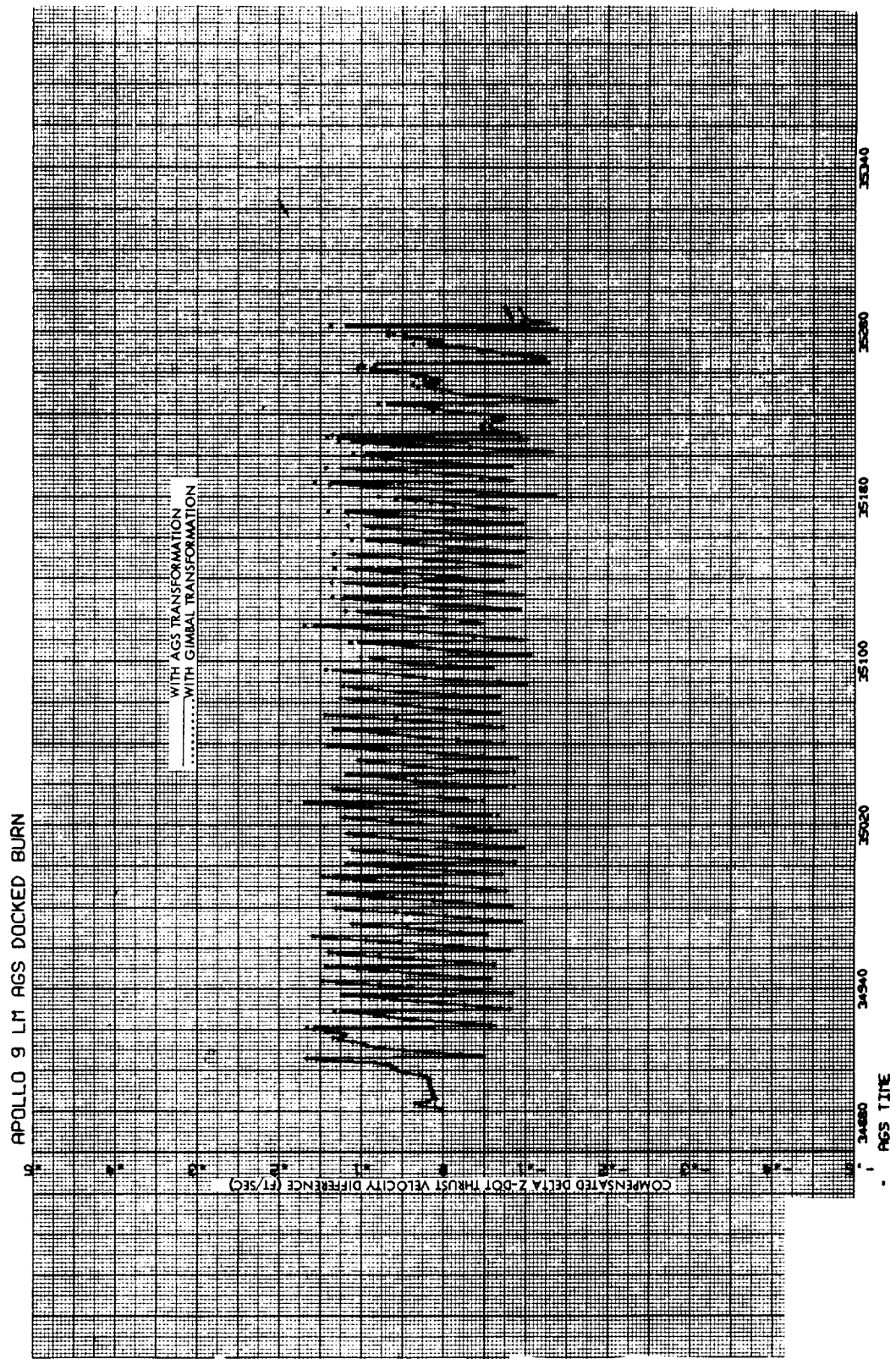


Figure 4-17. Compensated Thrust Velocity Differences (Z)

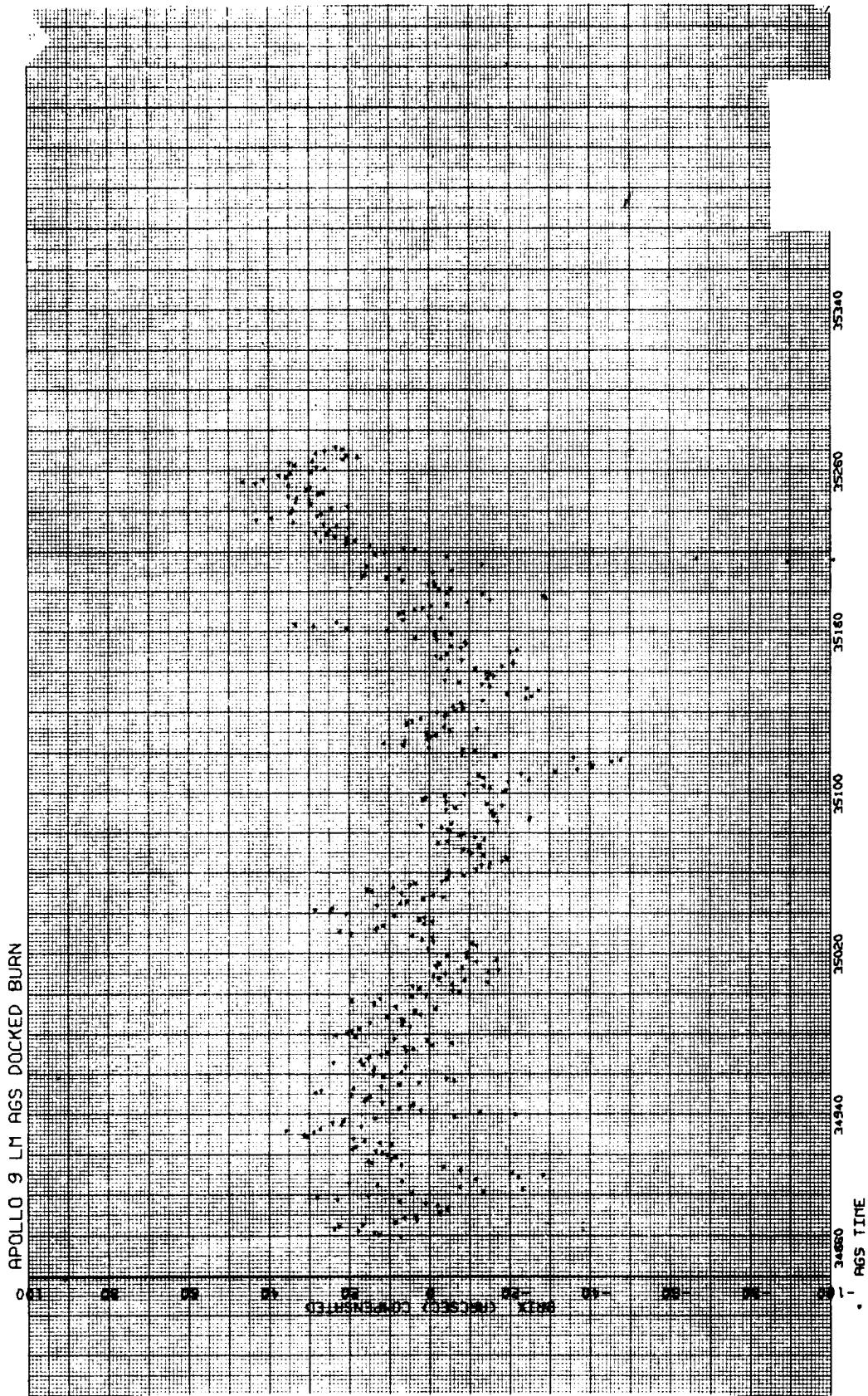


Figure 4-18. Integrated AGS/PGNCS Body Rate Differences After Compensation (X)

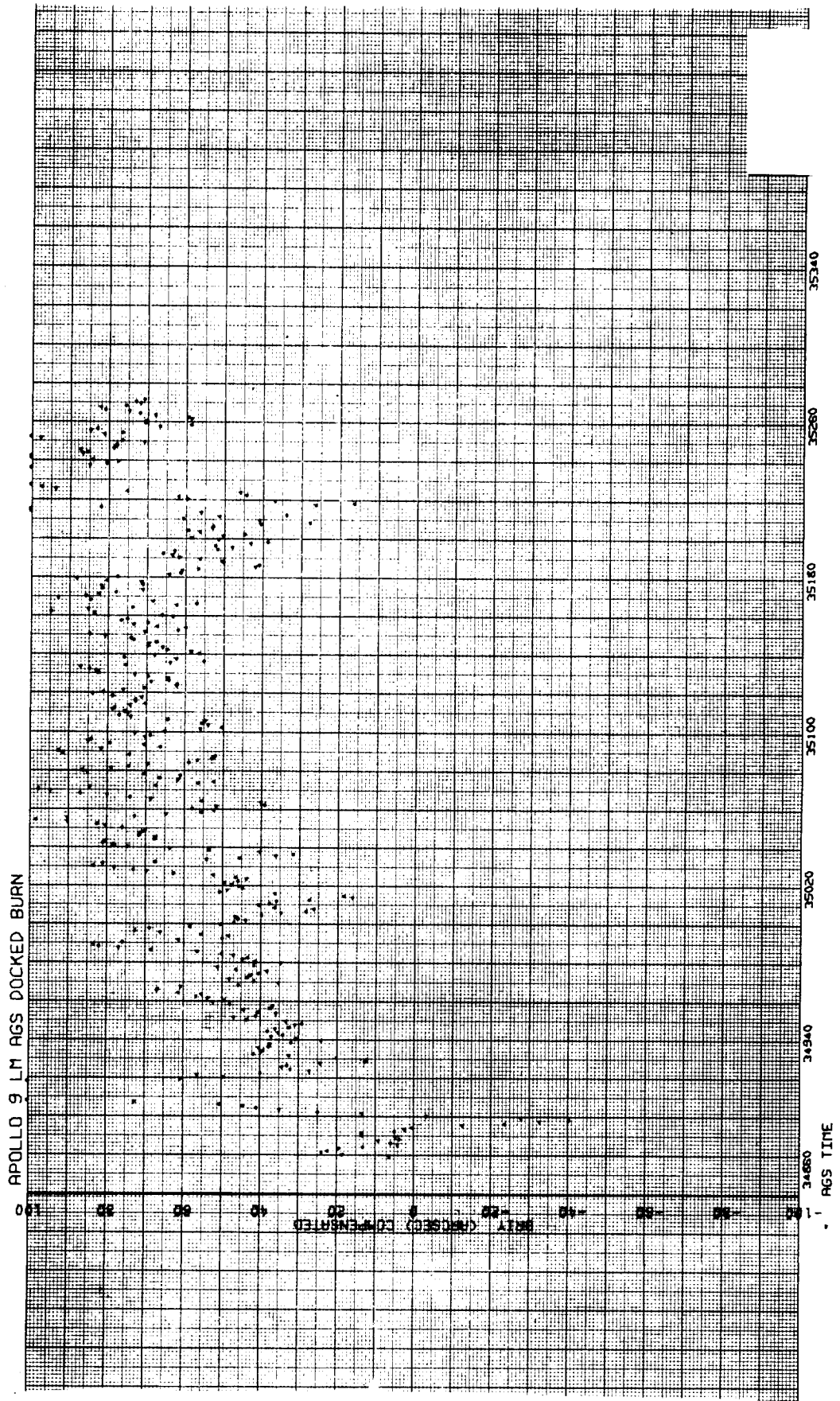


Figure 4-19. Integrated AGS/PGNCS Body Rate Differences After Compensation (Y)

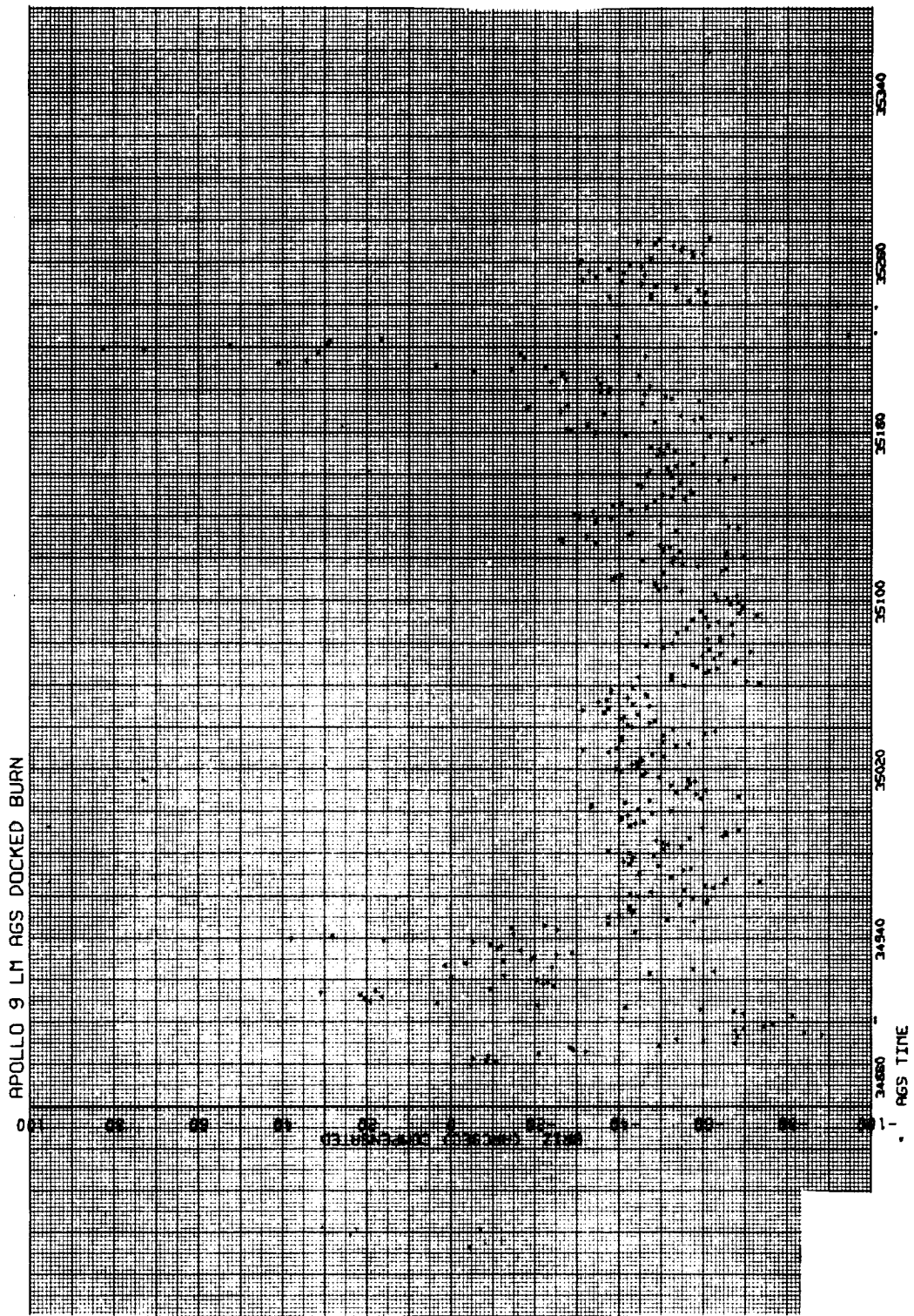


Figure 4-20. Integrated AGS/PGNCS Body Rate Differences After Compensation (Z)

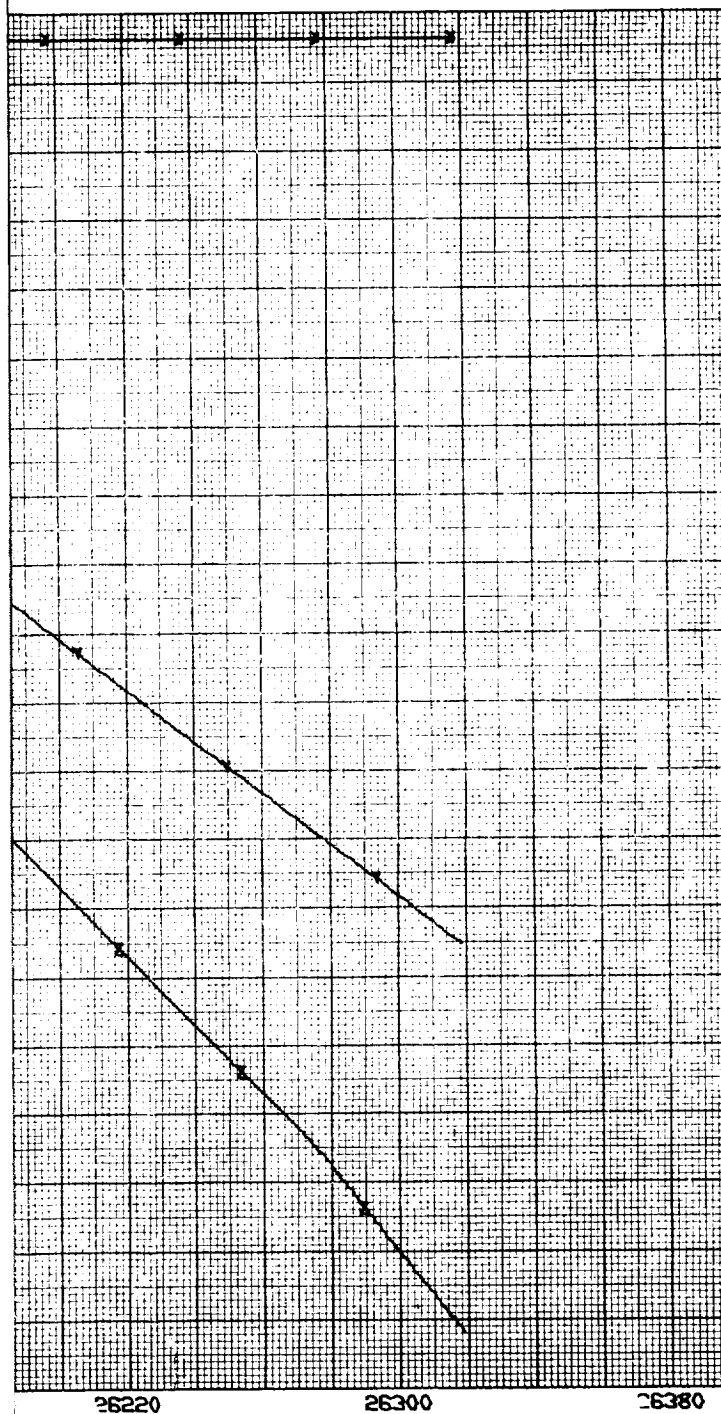
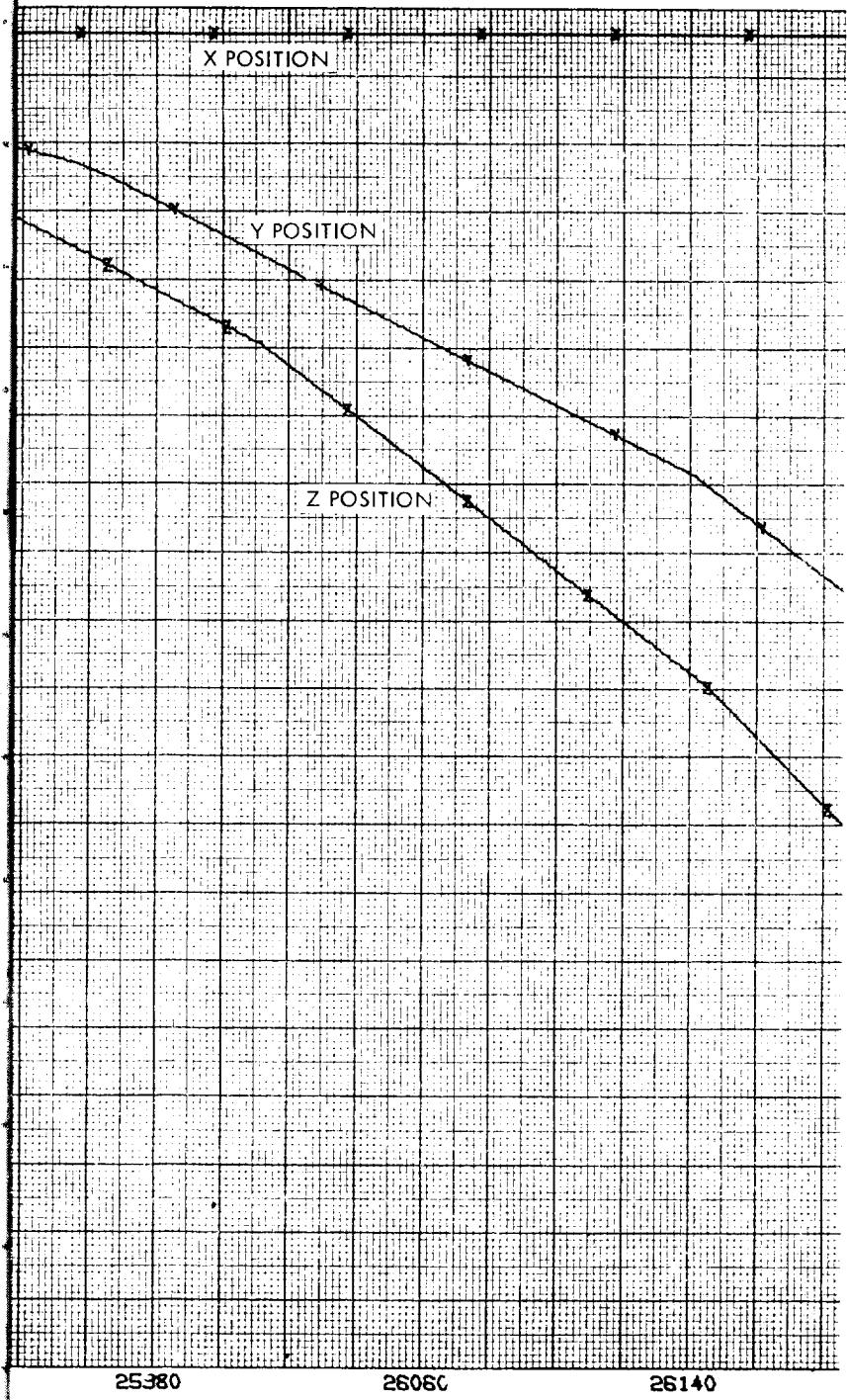


Figure 4-21. Thrust Position in Free Flight

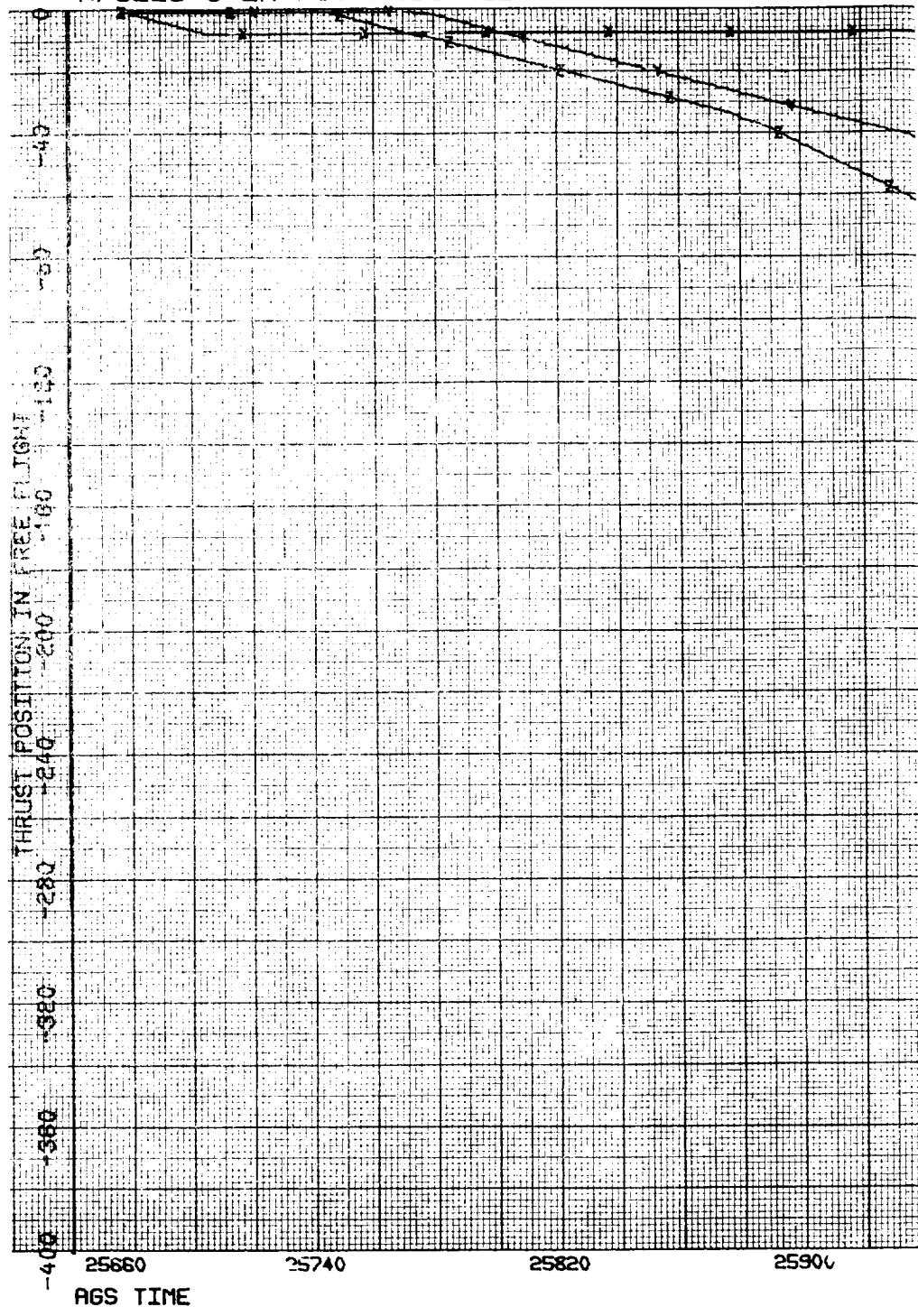


FOLDOUT, FRAME 2

www.pearsoned.com

© 2008 Pearson Education, Inc.

APOLLO 9 LM AGS FREE FLIGHT



EXPOSED FRAME 3

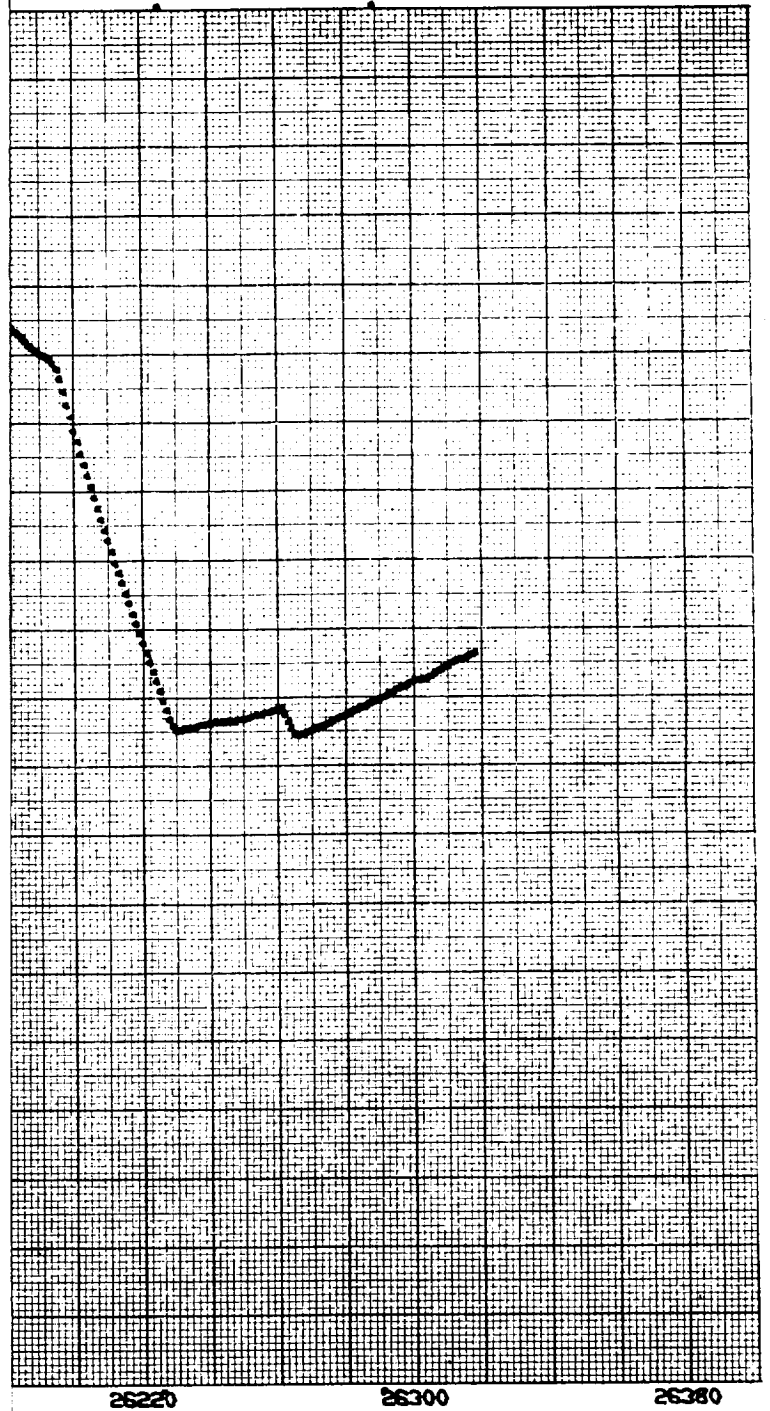
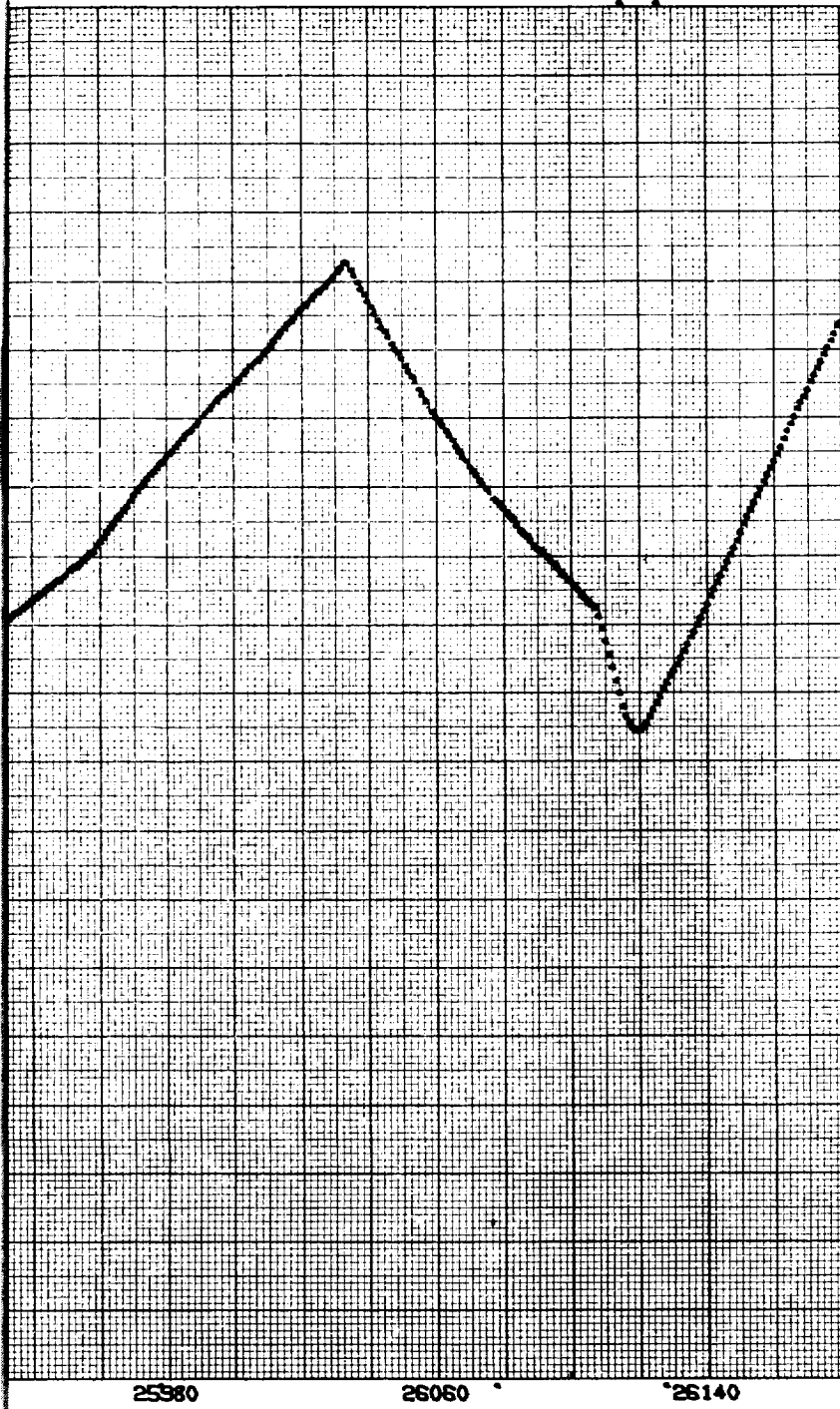
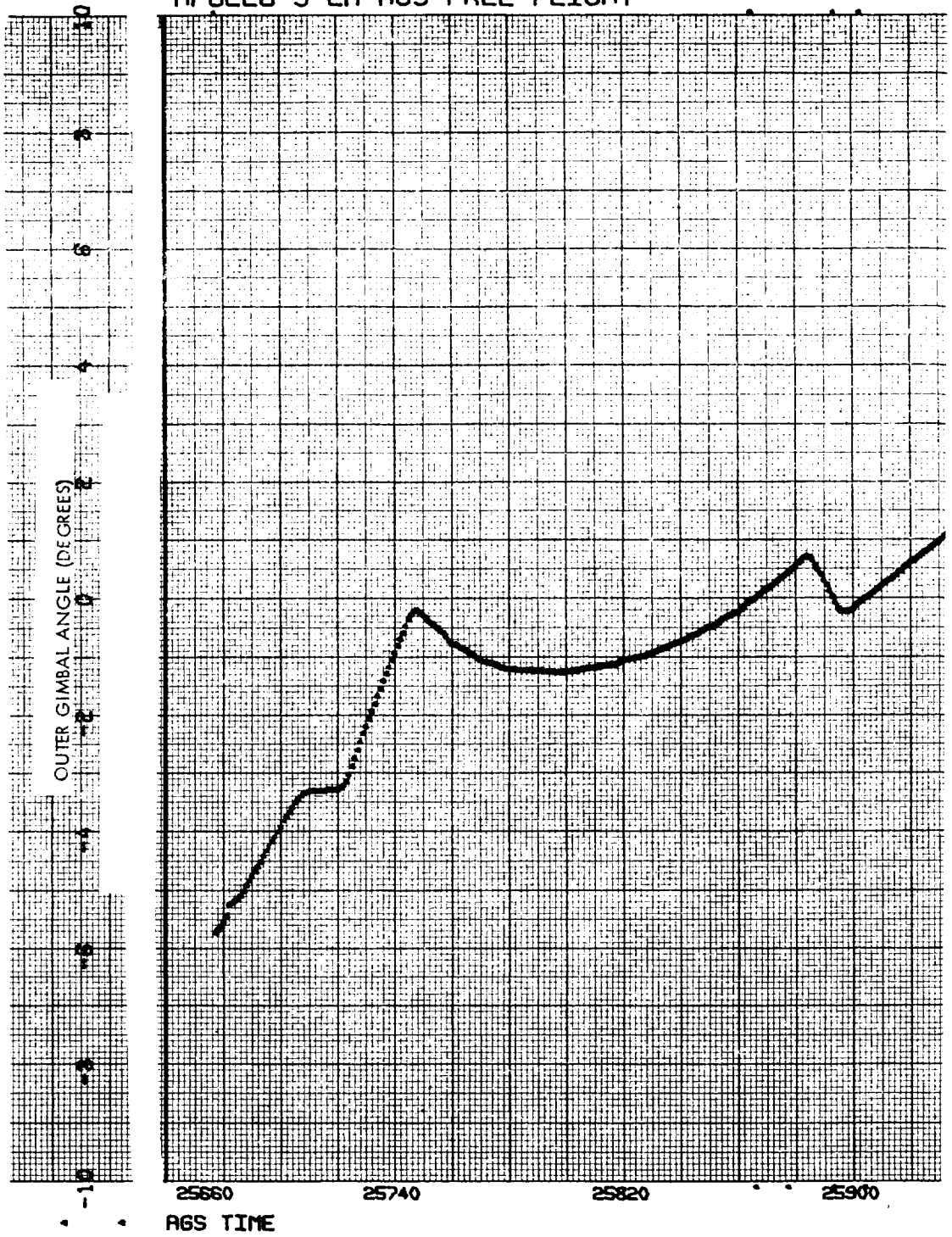


Figure 4-22. Outer Gimbal Angle



FOLDOUT FRAME *JD*

APOLLO 9 LM AGS FREE FLIGHT



FOLDOUT FRAME 3

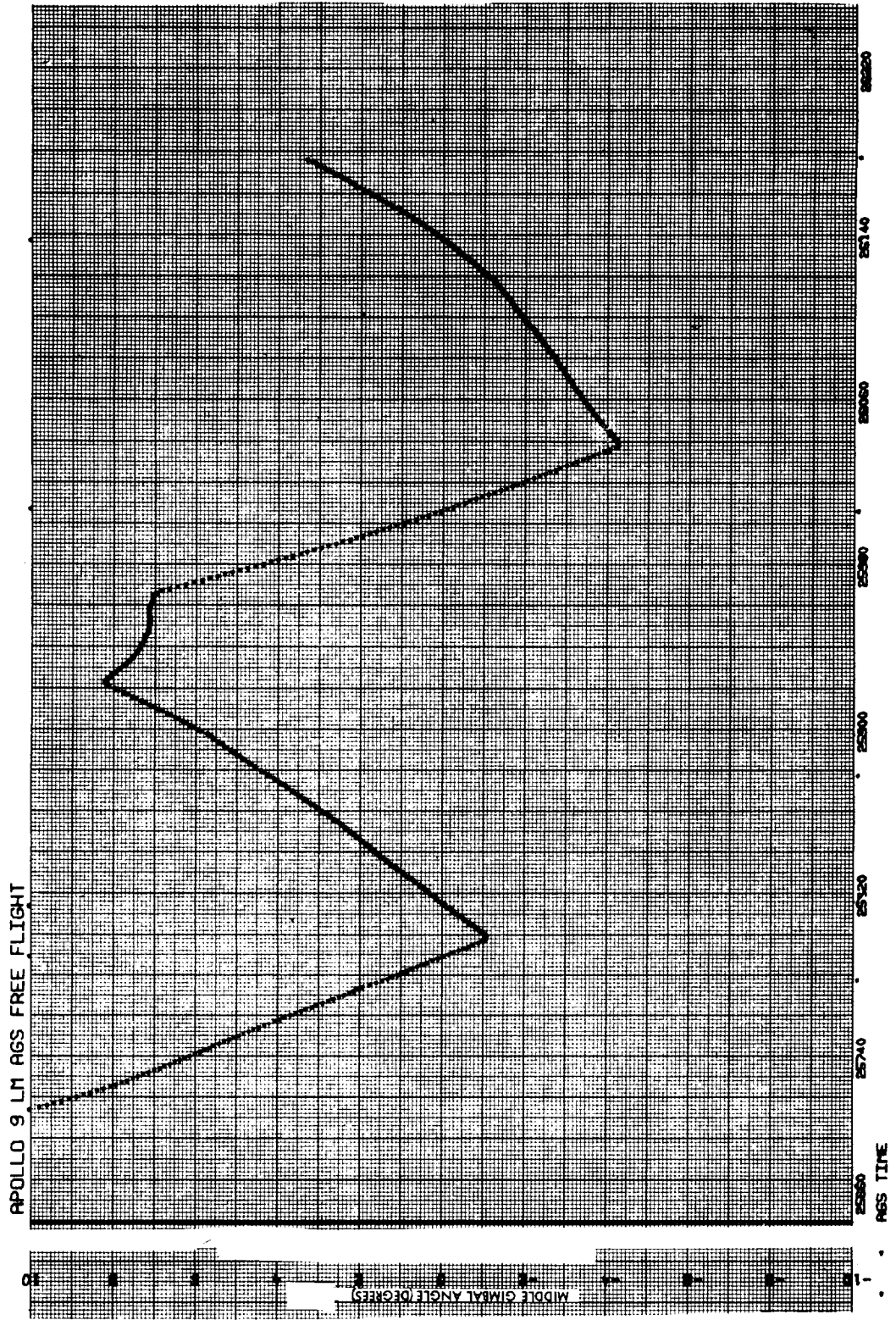


Figure 4-23. Middle Gimbal Angle

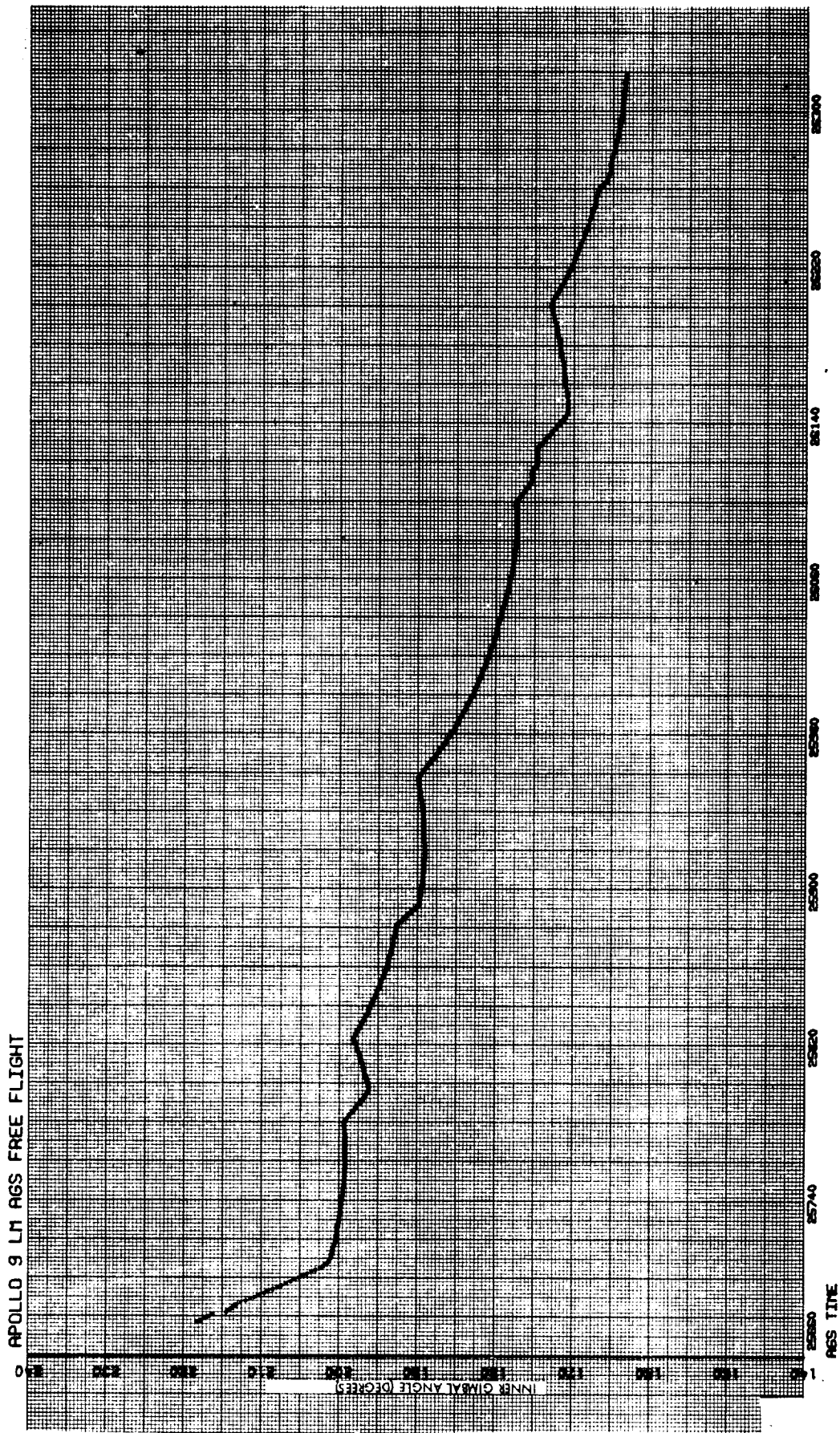


Figure 4-24. Inner Gimbal Angle

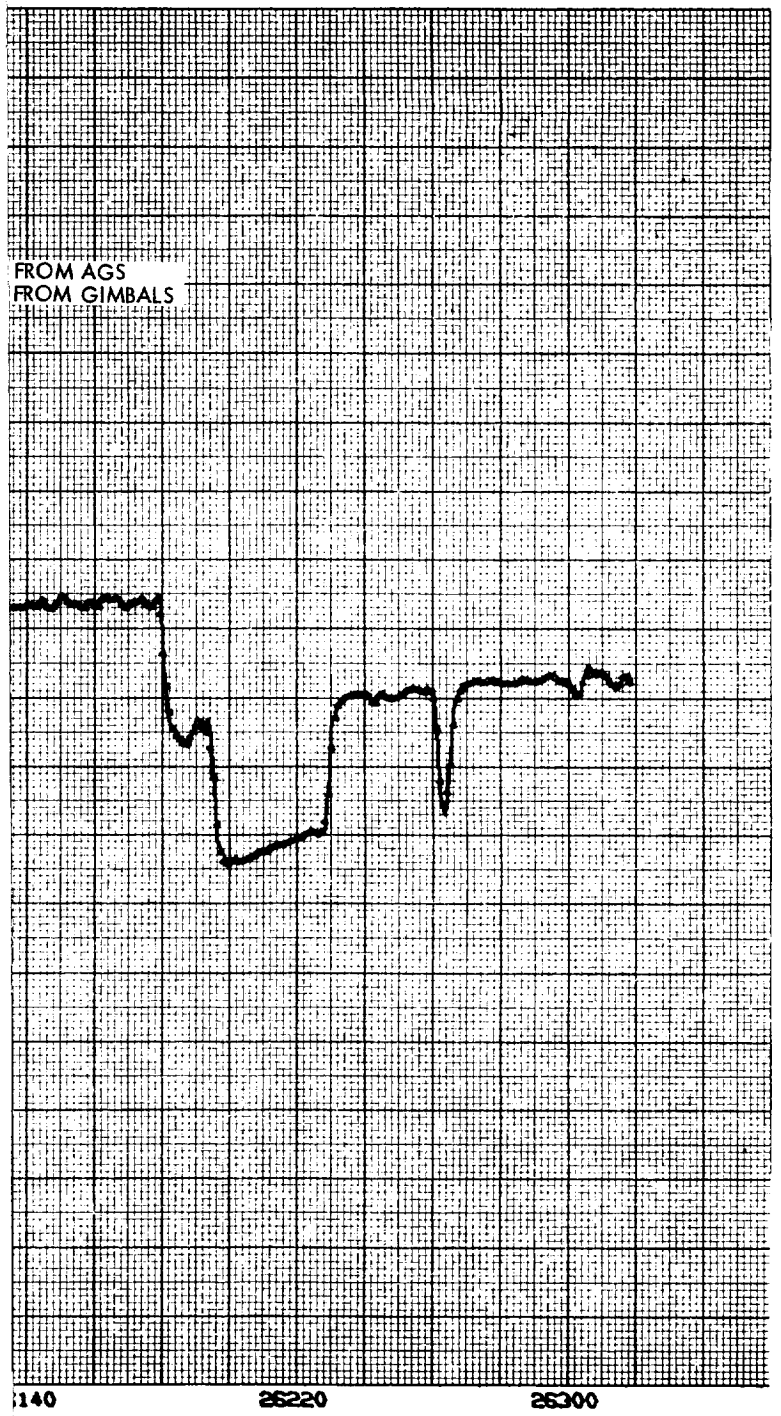
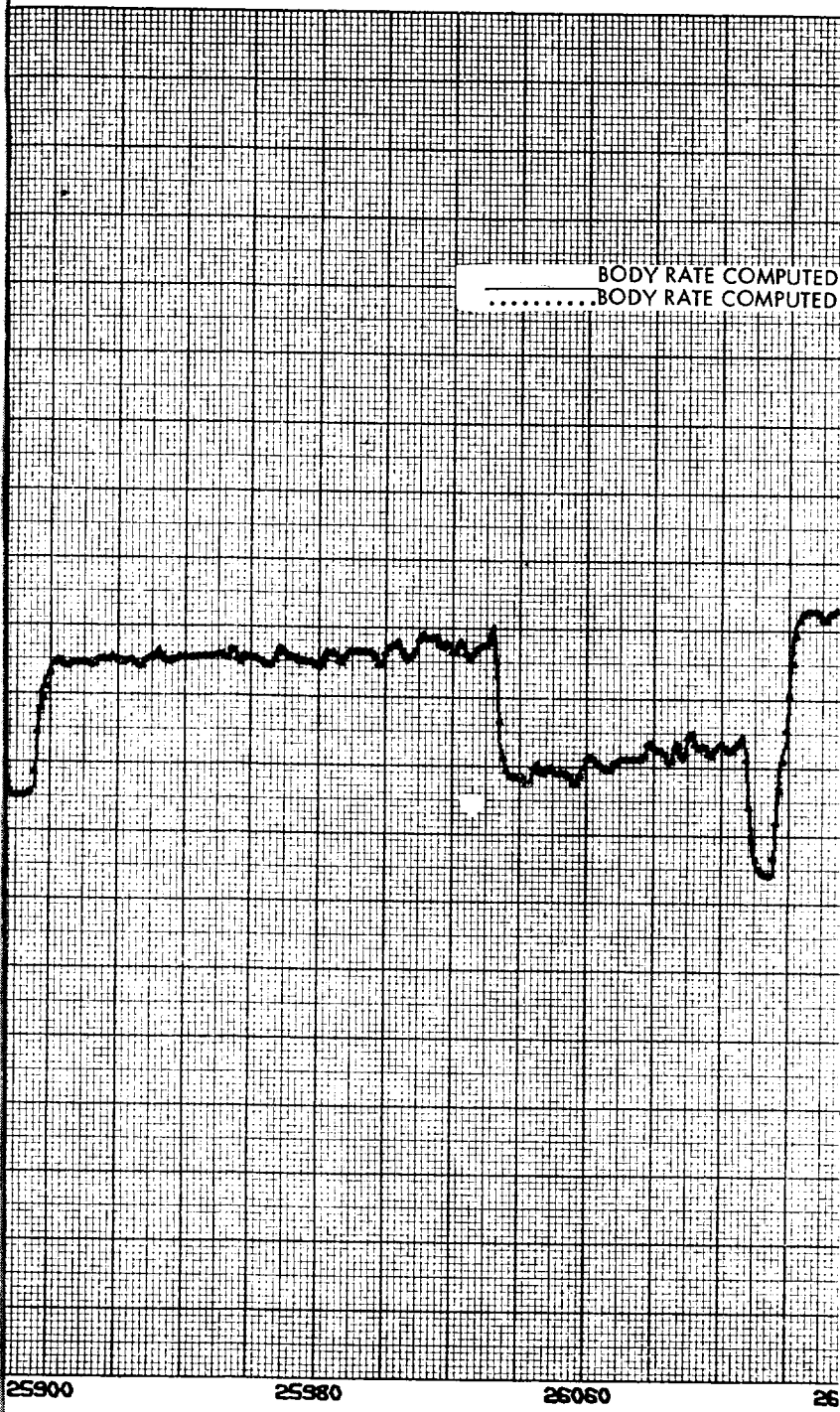
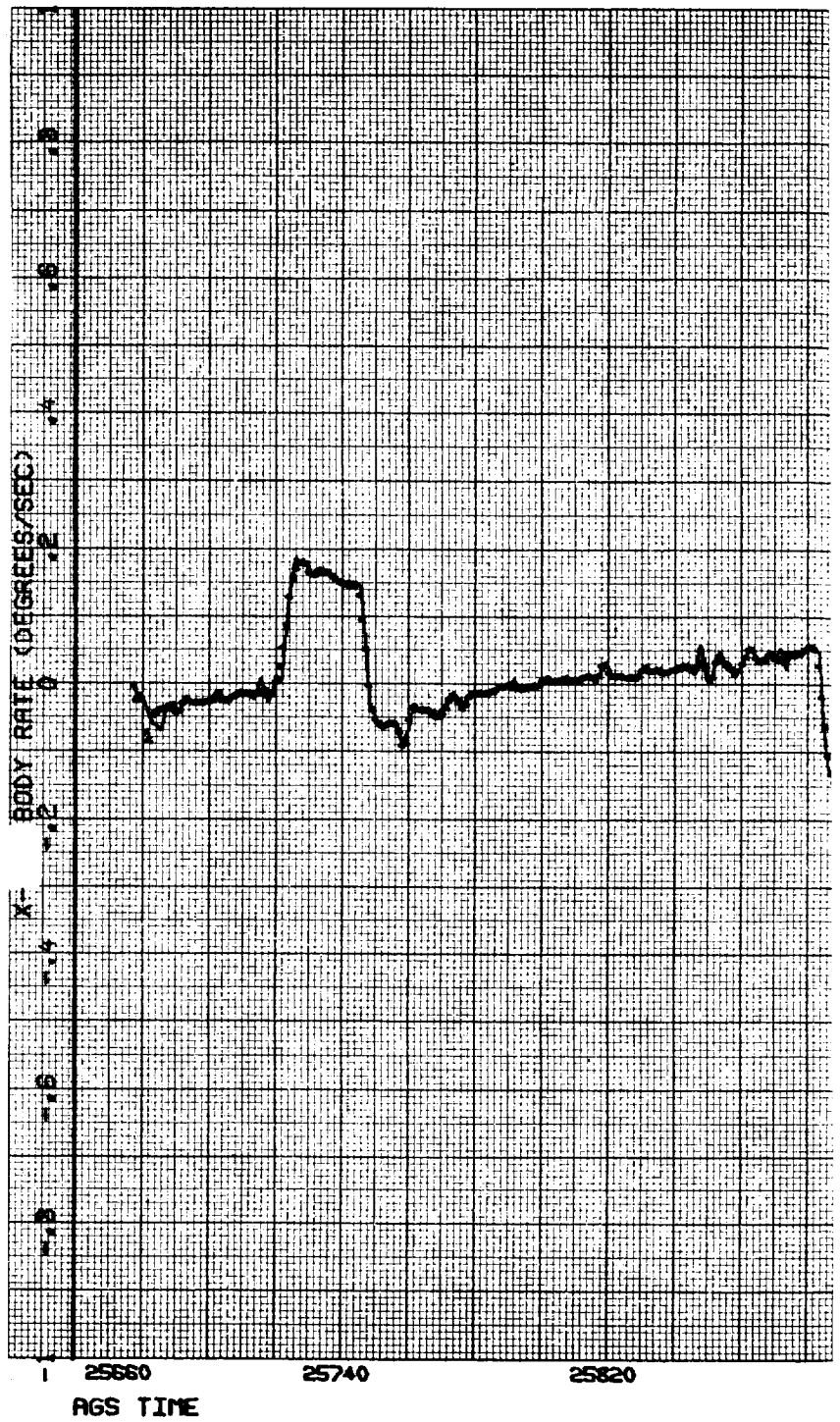


Figure 4-25. X Body Rate



FOLDOUT FRAME 2

APOLLO 9 LM AGS FREE FLIGHT



FOLDOUT FRAME 3

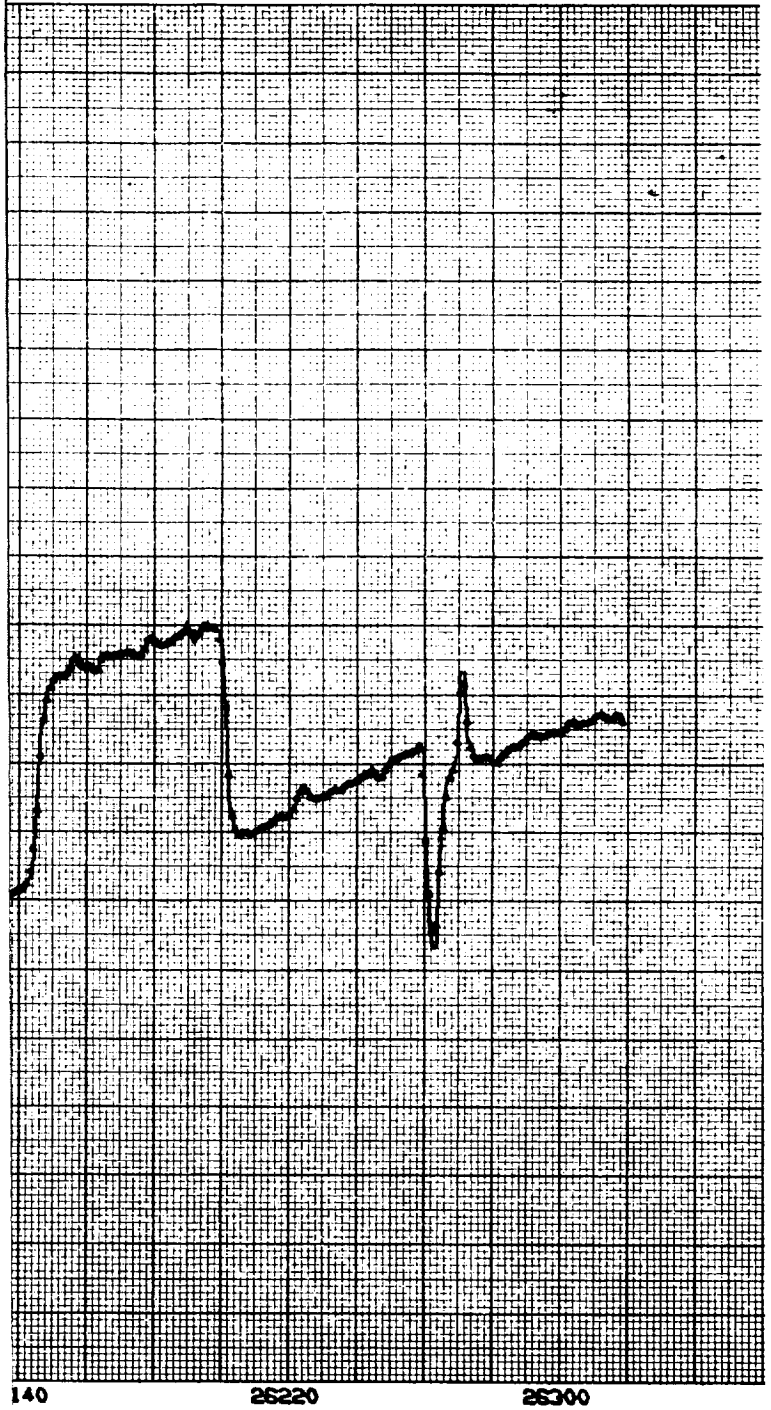
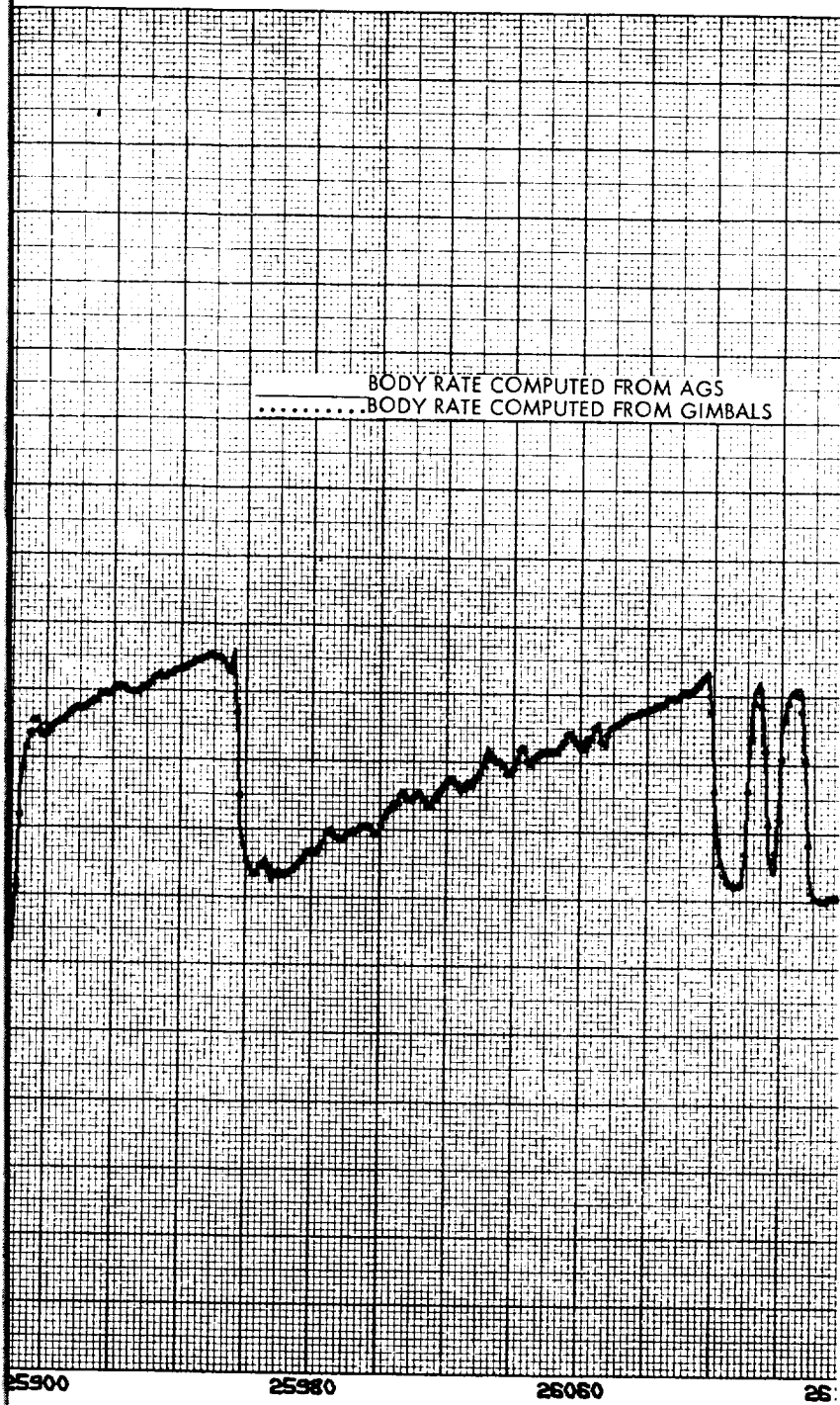


Figure 4-26. Y Body Rate

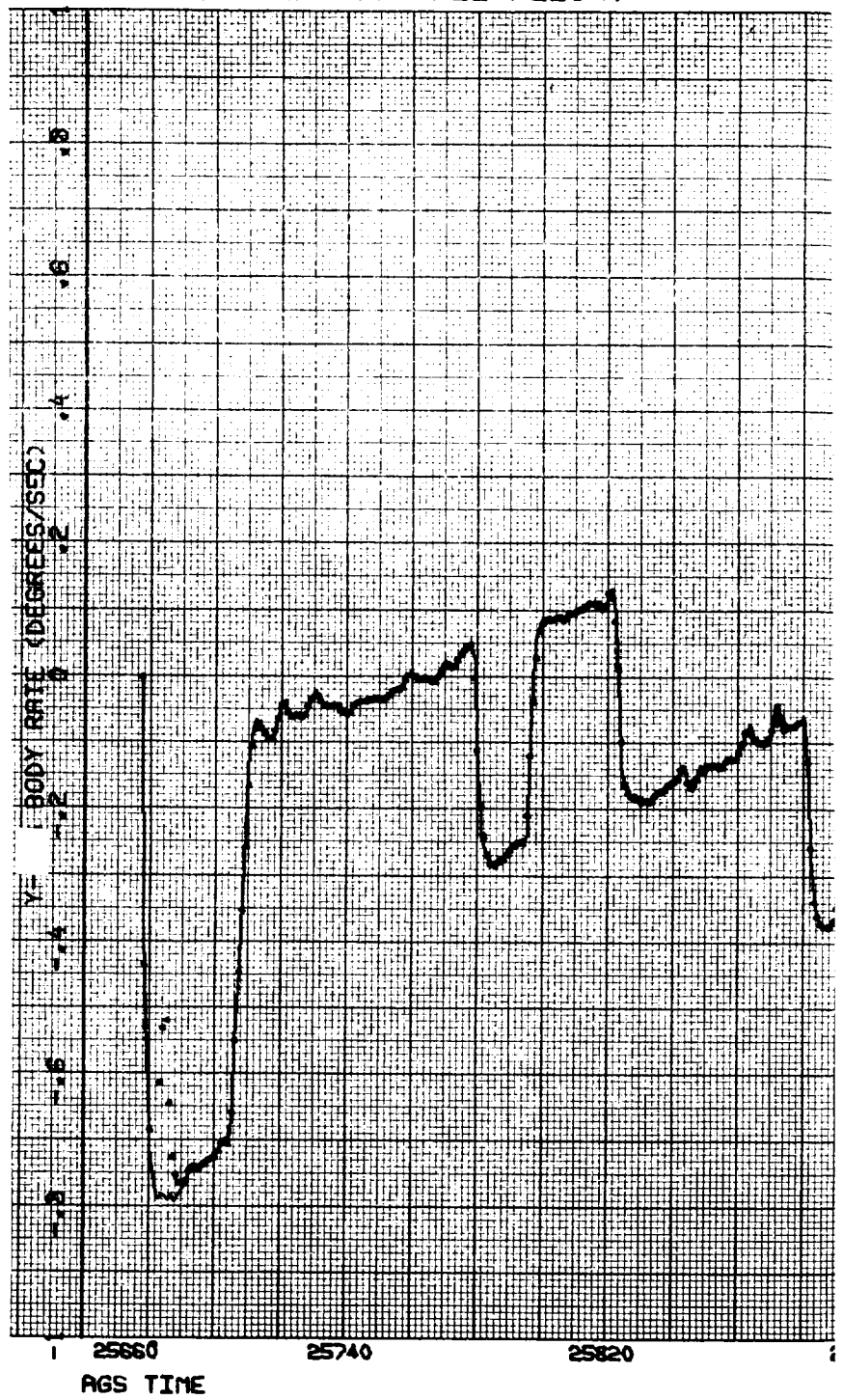


FOLDOUT FRAME 2

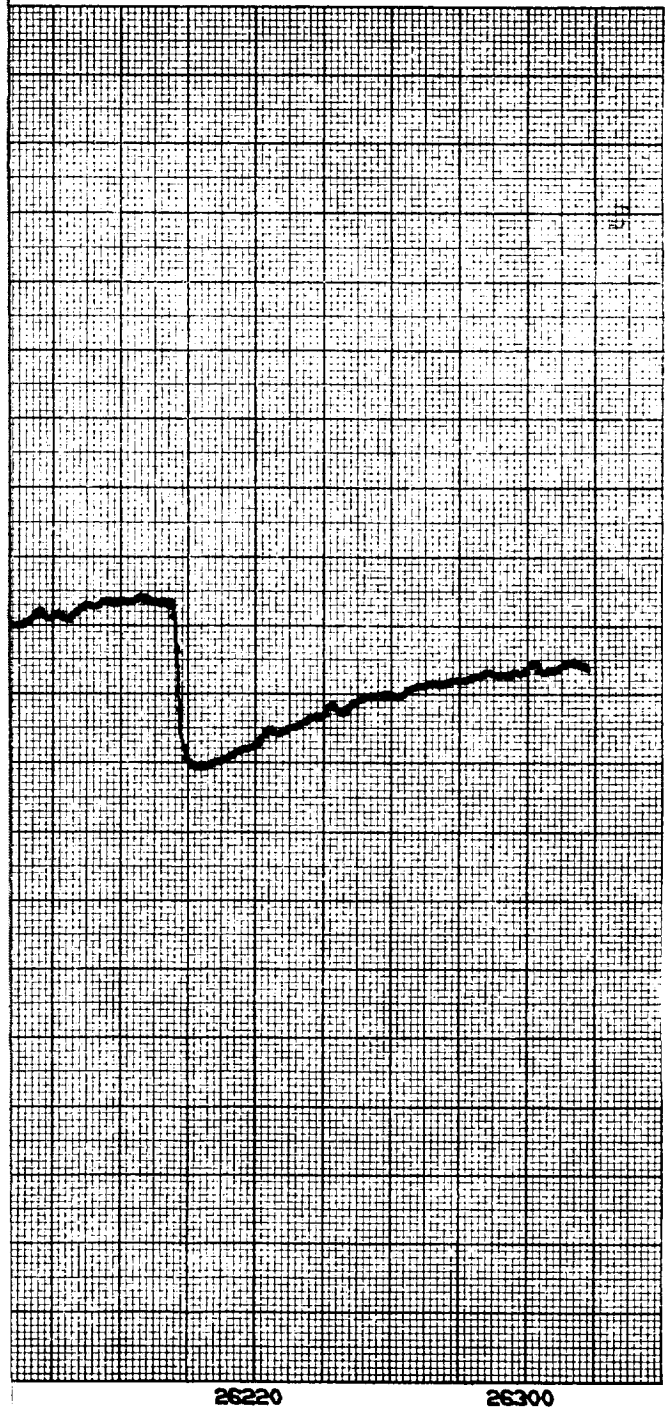
.

9. 1. 1. 1. 1.

APOLLO 9 LM AGS FREE FLIGHT

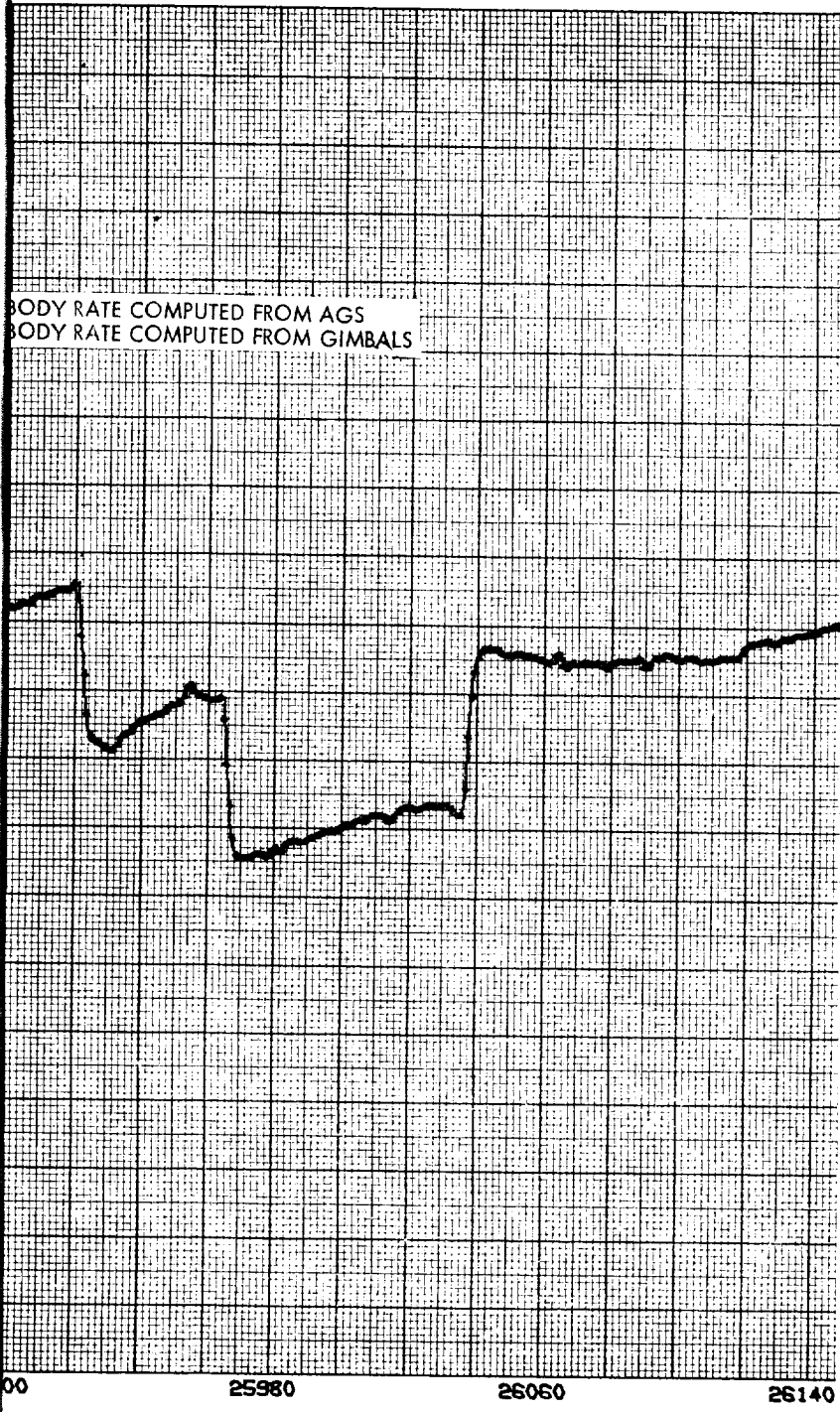


FOLDOUT FRAME 3



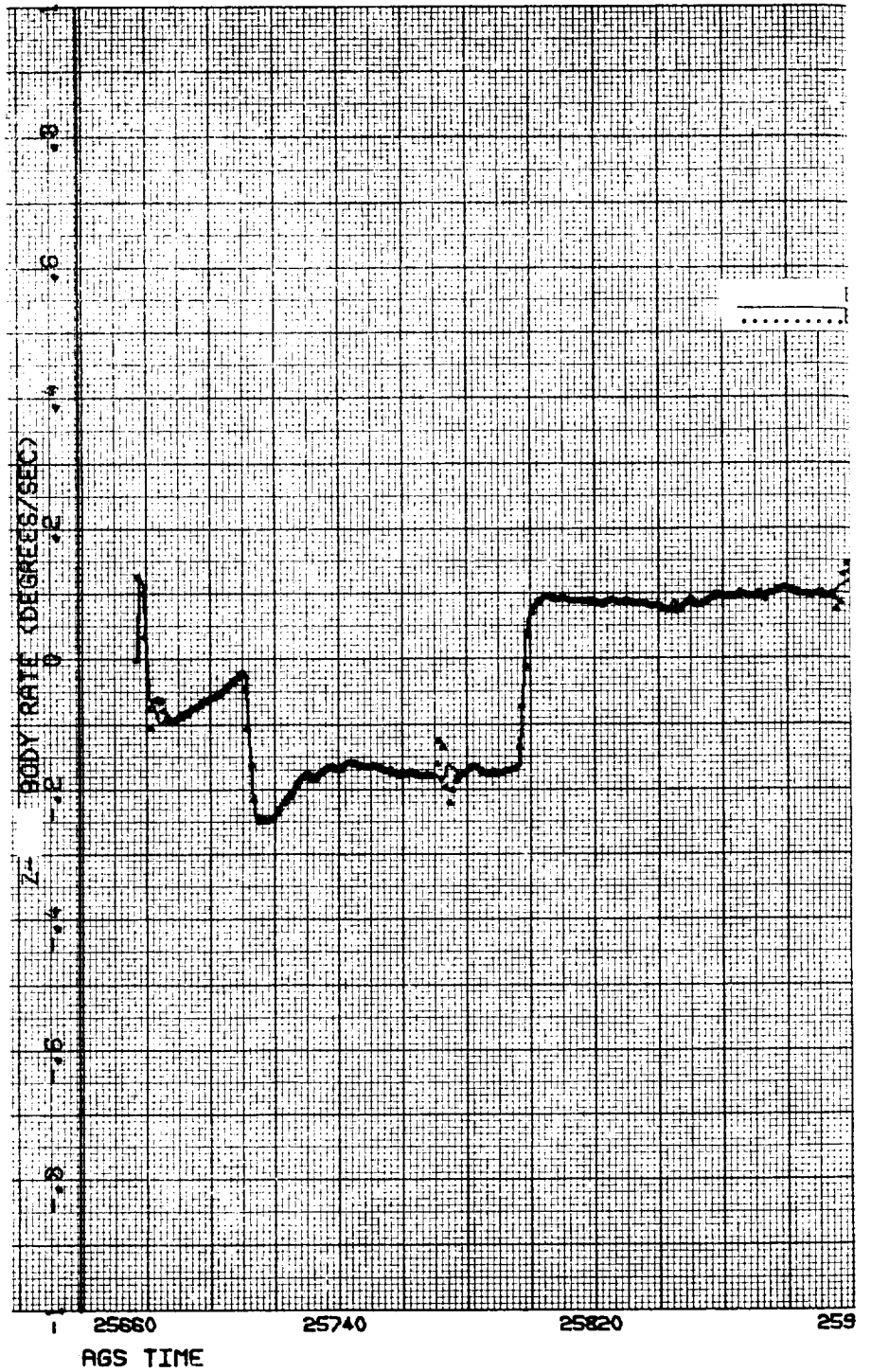
FOLDOUT FRAME |

Figure 4-27 Z Body Rate



FOLDOUT FRAME 2

APOLLO 9 LM AGS FREE FLIGHT



FOLDOUT FRAME 3

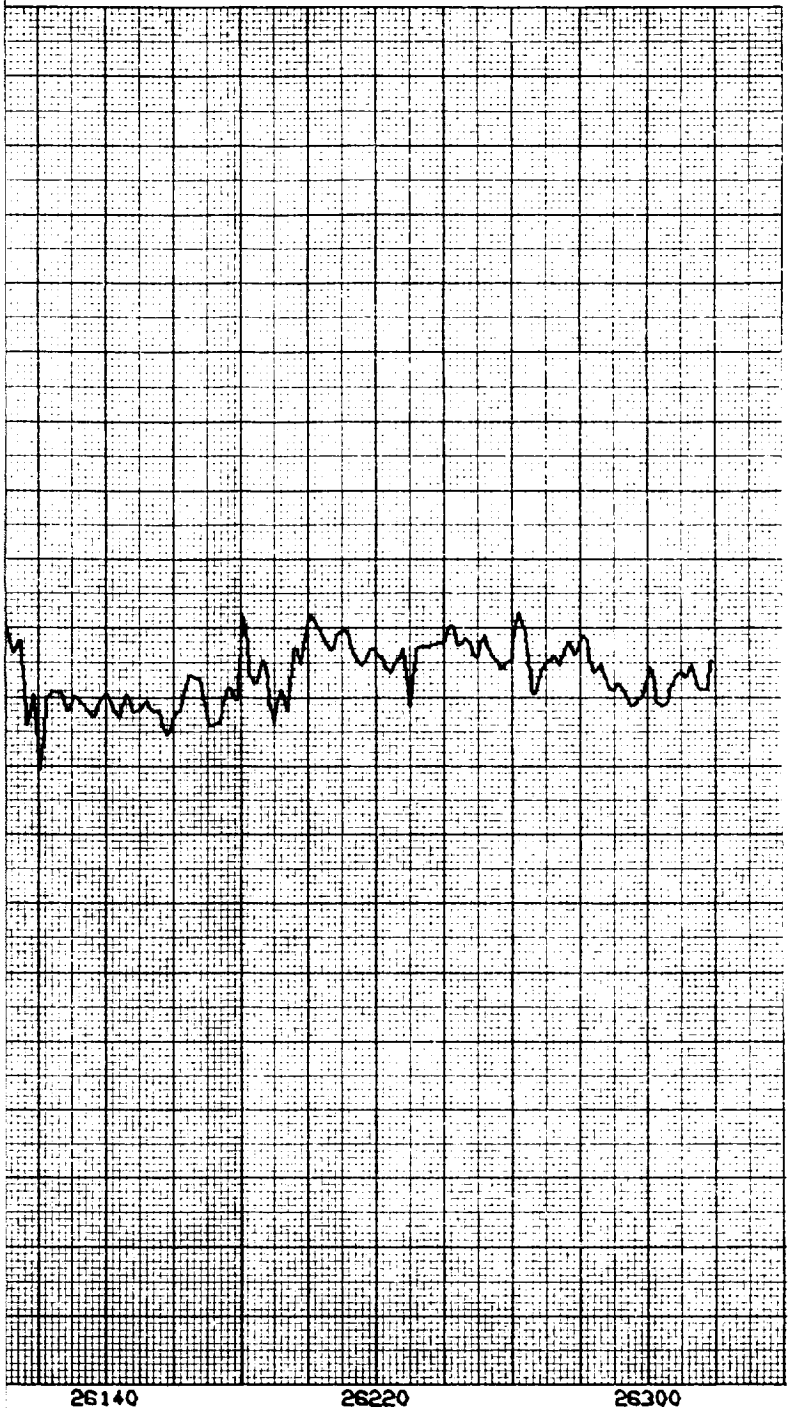
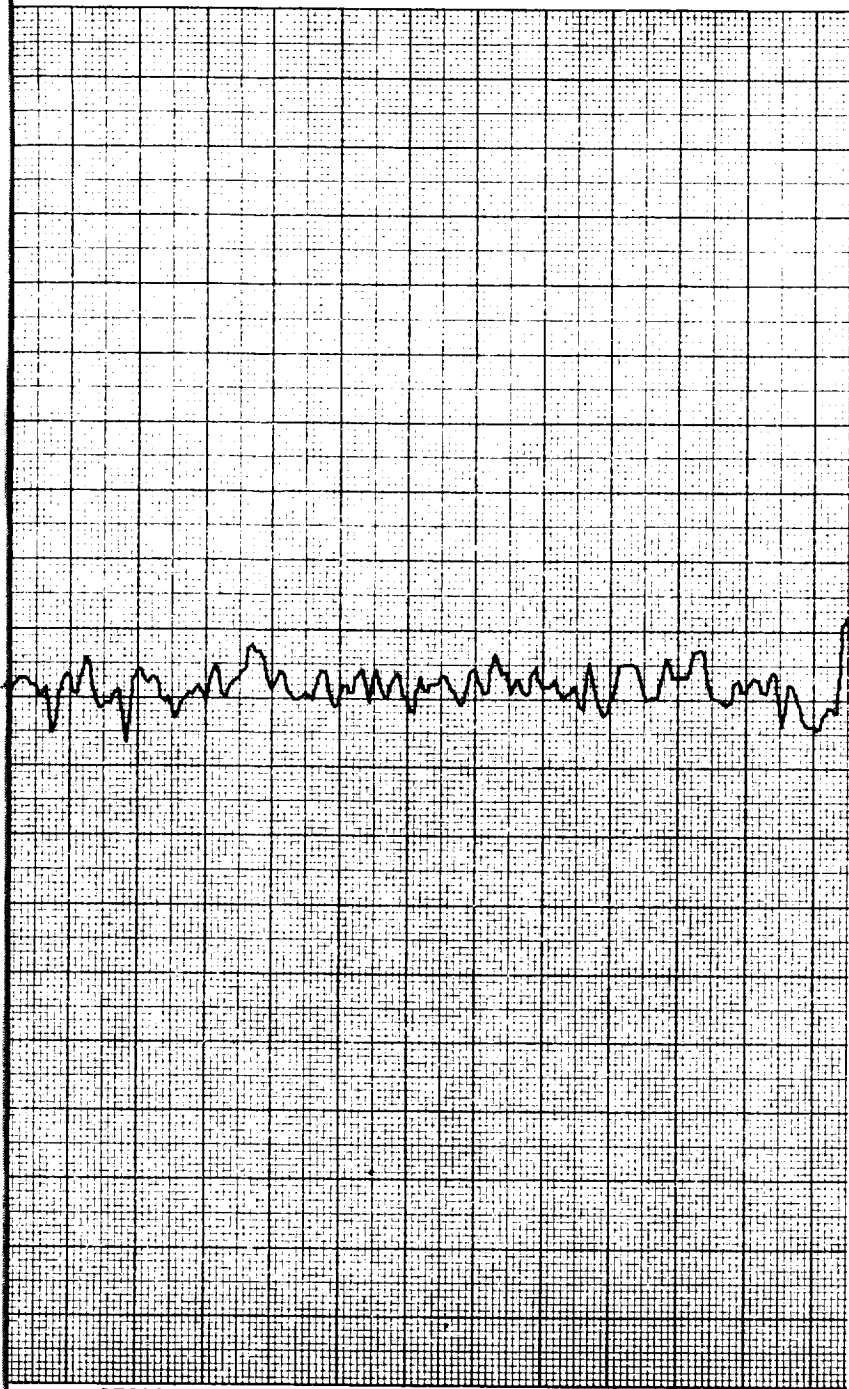


Figure 4-28. X Integrated Body Rate Difference

4-49

FOLDOUT FRAME



25900

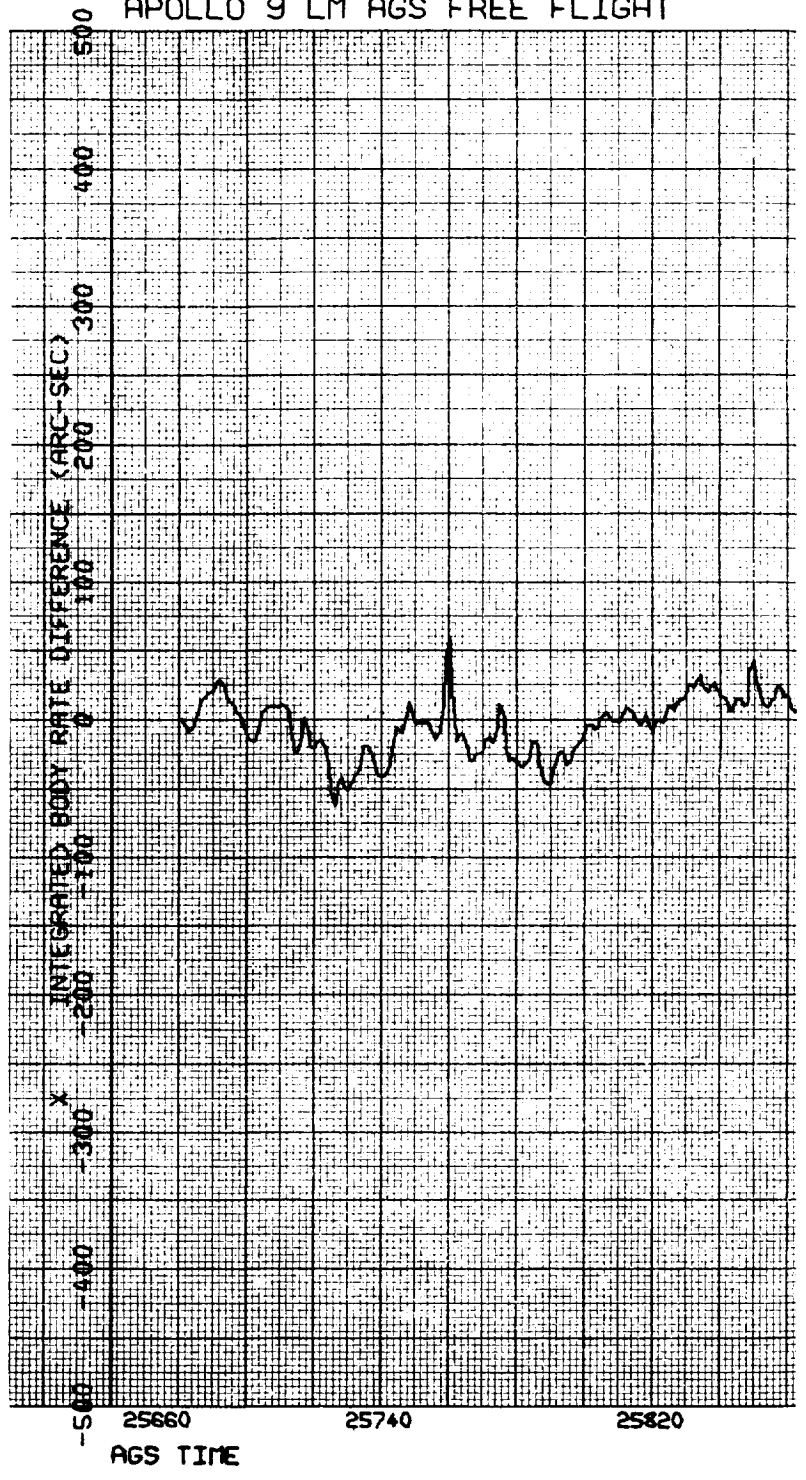
25980

26060

FOLDOUT FRAME 2

(1) 1000

APOLLO 9 LM AGS FREE FLIGHT



EOLDOUI FRAME 3

1000

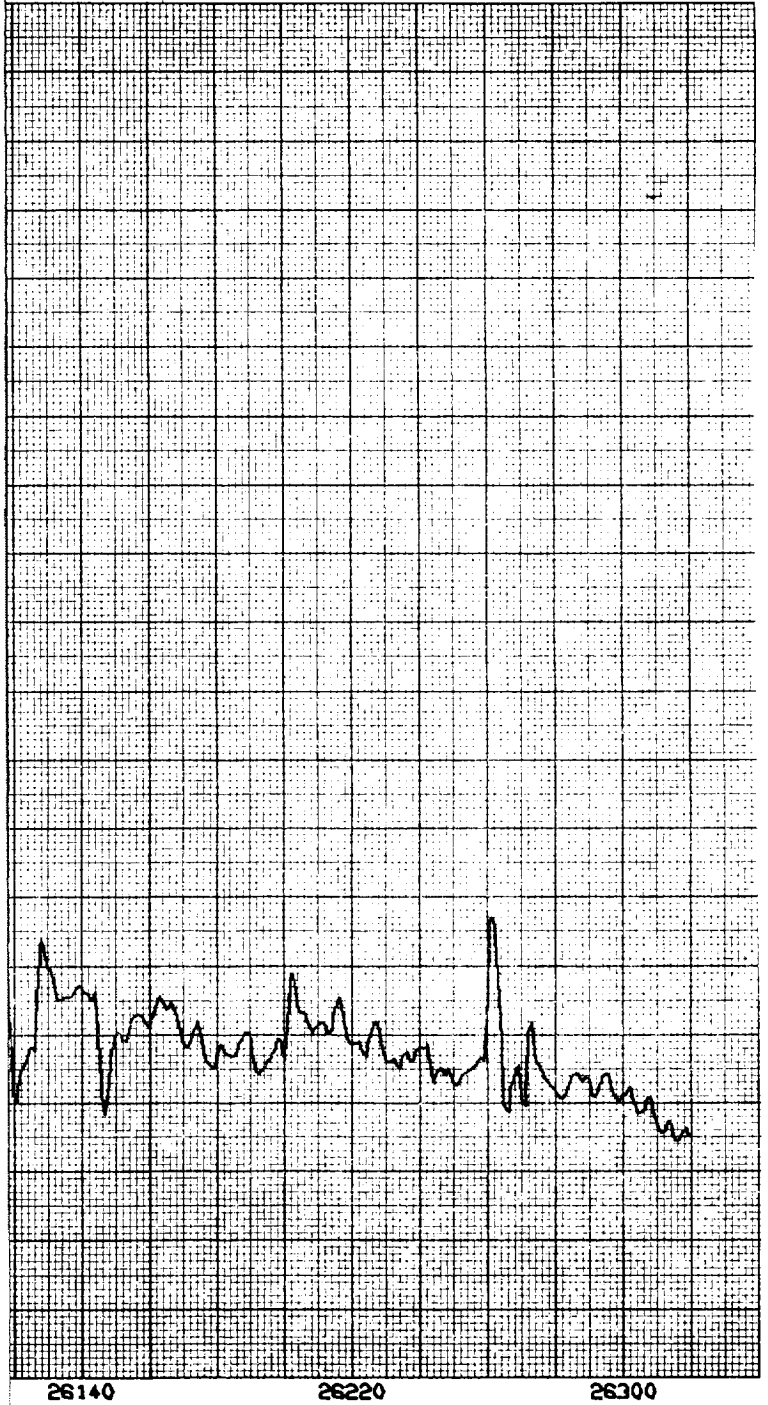
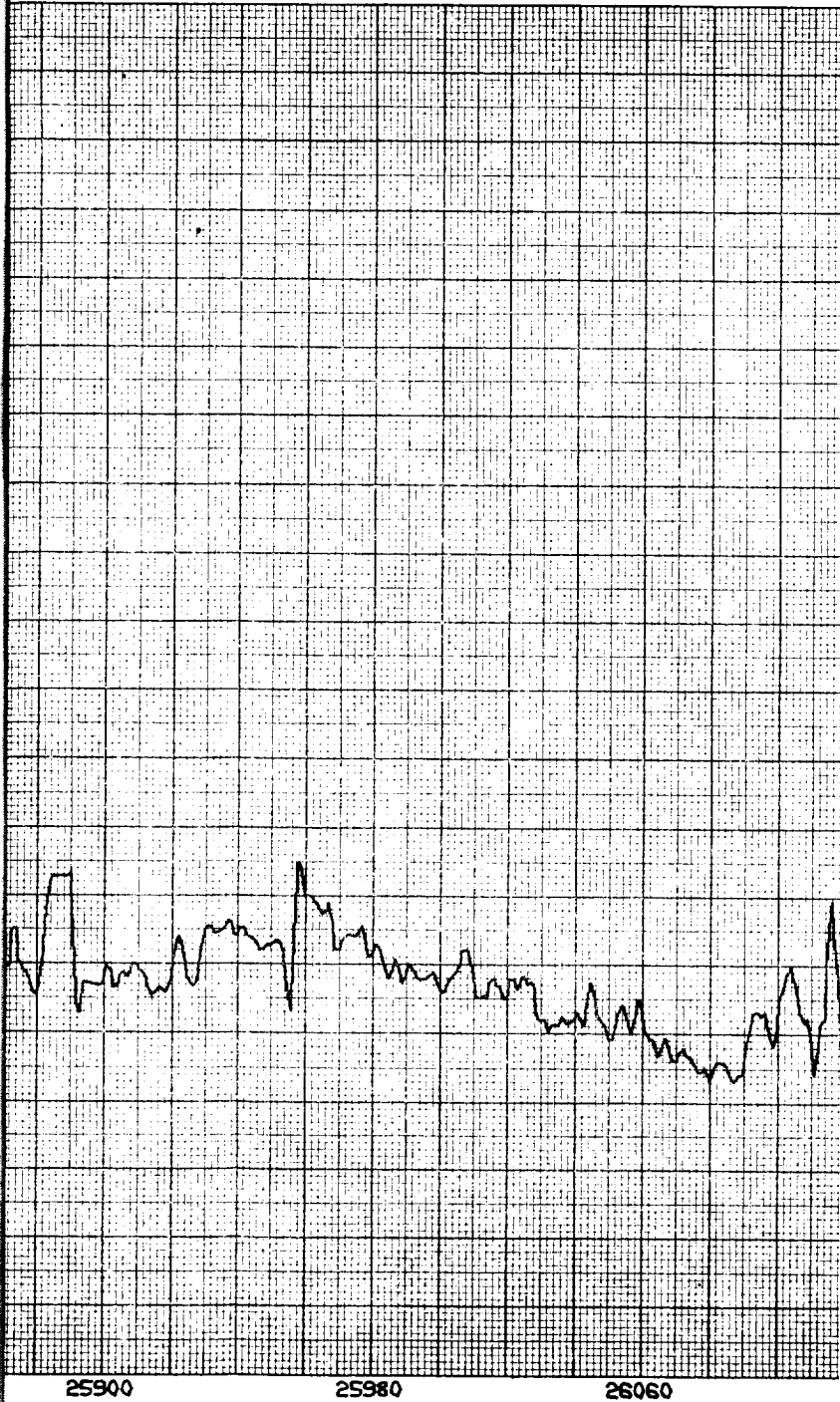
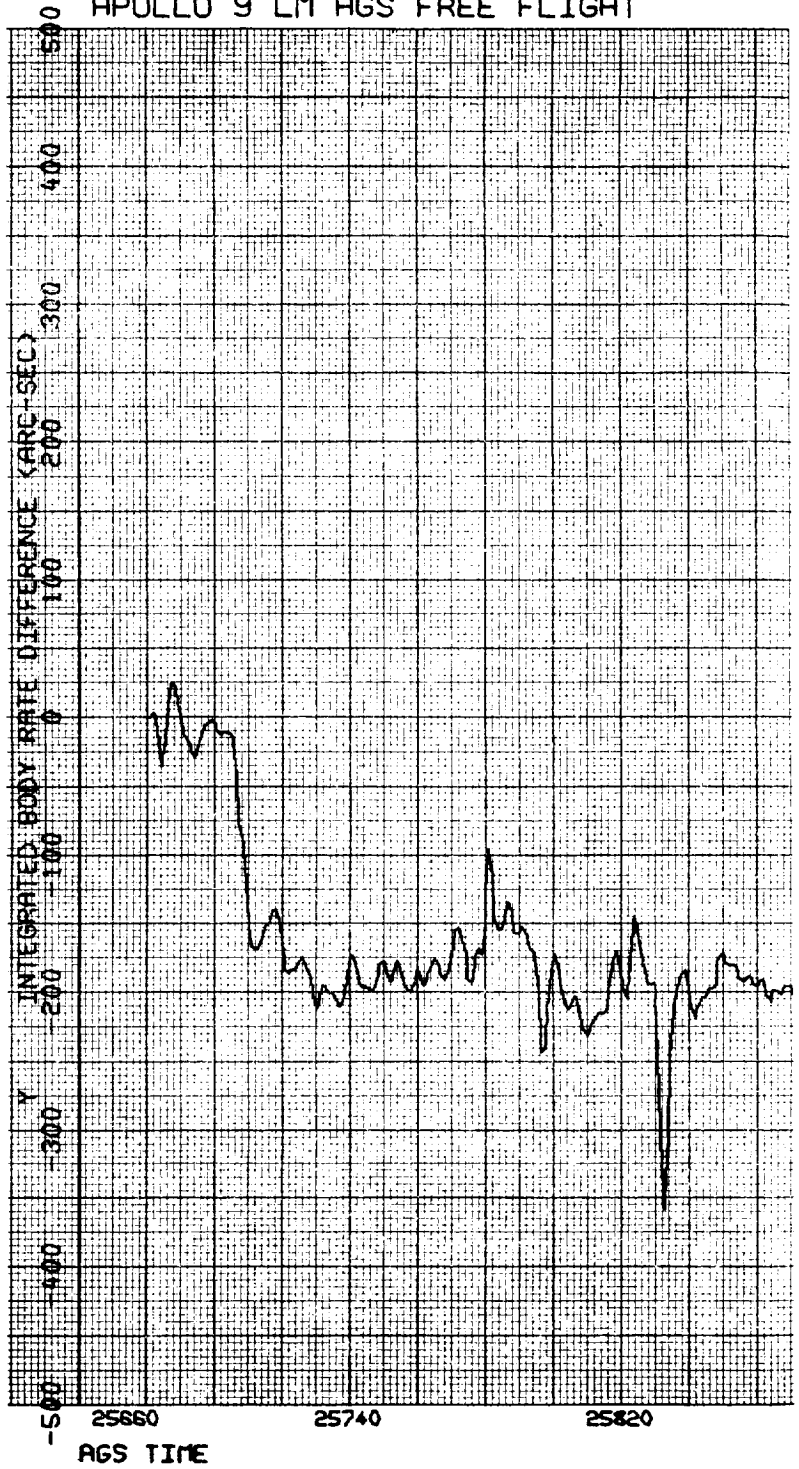


Figure 4-29. Y Integrated Body Rate Difference



EOLDOUT FRAME 2

APOLLO 9 LM AGS FREE FLIGHT



FOLDOUT FRAME 3

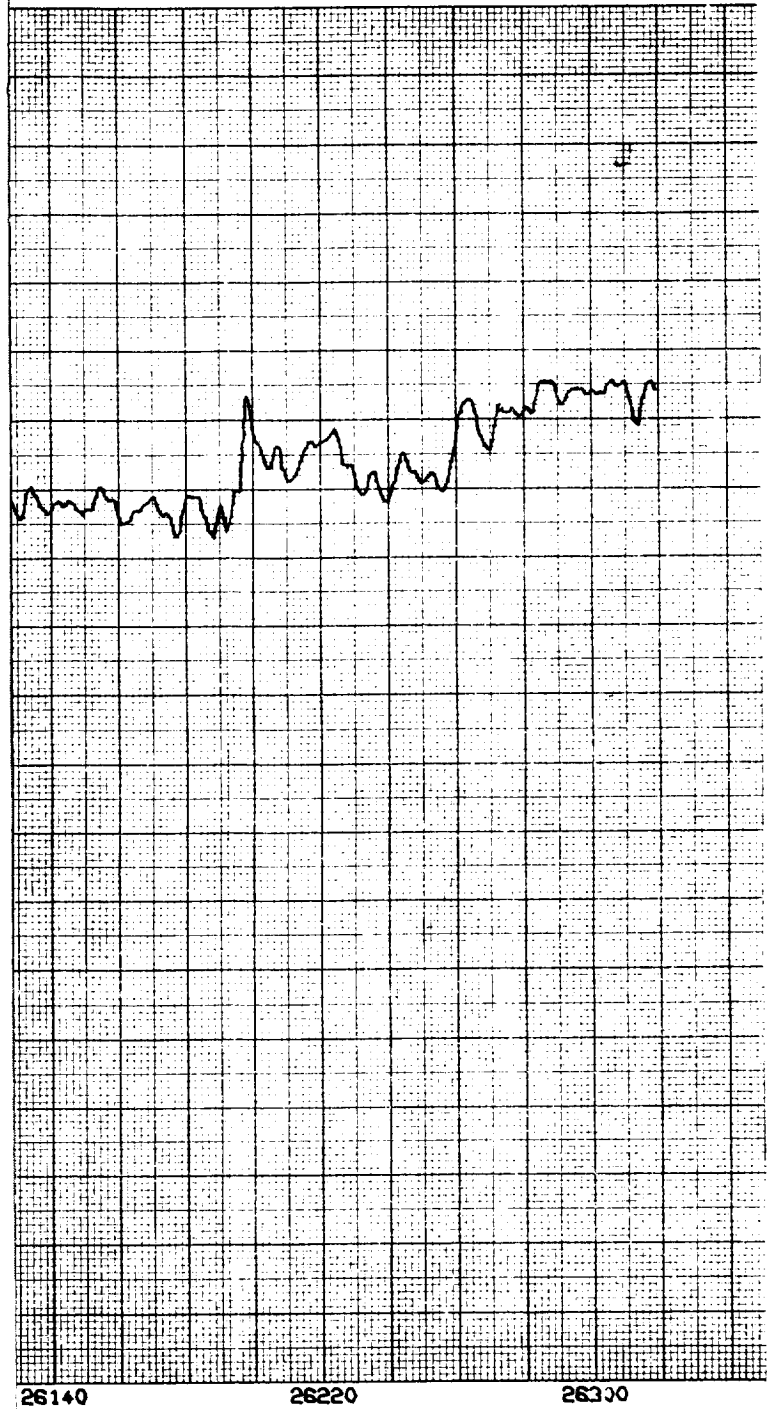


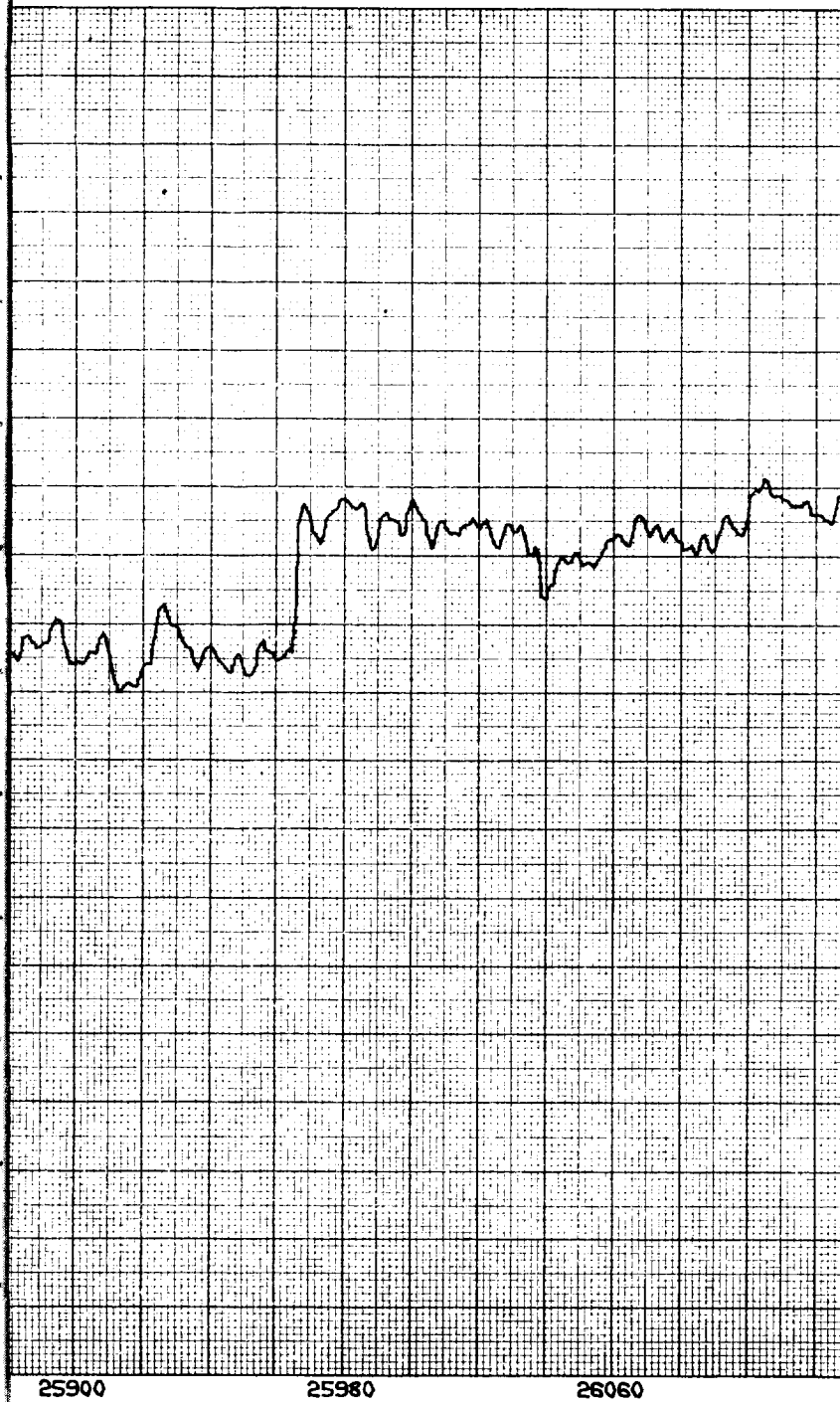
Figure 4-30. Z Integrated Body Rate Difference

FOLDOUT FRAME |

4-53

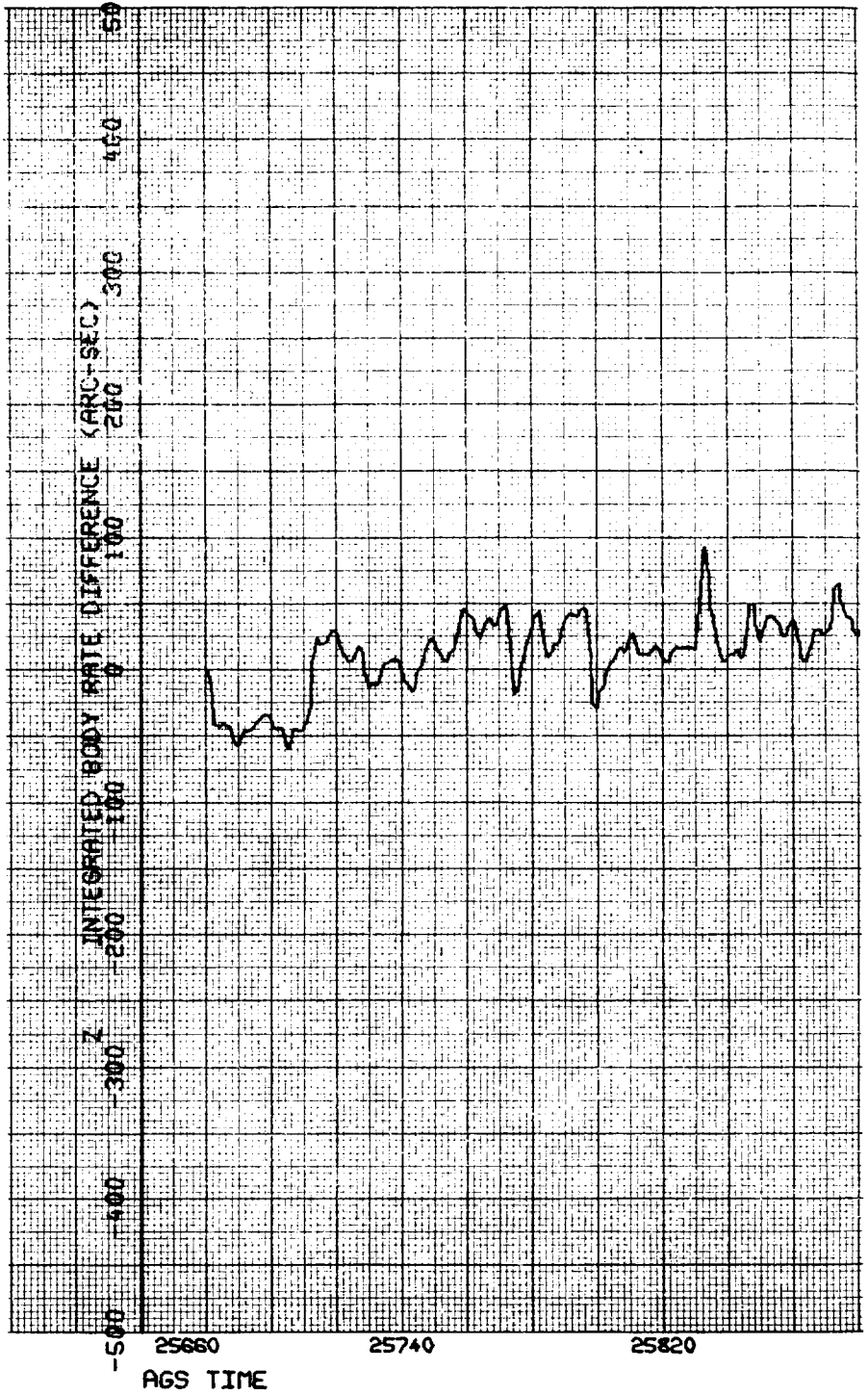
NASA — MSC

MSC 2838-70



FOLDOUT FRAME 2

APOLLO 9 LM AGS FREE FLIGHT



FOLDOUT FRAME 3

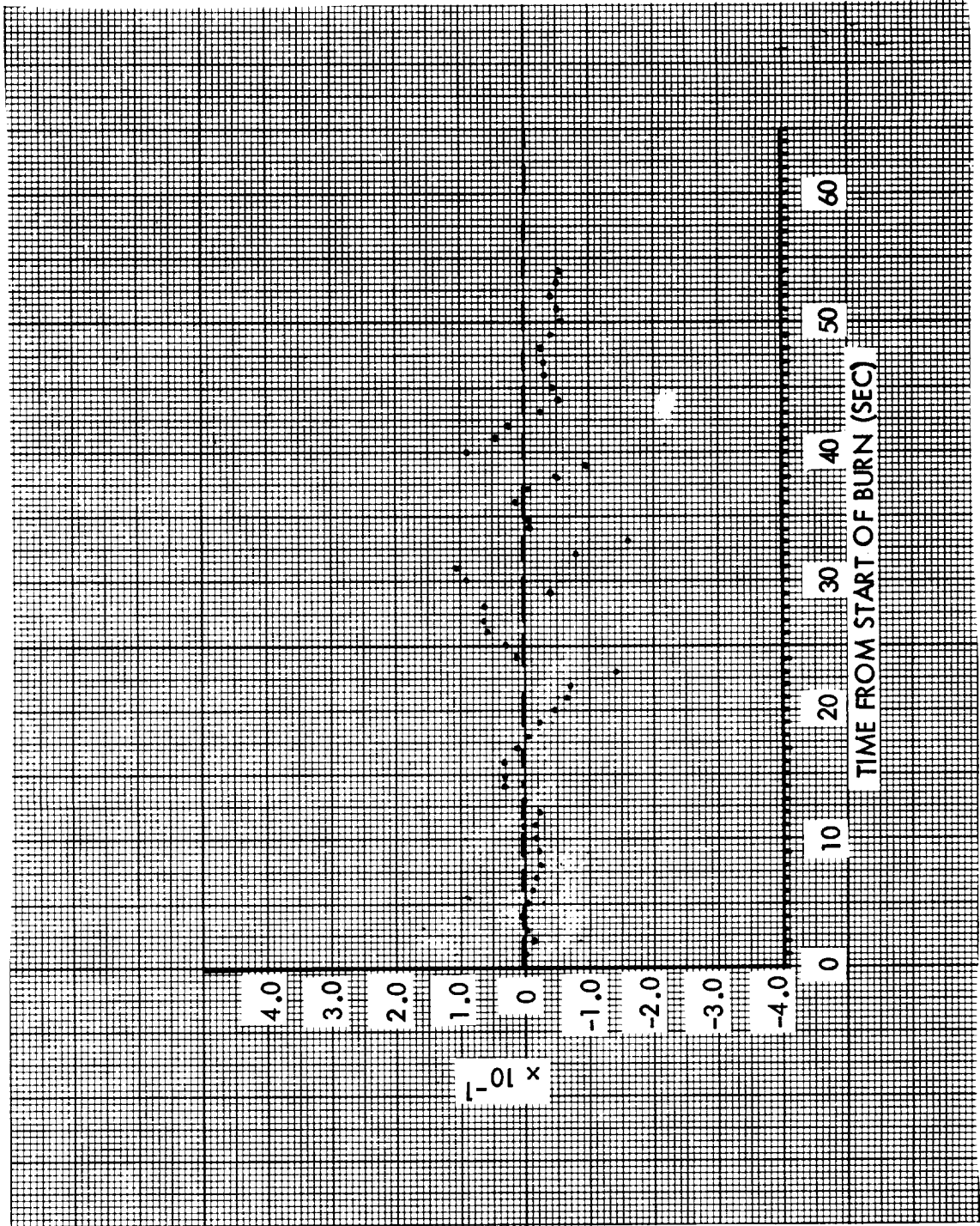


Figure 4-31. $\Delta \dot{X}$ Insertion Burn AGS/PGNCS Velocity Residuals

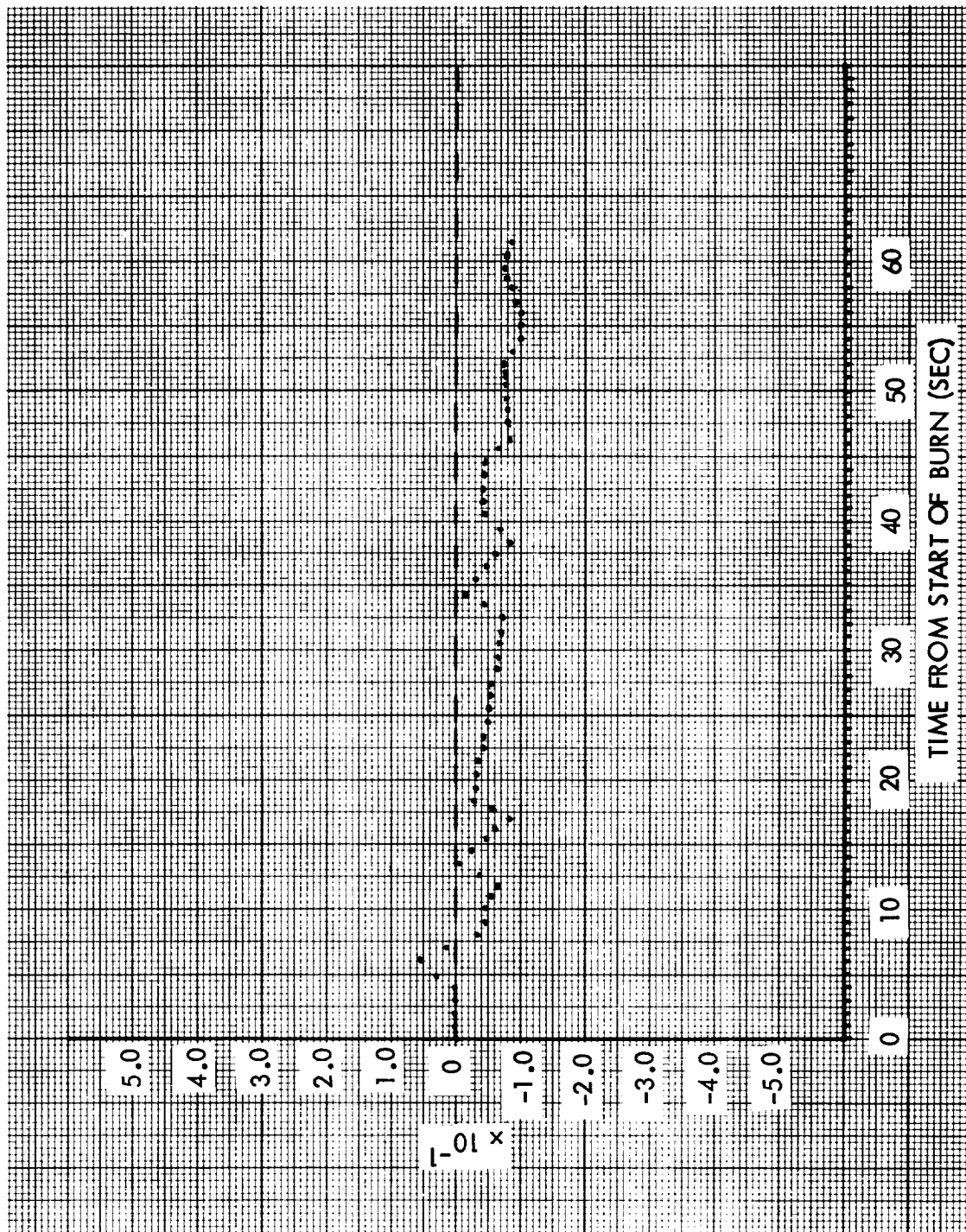


Figure 4-32. ΔY Insertion Burn AGS/PGNCS Velocity Residuals

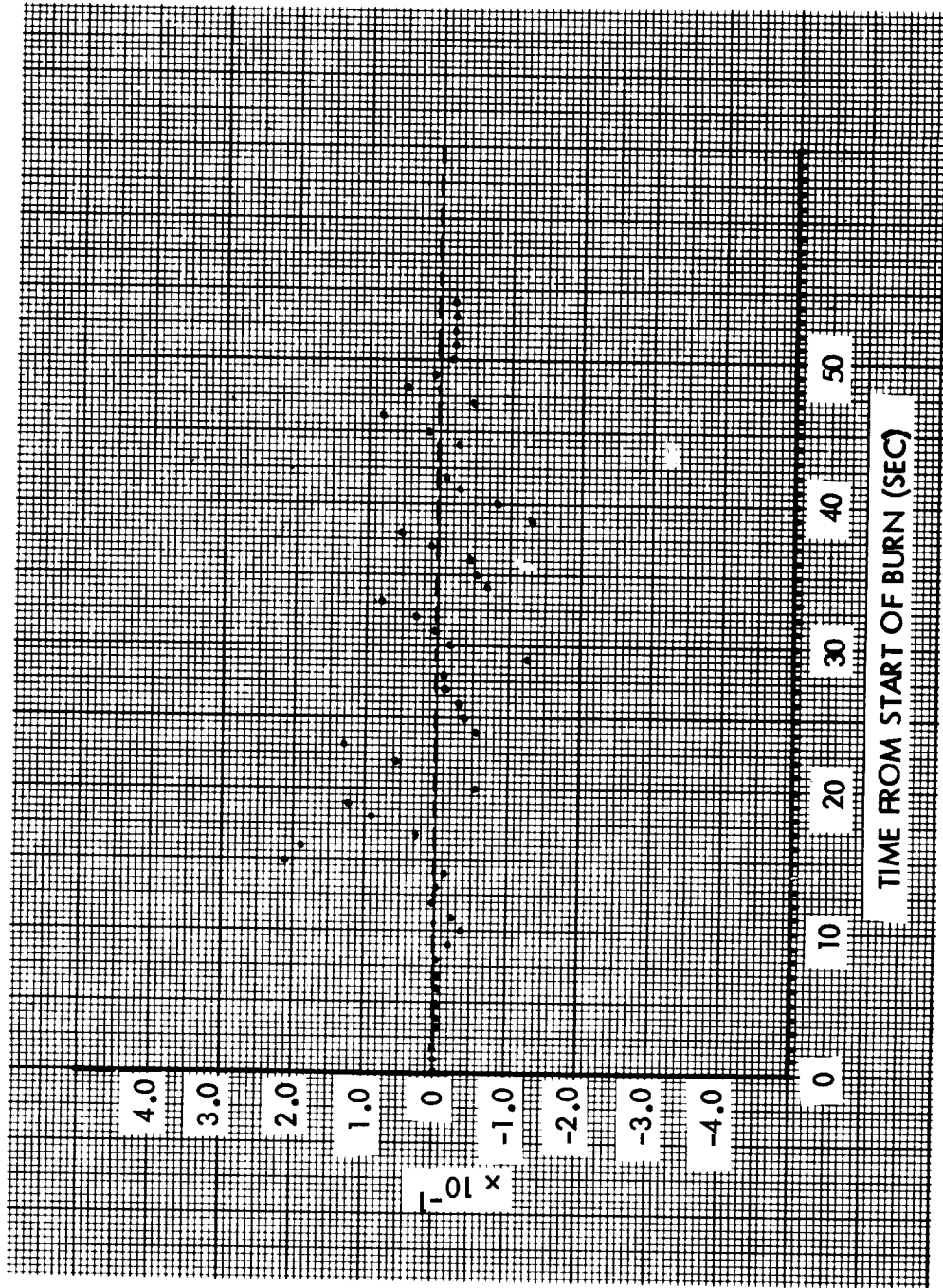


Figure 4-33. ΔZ Insertion Burn AGS/PGNCS Velocity Residuals

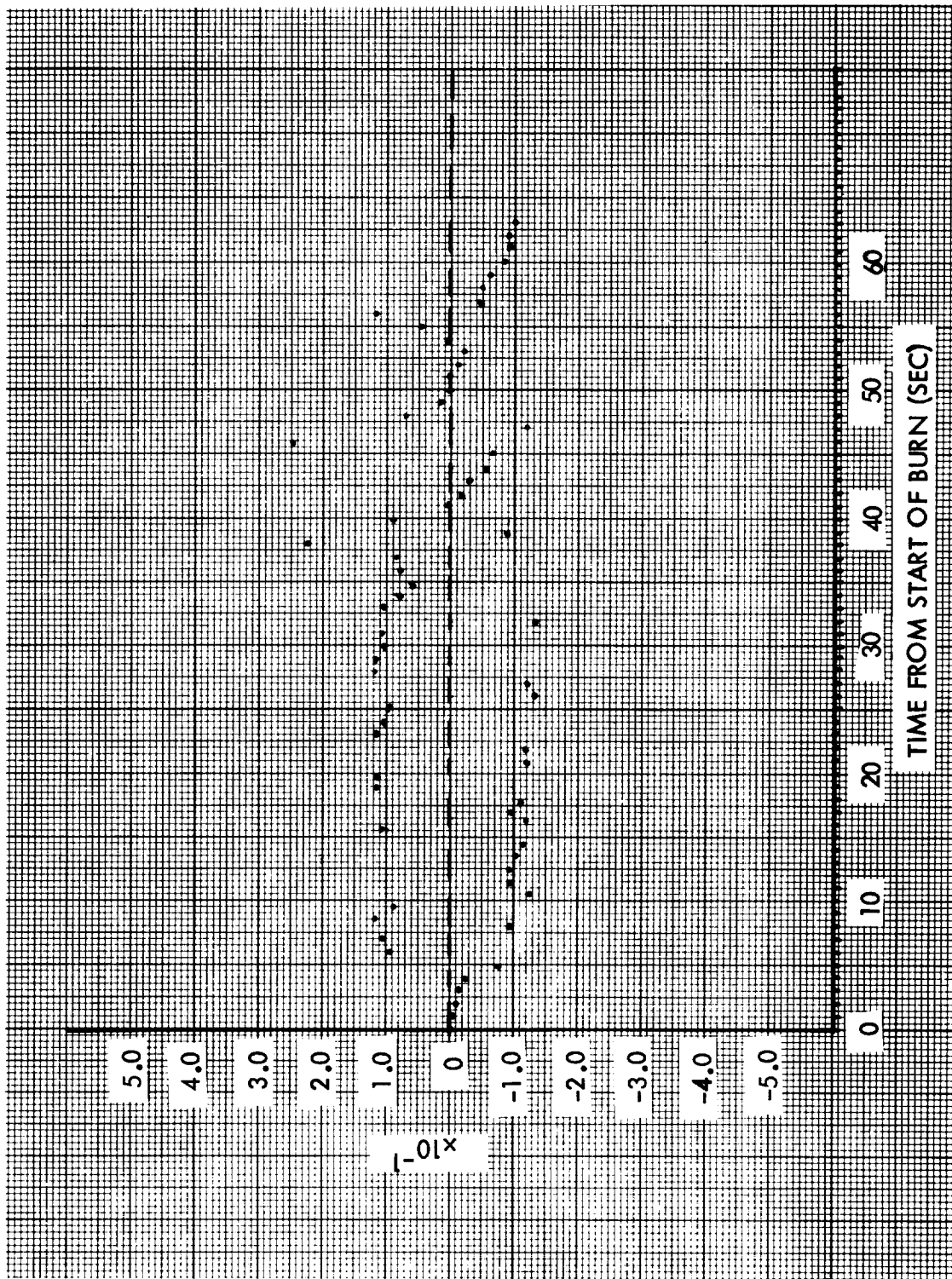


Figure 4-34. CSI Burn AGS/PGNCS Velocity Residuals

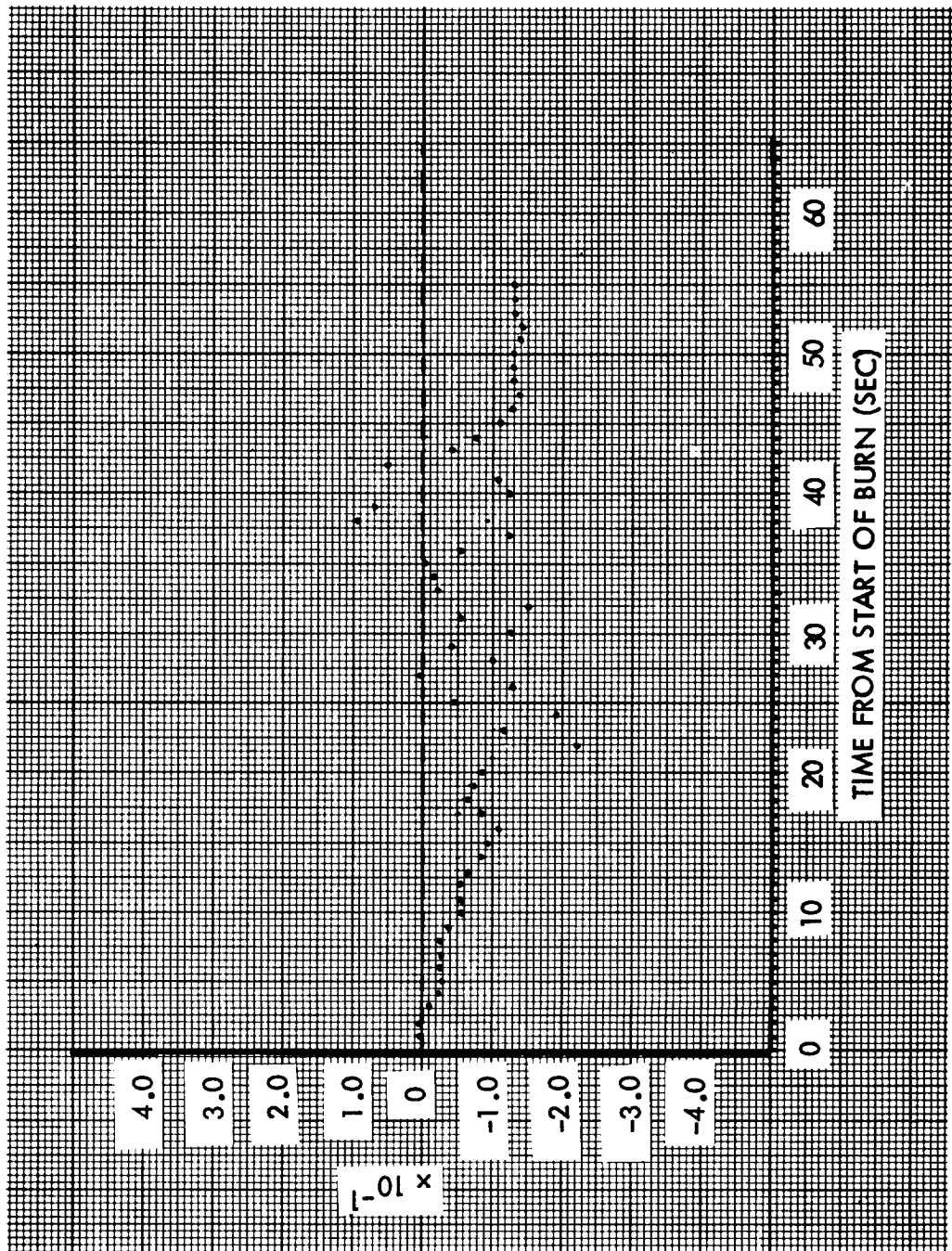


Figure 4-35. CSI Burn AGS/PGNCS Velocity Residuals (ΔY)

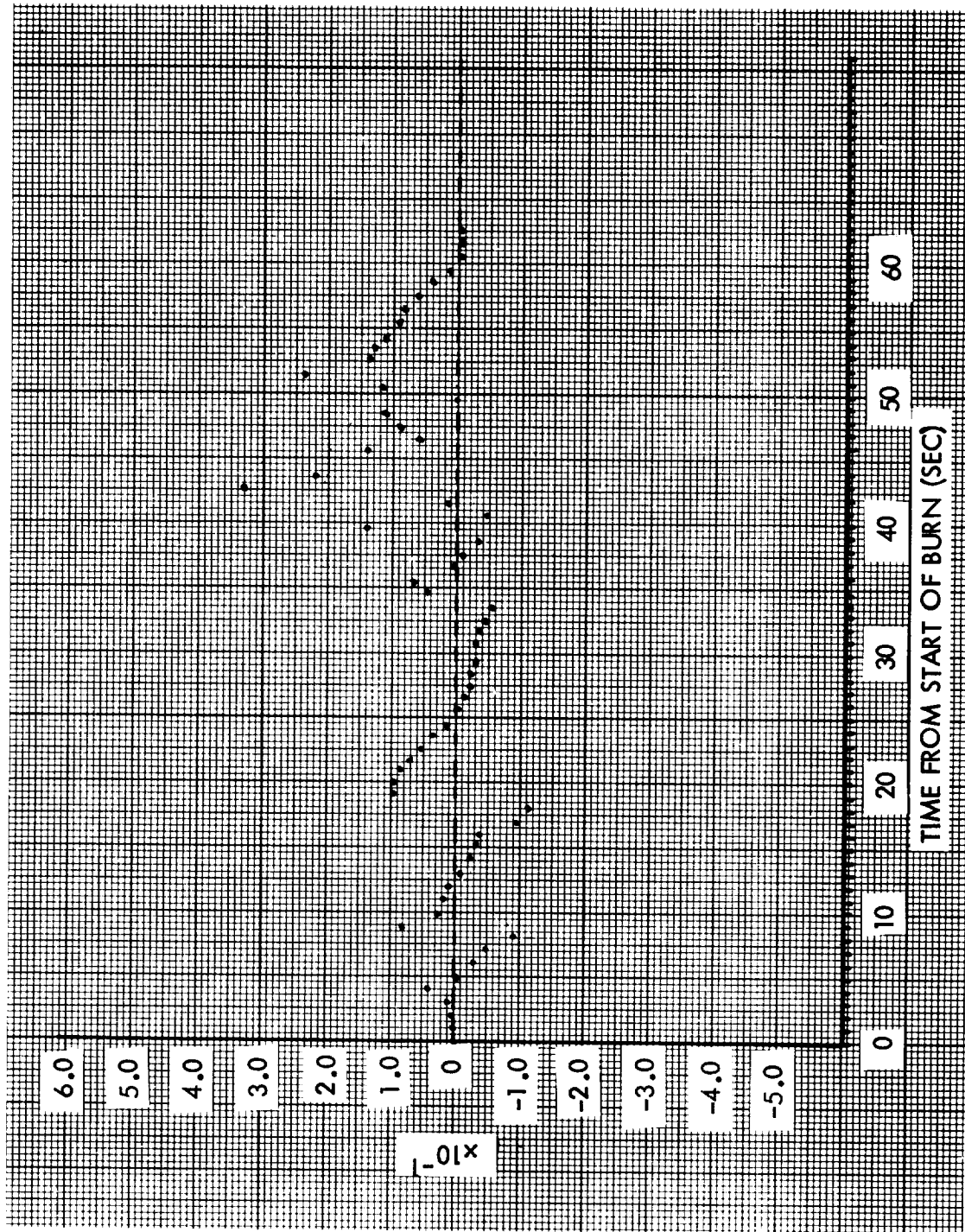


Figure 4-36. CSI Burn AGS/PGNCS Velocity Residuals (ΔZ)

5. FUNCTIONAL PERFORMANCE

This section describes the ASA flight environment and contains a discussion of functional performance and/or anomalies.

5.1 FLIGHT ENVIRONMENT

5.1.1 Flight Vibration Levels

Vibration levels during the two major burns were examined utilizing data from a set of linear instrumentation pickups mounted on the Guidance Nav-base. These data were used because the pickups were closest to the ASA. Typical peak vibration levels observed from oscillograms are given in Table 5-1. The vibration magnitudes during the burns were approximately the same as the levels observed prior to thrusting.

Table 5-1. Nav-Base Linear Vibration

Axis	Pre-Burn g(P-P)	Docked DPS Burn g(P-P)	APS Depletion Burn g(P-P)
X	1.2	1.2	1.3
Y	1.3	0.8	1.0
Z	0.5	0.5	0.6

The power spectral density profiles observed for translational vibration were well within the LSP-300-37F specification (reference 9). Values from the PSD time samples which are applicable to gyro and accelerometer frequency response ranges are given in Table 5-2.

5.1.2 Input Voltages

No AGS input power interruptions were reported. LM power sources and distribution systems apparently performed normally.

5.1.3 ASA Temperature

The ASA block temperature reading was the normal 120°F for most of the flight. An increase to 121°F was reported. Since this increase was within the telemetry instrumentation accuracy of $\pm 4^\circ\text{F}$, it was not considered a significant change.

Table 5-2. Sample Vibratory Levels

Axis	Pre-Burn Time Sample* — 49H40M 15s	Docked DPS Burn	APS Depletion Burn Time Sample* — 101H59M 11s	LSP 300-37F Values for Level II
X	DATA NOT CONSIDERED VALID			$1.6 \times 10^{-3} \text{ g}^2/\text{cps}$ at 70 cps
Y	$2.8 \times 10^{-6} \text{ g}^2/\text{cps}$ at 180 cps 0.087g (rms)	$2.8 \times 10^{-6} \text{ g}^2/\text{cps}$ at 180 cps rms value not available	$1.1 \times 10^{-4} \text{ g}^2/\text{cps}$ at 68 cps 0.105g (rms)	$1 \times 10^{-4} \text{ g}^2/\text{cps}$ at 180 cps $3.5 \times 10^{-3} \text{ g}^2/\text{cps}$ at 70 cps 0.69g rms
Z	$4.0 \times 10^{-6} \text{ g}^2/\text{cps}$ at 30 cps 0.065g (rms)	$6.8 \times 10^{-6} \text{ g}^2/\text{cps}$ at 30 cps rms value not available	$4.2 \times 10^{-5} \text{ g}^2/\text{cps}$ at 68 cps 0.091g (rms)	$4 \times 10^{-5} \text{ g}^2/\text{cps}$ at 30 cps $6 \times 10^{-4} \text{ g}^2/\text{cps}$ at 70 cps 0.67g rms

*PSD data obtained with 2000 cps low-pass filter-bandwidth of 6.09 cps.

5.2 AGS FUNCTIONAL ANOMALIES

Several AGS procedural difficulties were experienced during flight and are discussed in the MSC Mission Report. Two apparent functional anomalies were also indicated; a continuous AGS Caution and Warning light and inadvertent illumination of the DEDA Operation Error Light. The operator error light problem has been attributed to a faulty pushbutton on the DEDA. The continuous Caution and Warning light was not the result of an AGS functional failure and was probably caused by a failure in the Caution and Warning circuitry downstream of the AGS. This problem is discussed in detail below:

5.2.1 Caution and Warning Electronic Assembly (CWEA) Signal

The AGS Caution and Warning light was illuminated at AGS turn-on in the fifth period and remained on for the remainder of this phase. Subsequent investigation of the warning circuits and AGS performance confirmed the assumption that there had not been a functional failure in the AGS.

After verifying from downlink data that: 1) the AEA self-check was GO, 2) the ASA block temperature was steady at 120 degrees, and 3) the

ASA functional operation was nominal (low attitude and velocity drifts and good inflight calibration), it was presumed that the fault was an instrumentation (C and W System or in the cables feeding it) failure, and the indicator was disregarded for the balance of this period.

Shortly after rendezvous, the crew attempted to isolate the problem further. An AGS shutdown was performed. The AGS was then turned on, reinitialized, and aligned. After this sequence, the CWEA light was again illuminated.

The AGS functions monitored by the Caution and Warning System and the corresponding limits are:

<u>ASA Parameter</u>	<u>Warning Level</u>
+28 V precision	25.2 and 30.8 V
+12 V	10.8 and 13.2 V
400 Hz spin supply	385 and 415 Hz
Block temperature (thermostat)	More than $150 \pm 5^{\circ}\text{F}$
AEA	
Test Mode Fail Indicator (On if AEA fails self-test)	Off/On

Figure 4.2.3.1 is a block diagram illustrating the AGS/CWEA interface.

Independent positive verification exists from downlink data that:

- 1) The AEA self-test was GO, the test mode fail indicator was off
- 2) The ASA block temperature was normal, $120^{\circ} \pm 1^{\circ}$.

The AGS spin supply was not 15 Hz ($\approx 4\%$) high or low. This would have caused 4% errors in gyro scale factors and extreme errors in AGS attitude after large rotations. Data observed when the CWEA light was on did not indicate any such errors.

Data was examined during the interval between 92:35:49 and 92:54:41. This time interval was shortly after the LM separated from the CSM and included LM rotations performed in order that the CSM

could accomplish a visual inspection of the LM exterior structure, Tabulated below are the net rotation angles, the anticipated errors if a 4% gyro scale factor existed, and the actual observed error.

<u>PGNCS Euler Angle</u>	<u>Measured Net Rotation</u>	<u>Expected Angular Error if Scale Factor Differed by 4%</u>	<u>Observed Error</u>
θ	200°	8°	0.031°
ψ	63°	2.5°	0.091°
ϕ	124°	5.0°	0.045°

The observed errors were determined by comparing the CDU angles and the AGS direction cosines over the time interval noted. This data indicated that no large scalefactor errors were present.

An inflight calibration of the gyros and accelerometers was performed with excellent results, thereby eliminating the +12 and +28 precision supplies as causes of the warning. Extrapolation of existing test and analysis data on power supply sensitivities gives estimates of greater than 1.0 deg/hr gyro drift and greater than 1000 ppm gyro scale factor error for a 10% change in either the 12- or 28-V precision supply. Flight data analysis shows no such change. Further, no failure history exists in which either of these supplies varied 10% or more and the ASA continued to operate.

The nonfunctional or instrumentation circuitry within the AGS incorporates several resistors, a thermostat, and an AEA output-driver circuit (see Figure 5-1). None of these components has any history of failure in the AGS. The thermostat has been completely reliable even during vibration testing, and is normally at 120°F , 30° below its set point of 150°F .

It was concluded that the C and W indication resulted from an instrumentation failure, presumably external to the AGS since the preponderance of the circuitry is external to the AGS.

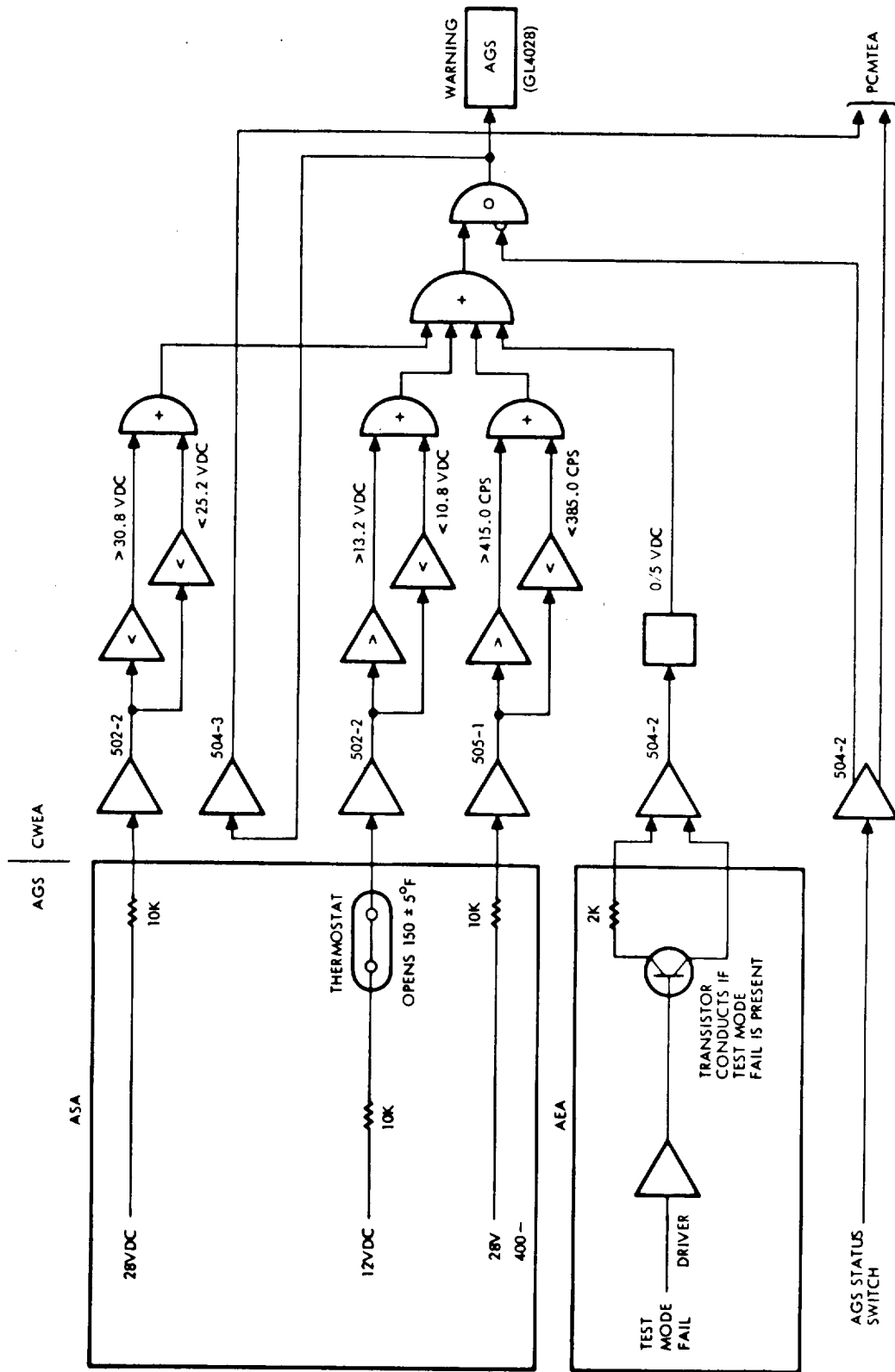


Figure 5-1. Block Diagram of CWEA-AEA Circuitry

|

6. REFERENCES

1. "LM AGS Postflight Data Reduction and Analysis Plan (U)," 05952-6196-T000, 8 March 1968, TRW Systems Group, Redondo Beach, California.
2. "LM AGS Capability Estimate," 03358-6134-R000, 15 May 1969, TRW Systems Group, Redondo Beach, California.
3. "Mission Requirements 'D' Type Mission," SPD8-R-005 Revision 1, 6 November 1968, NASA Manned Spacecraft Center, Houston, Texas.
4. "Apollo 9 Mission Report," MSC-PA-R-69-2, May 1969, NASA Manned Spacecraft Center, Houston, Texas.
5. "Apollo IX Guidance, Navigation and Control System Performance Analysis Report," 11176-232-R0-00, 15 May 1969, NASA Manned Spacecraft Center, Houston, Texas.
6. "Abort Guidance Section Software GFE Performance and Interface Specification (U)," LSP-500-1A, 4 February 1969, Grumman Aircraft Engineering Corporation.
7. "Estimates of Worst Case Gyro and Accelerometer Bias Shifts for In-Flight Calibrations," IOC 7222.14-626A, 20 November 1968, TRW Systems Group, Redondo Beach, California.
8. "ASA 015 Error Model KSC Data," IOC 7222.14-679, 27 January 1969, TRW Systems Group, Redondo Beach, California.
9. "Abort Sensor Assembly, Guidance, Navigation and Control Subsystem, Design Control Specification for," LSP-300-37F, 3 April 1968, Grumman Aircraft Engineering Corporation, Bethpage, New York.

|

APPENDIX I
PREFLIGHT HISTORY AND PERFORMANCE

The designated flights units were:

Unit
ASA 015
AEA 121
DEDA 112

The ASA operating time at launch was 752.5 hours.

The preflight stability of the ASA flight compensated parameters was very good as judged by comparisons with time stability values published in the "LM AGS Capability Estimate".

A summary of preflight testing of the ASA is shown in Table I-1. The ASA was sent to HSSC for heater modification after system level tests at KSC indicated an EMI problem when the ASA was in the fast warmup mode. Upon return to KSC the ASA was functionally checked prior to missile installation. Valid system performance was demonstrated.

Table I-2 shows a tabulation of the ASA calibration results for the flight compensated parameters. All results indicated normal performance. No waivers or discrepancies were reported for these values. Established test limits were exceeded for other parameters including accelerometer bias discrepancy and gyro asymmetry results, but these violations were waived as inconsequential.

The accelerometer bias discrepancy deviations were attributed to test fixture problems. The asymmetry violations were waived when considered in view of new proposed bounds.

On 16 January 1969, the Data Evaluation Committee at KSC reviewed the data and accepted ASA 015 for flight use.

Time-history plots of the gyro and accelerometer biases are shown in Figures I-1 and I-2.

Table I-1. ASA 015 Preflight Test History

<u>Dates</u>	<u>Location</u>	<u>Testing</u>
5/27-6/5/68	HSSC (Acceptance)	8 sets of cals and asymmetry test
6/8	GAEC/BPA	1 set of cals and asymmetry test
6/18-7/21	KSC/MSOB	2 sets of cals and 5 EPC's
8/2	(Shipped to HSSC for EMI fast warm-up modification)	
8/8	HSSC	2 sets of cals and asymmetry test after modification
8/10	KSC/LAB	ASA functional check
8/14-9/30	KSC/MSOB	3 EPC's
10/1/68-1/10/69	KSC/MSOB/VAB	5 sets of cals, 3 EPC's; accel. and gyro freq. response and gyro asymmetry test
1/16-2/13-69	KSC/PAD	6 EPC's (two sets)
2/12/69	KSC/PAD	Countdown Demonstration Test start
2/16/69	KSC/PAD	Final EPC
2/17/69	KSC/PAD	CDDT End
3/3/69	KSC/PAD	Launch

Table I-2. ASA 015 Field Test Performance

ASA 015 Performance Parameter	HSSC 5/27/68	HSSC 5/27/68	HSSC 5/28/68	HSSC 5/29/68	HSSC 5/30/68	HSSC 6/1/68	HSSC 6/3/68	HSSC 6/3/68	HSSC 6/3/68	HSSC 6/5/68	GAEC/BP 6/8/68
Gyro/PTSA Bias (IAV) B _X ^G	-0.19	-0.21	-0.24	-0.20	-0.17	-0.25	-0.19	-0.25	-0.19	-0.28	-0.35
(deg/hr) (OAV) B _Y ^G	-0.42	-0.43	-0.44	-0.48	-0.42	-0.44	-0.43	-0.49	-0.43	-0.46	-0.54
(OAV) B _Z ^G	-0.05	0.00	-0.07	-0.04	-0.11	-0.19	-0.09	-0.03	-0.09	-0.07	-0.34
Gyro/PTSA Scale ΔS_Y^G	-2326	-2324	-2364	-2333	-2337	-2335	-2332	-2325	-2325	-2324	-2314
Factor @ 2.62 °/sec ΔS_Y^G	-2431	-2428	-2442	-2443	-2465	-2458	-2474	-2455	-2455	-2435	-2447
ΔS_Z^G	2001	2025	2007	1996	2001	2051	2044	2040	2040	2041	2023
Gyro Spin Axis U _X ^S	0.31	0.28	0.29	0.36	0.33	0.24	0.30	0.26	0.30	0.37	0.07
Mass Unbalance (deg/hr/g)											
Accel/PTSA Bias (IAV) B _X ^A	20	11	21	5	7	21	32	5	32	18	27
(μg 's) (IAV) B _Y ^A	-33	-32	-18	-33	-31	-42	-40	-34	-40	-38	-20
(IAV) B _Z ^A	115	109	110	95	93	95	101	97	101	85	115
Accel/PTSA Scale Factor ΔS_X^A	-142	-138	-150	-166	-171	-190	-214	-221	-214	-233	-310
ΔS_Y^A	581	584	570	561	556	541	519	516	519	502	449
ΔS_Z^A	-1077	-1073	-1078	-1091	-1097	-1115	-1131	-1138	-1131	-1146	-1194

Table I -2. ASA 015 Field Test Performance (Continued)

ASA 015 Performance Parameter	KSC 6/18/68	KSC 6/29/68	KSC 7/13/68 (EPC)	KSC 7/15/68 (EPC)	KSC 7/21/68 (EPC)	HSSC 8/8/68	HSSC 8/8/68	KSC 8/14/68 (EPC)	KSC 8/29/68 (EPC)	KSC 9/30/68 (EPC)
Gyro/PTSA Bias (deg/hr)										
(LAV) B _X ^G	-0.19	-0.35	-0.18	-0.20	-0.35	-0.19	-0.21	-0.17	-0.35	-0.35
(LAV) B _Y ^G	-0.43	-0.64	-0.45	-0.39	-0.44	-0.44	-0.40	-0.46	-0.43	-0.43
(OAV) B _Z ^G	-0.18	-0.34	-0.71	-0.81	-0.65	0.01	0.00	0.17	-0.11	-0.13
Gyro/PTSA Scale ΔS _X ^G	-2307	-2337				-2305	-2330			
Factor 2.62 °/sec ΔS _Y ^G	-2415	-2450				-2419	-2432			
ΔS _Z ^G	2042	2015				2049	2029			
Gyro Spin Axis U _X ^S	0.15	0.50				0.63	0.64			
Mass Unbalance (deg/hr/g)										
Accel/PTSA Bias (LAV) B _X ^A	36	73				67	60			
(LAV) B _Y ^A	0	-9				9	9			
(LAV) B _Z ^A	127	121				140	142			
Accel/PTSA ΔS _X ^A	-414	-507				-684	-683			
Scale Factor ΔS _Y ^A	359	282				121	119			
ΔS _Z ^A	-1284	-1359				-1517	-1510			

Table I-2. ASA 015 Field Test Performance (Continued)

ASA 015 Performance Parameter	KSC 10/1/68	KSC 11/14/68	KSC 12/5/68	KSC 12/11/68 (EPC)	KSC 12/11/68 (EPC)
Gyro/PTSA Bias (deg/hr)	(IAV) B _X ^G	-0.25	-0.32	-0.27	-0.58
	(OAV) B _Y ^G	-0.49	-0.46	-0.47	-0.51
	(OAV) B _Z ^G	-0.29	-0.03	0.07	0.19
Gyro/PTSA Scale Factor 2.62°/sec (ppm)	ΔS_X^G	-2288	-2311	-2310	
	ΔS_Y^G	-2426	-2432	-2432	
	ΔS_Z^G	2030	2016	1975	
Gyro Spin Axis Mass Unbalance (deg/hr/g)	U _X ^S	0.79	0.68	0.74	
Accel/PTSA Bias (μg 's)	(IAV) B _X ^A	31	85	78	
	(IAV) B _Y ^A	7	41	19	
	(IAV) B _Z ^A	118	172	178	
Accel/PTSA Scale Factor (ppm)	ΔS_X^A	-829	-933	-943	
	ΔS_Y^A	6	-112	-128	
	ΔS_Z^A	-1612	-1707	-1709	

Table I-2. ASA 015 Field Test Performance (Continued)

ASA 015 Performance Parameter	KSC 12/11/68 (EPC)	KSC 1/6/69	KSC 1/10/69	KSC 1/16/69 (EPC)	KSC 1/16/69 (EPC)	KSC 1/16/69 (EPC)	KSC 2/13/69 (EPC)	KSC 2/13/69 (EPC)	KSC 2/13/69 (EPC)	KSC 2/16/69 (EPC)
Gyro/PTSA Bias (deg/hr)										
(LAV) B _X ^G	-0.50	-0.27	-0.27	-0.42	-0.43	-0.42	-0.41	-0.44	-0.33	
(OAV) B _Y ^G	-0.51	-0.45	-0.47	-0.58	-0.47	-0.57	-0.59	-0.59	-0.56	
(OAV) B _Z ^G	0.14	0.06	-0.06	-0.07	-0.09	-0.09	0.12	0.12	0.16	
Gyro/PTSA Scale Factor @ 2.62°/sec (ppm)										
ΔS _X ^G		-2339	-2316							
ΔS _Y ^G		-2473	-2440							
ΔS _Z ^G		2004	2006							
Gyro Spin Axis U _X ^S		0.92	0.96							
Mass Unbalance (deg/hr/g)										
Accel/PTSA Bias (μg's)										
(LAV) B _X ^A		127	124							
(LAV) B _Y ^A		40	45							
(LAV) B _Z ^A		194	185							
Accel/PTSA Scale Factor (ppm)										
ΔS _X ^A		-981	-993							
ΔS _Y ^A		-173	-185							
ΔS _Z ^A		-1753	-1756							

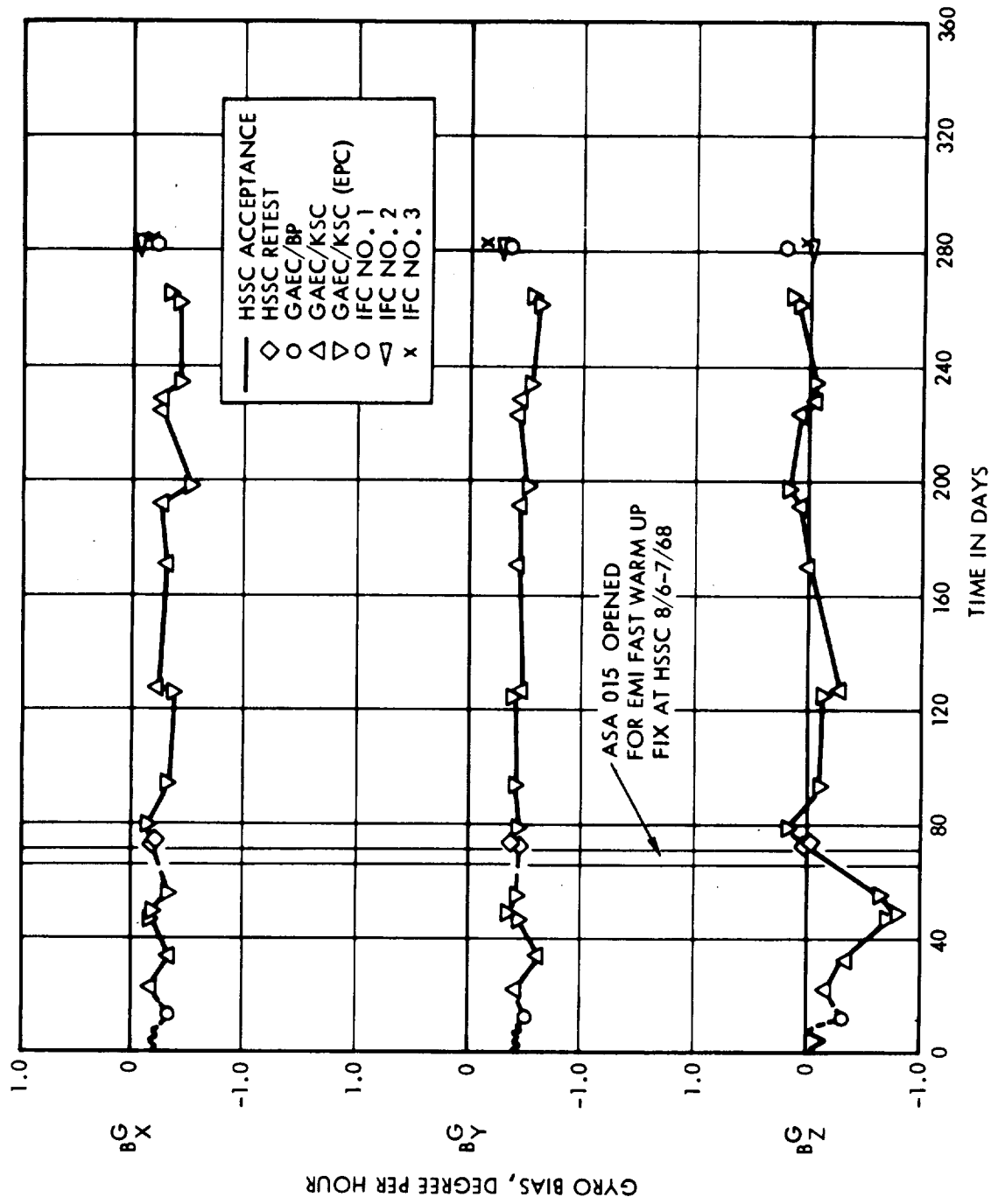


Figure I-1. ASA 015 History of Gyro Calibrations

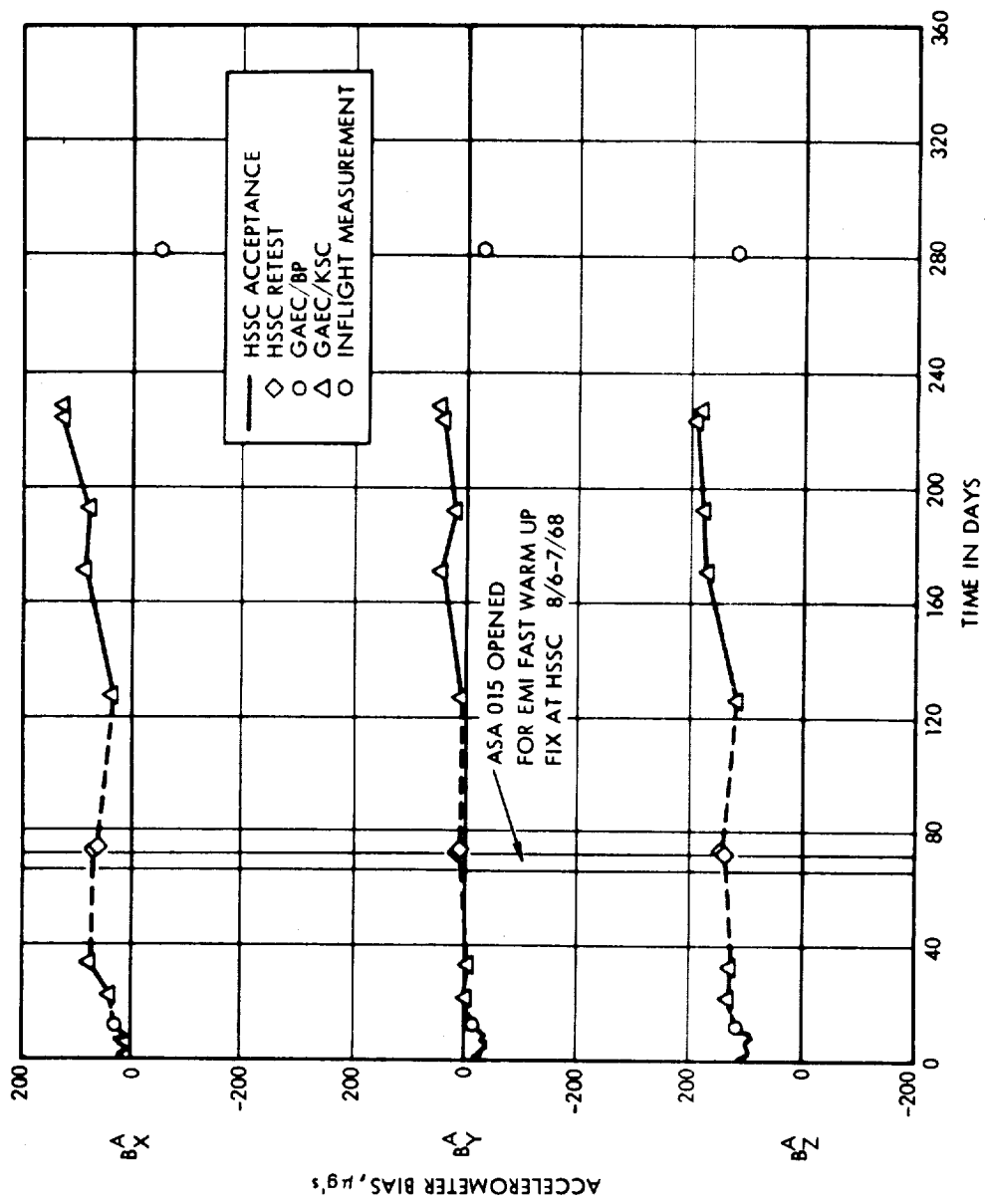


Figure I-2. ASA 015 History of Accelerometer Bias

APPENDIX II

TIMING ADJUSTMENTS

The following table lists the time increments between the AGS data (direction cosines and sensed velocities referred to the beginning of an AGS computation cycle): (1) the accelerometer count data, and (2) CDU angle data.

The values listed were determined by a curve fitting procedure in which errors due to timing are modeled as first derivatives and removed from the data by biasing the time base.

INTERVAL	CDU TIMEBIAS (SEC)	PGNCS ACCELERATION TIMEBIAS (SEC)
Docked DPS	+1.40	-0.29
Insertion	+1.14	+0.25
CSI	+1.20	+0.25
Depletion	+0.26	+0.33

The numbers tabulated are to be added to the nominal K factors in order to bias the AGS time base properly. The nominal K values are:

40 hrs (third period)

90 hrs (fifth period).

|

For the changing acceleration and attitude profile in an orbit insertion mode (lunar scaling) the quantization error would be less than 0.2 fps for a 450 sec burn.

The net result, for earth scaling, of the quantization induced computational error in accumulating sensed velocities in inertial coordinates is that while the errors are not large enough to impact mission performance, they are large enough to prevent the V_G residuals data at the end of burns to refine the estimate of AGS sensor performance.